

NORTHWESTERN UNIVERSITY

Tools and Methods for High-throughput Materials Synthesis Using Cantilever-free Scanning

Probe Lithography

A DISSERTATION

SUBMITTED TO THE GRADUATE SCHOOL

IN PARTIAL FULFILLMENT OF THE REQUIREMENTS

for the degree

DOCTOR OF PHILOSOPHY

Field of Materials Science and Engineering

By

Rustin Golnabi

EVANSTON, ILLINOIS

March 2021

© Copyright Rustin Golnabi 2021

All Rights Reserved

## ABSTRACT

### *Tools and Methods for High-throughput Materials Synthesis Using Cantilever-free Scanning Probe Lithography*

The advancement of nanotechnology is at least partially dependent on the ability to synthesize and arrange complex nanostructures on a substrate. Nanolithography, or the patterning of materials at the sub-micrometer length-scale, has been traditionally performed using a number of methods such as conventional photolithography, ion-beam etching, and electron-beam lithography. While most of these techniques demand complex multi-step procedures, often including vacuum environments, one recent development, polymer pen lithography (PPL), is a desktop fabrication tool that can be used to synthesize materials on a substrate at ultra-high-throughput and under ambient conditions. The technique uses an elastomeric array of pyramidal tips to physically transfer an ink to a substrate with the help of an atomic force microscopy (AFM) piezo.

High-throughput lithography techniques like PPL have established the field of nanocombinatorics, where megalibraries of materials are synthesized over a single substrate and screened for their properties. Advancing these lithography techniques such that we can perform all kinds of materials synthesis, including electrochemical or thermal synthetic methods in-situ, will greatly enhance our capabilities to create and use these combinatorial megalibraries. In addition, new high-throughput lithography techniques may enable simpler single-substrate biological studies and open the door to massively parallel 3D nanoprinting. In this thesis, I developed and investigated four different, yet inter-related cantilever-free scanning probe lithography techniques that expand lithography into unconventional materials synthesis localized

to a tip. Chapter 1 first reviews the traditional and newly emerging high-throughput lithography techniques as well as the path that has led towards the development of PPL. Chapter 2 describes a novel technique to use the existing technology to perform negative (rather than positive) lithography over a large substrate, while also investigating the technique's versatility in environments and inks as exemplified by DNA-nanoparticle assemblies within an aqueous system. Chapter 3 describes a technique termed thermal polymer pen lithography (t-PPL) and how it can be used to pattern over large areas. This system may be used to either deliver heat directly to a thermally sensitive substrate or deliver thermally-sensitive materials to a substrate with precision using a heated pen array. In Chapter 4, an invention called electrochemical PPL (ePPL) is described, wherein the typical elastomer pen array is replaced with a hydrogel one, and a potential difference is used to locally reduce metals onto a cathodic surface. Alloy nanostructures can be synthesized using this technique across large areas, achieving control over feature size, composition, and placement. Resolution down to 210 nm and height control up to a few microns is observed. Next, Chapter 5 describes the conceptual design and fabrication of an optoelectronic heater to be used for photo-actuated PPL. Due to the use of a single backing layer in this technique, PPL is intrinsically limited to the repetition of patterns over a single large-area substrate. This work represents one possibility for using light to actuate individual pens and pattern features arbitrarily at both high speed and high-throughput. The optoelectronic heater provides 1.5 microns of PDMS expansion, with sub-second time response in the current-profile.

Finally, Chapter 6 summarizes these advances and provides a future outlook for these techniques and the field of massively parallel nanolithography as a whole. Each of these innovative methods represents a distinct path forward for nanolithography with conditions and

materials that have been hitherto unavailable to scientists and researchers. With each new tool and technology, new avenues for exploration are revealed in the fields of combinatorics, prototyping, and cellular studies.

---

Thesis Advisor: Prof. Chad A. Mirkin

## ACKNOWLEDGEMENTS

First, I thank my advisor, Professor Chad Mirkin. While joining his lab was intimidating at first, I am forever grateful for his mentorship and guidance because he challenged me to become both a better scientist and communicator. He provided me with the freedom to explore the science that I found most interesting and the tools with which to do so. And while I worked on the details of my research, he always encouraged and pushed me to keep an open mind by suggesting unique directions for my projects and reminding me of the bigger-picture. In addition, I am very grateful to the endless help of the excellent staff he has brought together, namely Dr. Tanushri Sengupta, Pam Watson, Dr. Sarah Petrosko, Elizabeth Forest, and in particular, Dr. Sara Rupich. Sara has always provided invaluable suggestions and scientific critiques, and she has helped to make everything I wrote or presented a thousand times better. I also thank Professor Vinayak Dravid, one of my committee members who has never failed to make me smile and feel welcome when I spent time in his lab and offices. In addition, I thank Professors Jiaying Huang and Horacio Espinosa, my other committee members who have provided helpful suggestions, especially during my Qualifying Exam.

I never would have gotten through this experience with my sanity intact if it were not for my lab-mates. Not only are they fantastic scientists to work with and bounce ideas off daily, but they have also become great friends. In particular, I would like to thank EunBi Oh. We worked together nearly every day troubleshooting the myriad problems we would encounter, often followed by lunch or coffee while we vented about anything and everything. I also thank my friends and colleagues Liban Jibril, Dr. Abha Gosavi, Donghoon Shin, Namrata Ramani, Dr. Liliang Huang, Dr. Jinghan Zhu, and Kent Miao, not only for being excellent collaborators but

also for making the lab more tolerable, and, at times, even a fun place to work. Finally, I thank my mentor Dr. David Walker, for always being tough on me but simultaneously believing in me and helping me to become an infinitely better scientist who thinks critically and creatively about every problem he encounters. He is one of the smartest people I know, and I am so grateful for the opportunity to have learned from him.

Outside of the lab, I have been unbelievably fortunate with the amount of support I have had from all my friends and family. At Northwestern, Dr. Xiaomi Zhang, Will Kellogg, and Dr. Cesar Villa have grown to become what I believe will be lifelong friends. From grade school and college, thank you to Julienne Cham, Dr. Christina Le, Toni Guiriba, and Arman Mohsen-Nia for always being there for me and willing to listen or help with anything at the drop of a hat.

I thank my entire family for their love and support. In particular, my sister, Sima, has always believed in me and given me the kind of advice only an older sister can give. She is the one who helped me discover my career path, and she has always kept me grounded and has been the voice of calm when I needed it. In addition, I thank my brother-in-law, Paymon, for his support, as well as my entire extended family all across the globe. I extend my sincerest thanks to my soon-to-be mother-in-law, father-in-law, and brother-in-law, Arya, who have welcomed me into the family with open arms and open hearts. From the weekly games and movies, to the countless home-cooked meals I was lucky enough to bring home after every visit, they have become one of the greatest blessings in my life. Finally, I thank my parents who have given everything for me, without hesitation, and were always a daily phone-call or a quick flight away no matter what I needed. They have made me the man I am today, and any success I may have is theirs to share.

Last, but certainly not least, I thank my fiancée, Roya. I met Roya within two months of starting at Northwestern, and I can't believe I'll be marrying my best friend this spring. She motivates me to be a better student and a better person. With her immeasurable love, support, and partnership, she has been my biggest cheerleader, and she has ensured that I never lose my self-confidence. Without her, I am not sure that I would have finished this degree, let alone this dissertation. Thank you, Roya, for everything.

## **DEDICATION**

This dissertation is dedicated to Roya and my parents. Your unconditional love and support are what made this possible.

## TABLE OF CONTENTS

<b>ABSTRACT.....</b>	<b>3</b>
<b>ACKNOWLEDGEMENTS.....</b>	<b>6</b>
<b>DEDICATION.....</b>	<b>9</b>
<b>TABLE OF CONTENTS.....</b>	<b>10</b>
<b>LIST OF FIGURES.....</b>	<b>12</b>
<b>LIST OF TABLES.....</b>	<b>18</b>
<b>LIST OF ABBREVIATIONS.....</b>	<b>19</b>
<b>CHAPTER ONE: INTRODUCTION TO CF-SPL .....</b>	<b>20</b>
1.1 Polymer Pen Lithography.....	21
1.2 Ink and architectural advancements in CF-SPL .....	28
1.3 Future Outlook of CF-SPL .....	37
<b>CHAPTER TWO: NEGATIVE POLYMER PEN LITHOGRAPHY.....</b>	<b>39</b>
2.1 Introduction.....	40
2.2 Results and Discussion.....	41
2.3 Conclusions.....	48
<b>CHAPTER THREE: THERMAL POLYMER PEN LITHOGRAPHY .....</b>	<b>50</b>
3.1 Introduction.....	51
3.2 t-PPL Development and Technology .....	53
3.3 Conclusions and Future Outlook.....	61
<b>CHAPTER FOUR: ELECTROCHEMICAL POLYMER PEN LITHOGRAPHY.....</b>	<b>64</b>
4.1 Introduction.....	65
4.2 Experimental Section .....	67
4.3 Single Metal Patterning.....	71
4.4 Multimetallic Patterning.....	81
4.5 Conclusion .....	86
<b>CHAPTER FIVE: ACTIVE POLYMER PEN LITHOGRAPHY .....</b>	<b>87</b>
5.1 Introduction.....	88
5.2 Conceptualization of Photo-actuation .....	97

	11
5.3 Optoelectronic Heating Device.....	102
5.4 Future prospects.....	108
<b>CHAPTER SIX: CONCLUSIONS AND FUTURE OUTLOOK.....</b>	<b>112</b>
6.1 Summary and Conclusions.....	113
6.2 Future Outlook.....	114
<b>REFERENCES.....</b>	<b>117</b>
<b>CURRICULUM VITAE.....</b>	<b>129</b>

## LIST OF FIGURES

- Figure 1.1** Schematic representation of dip-pen nanolithography (DPN). As an inked atomic force microscopy (AFM) tip comes into contact with a substrate, a water meniscus forms, which enables the transport of molecules from the tip to the substrate with high resolution.<sup>7</sup>..... 22
- Figure 1.2** The rapid progression of DPN to polymer pen lithography (PPL) over nine years is shown, where throughput has increased by several orders of magnitude. The time needed to pattern 1 cm<sup>2</sup> with 1 billion 100-nm dot features is plotted against the year of technology development.<sup>11</sup> ..... 24
- Figure 1.3** PPL uses deformable elastomer tips as the cantilever and piezo scanners to control the movement of the pen array. An example of a patterned array of 16-mercaptohexadecanoic acid (MHA) particles is shown, depicting the logo of the 2008 Beijing Olympics.<sup>9</sup>..... 26
- Figure 1.4** (a) A PPL array before inking is (b) inked using two spray guns delivering two different aqueous molecular inks. (c) By patterning using this coated array, a compositional gradient of particles is deposited onto a substrate. (d) By selective chemical vapor deposition (CVD) growth, in this case single-walled carbon nanotubes (SWCNTs) are grown and simultaneously analyzed using Raman spectroscopy in order to identify the optimal catalyst for SWCNT growth.<sup>1</sup> ..... 29
- Figure 1.5** PPL provides precision control over resolution by varying z-piezo extension of the pen array or varying the deposition time. (a) Here, dot size of MHA features is plotted against relative z-piezo extension, using an array of 15,000 pens at room temperature with relative humidity of 40%. (b) Optical image of a 4-inch wafer containing 11 million polymer pens. (c) Shown is an optical micrograph of etched gold circuit patterns having both nanometer and micrometer-sized patterns. (d) Periodic array of prostate specific antigen labeled with AlexaFluor antibodies is patterned, demonstrating the ability to control feature size based on both increased force (z-extension) and dwell time.<sup>14</sup>..... 30
- Figure 1.6** (a-d) MHA-fibronectin dot pattern designs on the left and representative fluorescence micrographs of the actin cytoskeleton in human mesenchymal stem cells seeded on each pattern (right).<sup>15</sup>..... 32
- Figure 1.7** Hard transparent arrays use a thin silica coating in order to reduce minimum feature size and keep pen-to-pen variation minimal by redistributing the force to the backing layer rather than the tips.<sup>21</sup> ..... 34

- Figure 1.8** (a) Beam pen lithography (BPL) uses a digital micromirror device (DMD) to individually actuate pens in a pen array. (b) These pens are coated with an opaque (typically Au) thin film, and etched at each tip using either focused ion beam, photolithography, or mask-enabled etching processes, such that small, subwavelength apertures allow light to penetrate to the material that is being patterned. One notable advancement in the BPL architecture has been observed using microfluidic channels to flow different chemical reagents onto a substrate without ever replacing the array, thus enabling multicomponent structural printing, such as for brush copolymers.<sup>24</sup> ..... 36
- Figure 2.1** Substrate and nanoparticle multilayer preparation and patterning process are schematically illustrated..... 41
- Figure 2.2** (a) A 30  $\mu\text{m}$ -pitch polydimethylsiloxane (PDMS) PPL array, as seen by optical microscope, with sharp tips, as observed in (b), was used to negatively pattern “N” shapes from a DNA-mediated nanoparticle assembly. The sample was then embedded in silica to observe in the solid state under a scanning electron microscope (SEM) (c, d), where the localized removal of programmable atom equivalents (PAEs) is apparent. The non-silica-embedded sample was imaged using optical microscopy in water as well (e). ..... 44
- Figure 2.3** Tilting the stage during patterning creates a gradient feature size in both point (a) and line (b) features across a single substrate. These dimensions are plotted against calculated z-distance in order to provide size control during patterning from 100 nm to 5  $\mu\text{m}$ . Scale bars = 1  $\mu\text{m}$ . ..... 45
- Figure 2.4** Patterns were successfully backfilled with new PAEs..... 46
- Figure 3.1** Schematic of thermal scanning probe lithography (above) and its capability (below) for ultra-high-resolution, spatially-precise patterning of silicon using a thermal resist (poly(phthalaldehyde)).<sup>41</sup> ..... 52
- Figure 3.2** Schematic of thermal PPL (t-PPL) pen array. The PDMS PPL array is affixed to an aluminum plate, serving as the backing layer, then coated with a thin film of Au in order to provide more efficient thermal conduction while also enhancing resolution consistency. A ceramic heater is adhered to a PPL array using polyimide tape (thermally resistant) for easy replacement while also providing insulation for instrument safety..... 54
- Figure 3.3** Images of pen array loaded into TERA-fab M-series instrument for patterning (left) and t-PPL pen array (right)..... 56

- Figure 3.4** t-PPL delivers localized heat at each tip location. Using an image-reversal photoresist (AZ 5214E), where a crosslinking agent in the resist formulation activates at temperatures above 110 °C, areas of a photoresist were selectively crosslinked using t-PPL..... 58
- Figure 3.5** t-PPL tips coated (top half) with gelatin methacryloyl (GelMA), ready to be patterned..... 59
- Figure 3.6** Patterned GelMA features on an Si substrate, as seen under an optical microscope. .... 60
- Figure 3.7** Example of thermal dip-pen nanolithography being used to pattern nanoparticles with high resolution and in a straight line for potential use in electronics for circuit building and repair.<sup>45</sup> ..... 62
- Figure 4.1** Exaggerated 3D rendering of electrochemical PPL (ePPL) procedure. As a metal salt-embedded hydrogel is brought into contact with a cathodic surface repeatedly using a piezo, metal micro/nano-structures are reduced sequentially. .... 66
- Figure 4.2** Experimental setup of ePPL. (a) Schematic of a three-electrode cell designed to hold the hydrogel array, electrolyte, and reference and counter electrodes in place during patterning. (b) Optical image of fabricated polyacrylamide hydrogel pen arrays, which were prepared by curing the hydrogel within a silicon master (scale bar = 30 μm). Images on the right show a pen array during the patterning process, highlighting how contact was determined: pens (top) out-of-contact and (bottom) in-contact with the substrate (working electrode) (scale bars = 15 μm). (c) Photograph of the experimental setup in a Park AFM, showing the cell, electrodes, electrical leads, and optical microscope used for leveling. .... 71
- Figure 4.3** CV scans for a Ni-embedded hydrogel 3-electrode cell at three different scan rates, indicating both reduction and oxidation potential peaks..... 72
- Figure 4.4** Patterning capabilities of ePPL. Optical micrographs of patterns of (a) Ni on an Au substrate (scale bar = 100 μm), (b) Ag on an indium tin oxide (ITO) substrate (scale bar = 20 μm), and (c) Pt on an Au substrate (scale bar = 100 μm). The Pt pattern consists of an array of 13 dots arranged as the letter “N” at each pen location. AFM images of (d) a single “N” (scale bar = 10 μm) and (e) a single Pt particle (scale bar = 500 nm). (f) The associated line scan of the particle in panel (e)..... 73
- Figure 4.5** Control patterning experiment shows that an applied voltage is needed for metal deposition to occur. An Au-coated Si wafer was scratched with a cross and

imaged before (a) and after (b) typical Ni patterning with 0 V applied. No patterned features are observed. Scale bars = 50 nm. .... 74

**Figure 4.6** Optical images of a substrate with Ni features before and after extensive rinsing indicate the presence of reduced metal. (a) An Au-coated Si wafer was patterned with an array of 3 Ni features from each tip (b) washed thoroughly with water, and then (c) sonicated for 30 s in water. While the features faded after agitation, this experiment shows that the patterned features are reduced metal on the substrate and not salt residue. Scale bars = 30  $\mu\text{m}$ . .... 75

**Figure 4.7** X-ray photoelectron spectroscopy (XPS) patterns of the patterned samples confirm the presence of metal on the respective substrates. (a) Ni features on an Au-coated Si wafer. The peaks at 856 eV and 873 eV (left) are expected Ni 2p peaks. Au 4f peaks are observed at 84 eV and 87.7 eV (right). (b) The peak at 73 eV (left) indicates Pt on Au-coated Si substrate with Au 4f peak at 84 eV (right). (c) The presence of the Ag is confirmed by the peaks at 367 eV and 373.6 eV (left), and the peaks at 486 eV and 494.5 eV (right) are assigned to Sn 3d from the ITO-coated glass slide. The main peaks in the deposited features are all oxides due to rapid oxidation upon exposure to ambient conditions. .... 76

**Figure 4.8** Scanning electron micrographs of patterned Pt features on Au-coated Si wafer, highlighting the high-resolution capability of ePPL. The black features indicate Pt particles with diameters ranging from ~210 nm to 280 nm. Scale bars = 500 nm. .... 78

**Figure 4.9** Feature dimensions are controlled by deposition time and layering. (a) Optical and AFM images of a pattern consisting of 4 Ni features where height was controlled by varying the deposition time. (b) Optical and AFM images of a pattern with 2 Ni features where size is controlled by depositing multiple layers of Ni, 60 s at a time. Features shown are 10 vs. 1 layer. Scale bars = 5  $\mu\text{m}$ . .... 79

**Figure 4.10** Schematic depicting the hypothesized mechanism of ePPL deposition. (1) First, metal reduction occurs preferentially from the meniscus that forms between the tip and the substrate upon contact. (2) Once ions are depleted from the meniscus, reduction occurs directly from the hydrogel, at the tip-substrate interface. (3) When the tip is lifted, the shape and size of the resulting structure corresponds to the shape of the tip-substrate interface, along with a very thin layer from the meniscus. .... 79

**Figure 4.11** Deposition of Ni-Co alloys. (a) Optical micrograph of a large-area pattern of >10  $\mu\text{m}$  Ni-Co features. The large feature size enables accurate elemental characterization. Inset shows a single feature. (b) XPS characterization of these

- patterns indicates that both the Ni and Co are present mainly as oxides. Auger peaks have been subtracted for clarity..... 81
- Figure 4.12** Optical micrograph of Ni-Co particles patterned on an Au substrate. Scale bar = 50  $\mu\text{m}$ ..... 82
- Figure 4.13** (a) AFM height profile of a large Ni-Co feature, and (b) AFM line scan across the large feature in (a), location indicated by dashed line. Scale bar = 3  $\mu\text{m}$ ..... 82
- Figure 4.14** Energy-dispersive X-ray spectroscopy (EDS) characterization of a Ni-Co feature indicates the presence of both Ni and Co in the deposited region. Ni-Co was patterned on an Au-coated  $\text{SiO}_2$  wafer with a chromium adhesion layer. Corresponding metal peaks are labeled. Scale bar = 5  $\mu\text{m}$ ..... 88
- Figure 5.1** Illustration of actuated DPN using thermal bimorphs. This method is difficult to scale up, fragile, and expensive to manufacture.<sup>78</sup>..... 89
- Figure 5.2** Schematic of pneumatic chambers and optical image of fabricated chambers behind PPL tips. The air pressure inside the chambers expands to “push” each tip towards the substrate for patterning.<sup>80</sup>..... 90
- Figure 5.3** Illustration and image of actuated PPL using patterned resistive heaters.<sup>81</sup>..... 92
- Figure 5.4** Depiction of actuated BPL. A DMD array is used to program and control the light output through the aperture at the apex of each pen and onto the substrate for large area arbitrary nanoscale light patterning.<sup>24</sup>..... 93
- Figure 5.5** Conceptualization for active PPL. A DMD projector will illuminate the area behind select pens within an array which will thermally expand and selectively deposit material onto the substrate. .... 96
- Figure 5.6** Schematic of active PPL design. A potential is applied across a transparent conducting oxide layer (i.e., ITO) and a reflective metal layer (i.e., Ag), with a mostly insulating layer of photoconductive hydrogenated amorphous silicon (a-Si:H) in between. By guiding the flow of electrons through the a-Si:H layer, the resistive heating can be localized to micron-scale regions, thereby thermally expanding each PDMS pen sitting atop that region..... 99
- Figure 5.7** The setup used for characterization of the optoelectronic heating (OEH) device is shown where an external power source applies a potential to the contact pads of the two electrodes; meanwhile, a DMD projects light from a red LED orthogonal to the device in order to illuminate the amorphous silicon. Measurements from an

	AFM cantilever, infrared (IR) camera, or probe station would be collected from above the device. ....	100
<b>Figure 5.8</b>	Layers of thin film deposition are shown for OEH device fabrication. An example of a completed device is shown in the corner of the figure. ....	103
<b>Figure 5.9</b>	I-V profile of OEH device was measured on the right, and the literature result is shown on the left for visual comparison. ....	104
<b>Figure 5.10</b>	More electronic properties of the OEH device were measured, including a) response to different light intensities, and b) time-response of the photocurrent. ....	105
<b>Figure 5.11</b>	The AFM tip deflection over a layer of expanding PDMS is shown over time. The markers indicate when light is turned on (red) and off (black).....	106
<b>Figure 5.12</b>	Schematic depicting how insulating features may be patterned between pens on the Ag backing layer, and a thermoelectric cooler may be integrated for improved reaction time and overall temperature control.....	108
<b>Figure 5.13</b>	Basic understanding of proposed active PPL mechanism. The working electrode will be replaced with the OEH device which can use the changing conductivity to apply potential selectively in regions where patterning is to occur. In this way, ePPL patterning could become a fully functional tool for arbitrary desktop nanolithography and 3D printing of metal nanostructures. ....	109

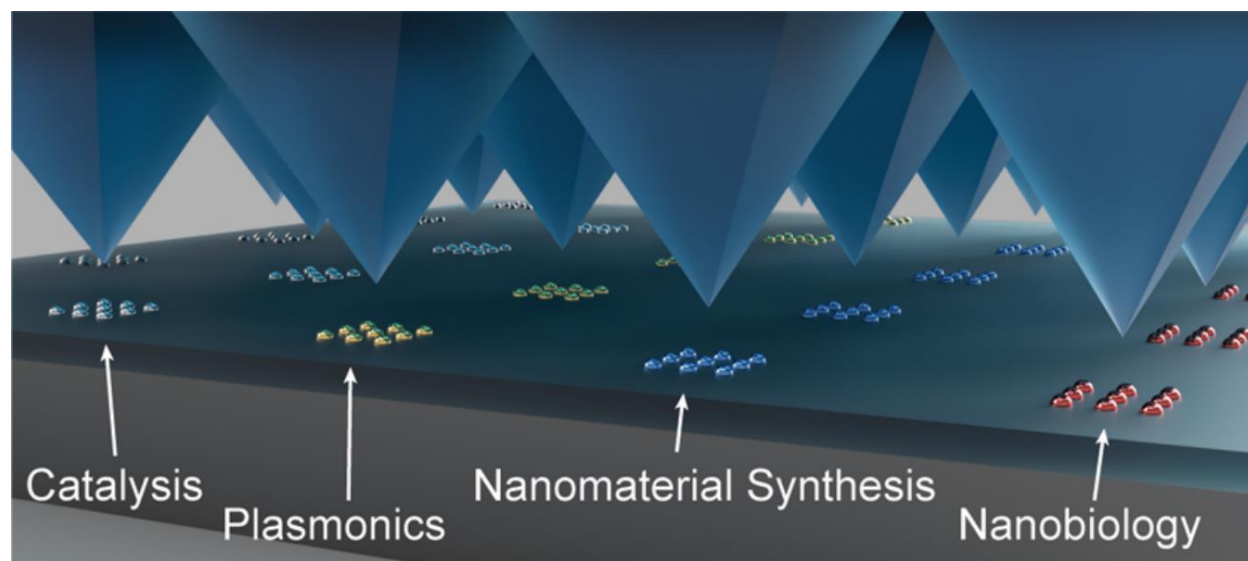
## LIST OF TABLES

<b>Table 4.1</b>	Applied voltages and minimum deposition times used for each metal deposition. .....	69
<b>Table 4.2</b>	Chemical composition of Ni–Co deposited alloys as obtained by X-ray photoelectron spectroscopy (XPS). .....	84

## LIST OF ABBREVIATIONS

<b>AFM</b>	atomic force microscopy
<b>a-Si:H</b>	hydrogenated amorphous silicon
<b>BPL</b>	beam pen lithography
<b>CF-SPL</b>	cantilever-free scanning probe lithography
<b>CPE</b>	controlled potential electrolysis
<b>CVD</b>	chemical vapor deposition
<b>DMD</b>	digital micromirror device
<b>DPN</b>	dip-pen nanolithography
<b>ePPL</b>	electrochemical polymer pen lithography
<b>HSL</b>	hard-tip, soft-spring lithography
<b>IR</b>	infrared
<b>ITO</b>	indium tin oxide
<b>MHA</b>	16-mercaptohexadecanoic acid
<b>n-PPL</b>	negative polymer pen lithography
<b>OEH</b>	optoelectronic heating
<b>OET</b>	optoelectronic tweezers
<b>PAE</b>	programmable atom equivalent
<b>PDMS</b>	polydimethylsiloxane
<b>PPL</b>	polymer pen lithography
<b>SEM</b>	scanning electron microscope
<b>SPBCL</b>	scanning probe block copolymer lithography
<b>SPL</b>	scanning probe lithography
<b>SWCNT</b>	single-walled carbon nanotube
<b>t-PPL</b>	thermal polymer pen lithography
<b>t-SPL</b>	thermal scanning probe lithography

## CHAPTER ONE: INTRODUCTION TO CF-SPL



## 1.1 Polymer Pen Lithography

In materials science, nanomaterials have been determined to provide dramatically different properties than their bulk counterparts because of quantum effects as well as increased surface area to volume ratios. As research in the field progresses, so does the need for methods to synthesize nanomaterials efficiently and with low cost. Most importantly, as new nanomaterials are discovered every day, a systematic way to synthesize them rapidly in a variety of ways and without the need for complex post-processing techniques is necessary. In order to create such combinatorial megalibraries and synthesize materials using light, electrochemistry, mechanical force, or heat, new high-throughput nanofabrication methods will be required.

The current staples of nanofabrication include photolithography<sup>2</sup> and electron beam lithography<sup>3</sup>. These methods have significant drawbacks, however, especially in materials science research. Photolithography is mask-limited, meaning that each new variation in a pattern requires a new mask, resolution-limited, and materials-limited (not easily adaptable to soft materials). Electron beam lithography is throughput-limited and high-cost. It is also likewise limited in terms of materials flexibility. One approach that has been developed to work around some of these limitations is microcontact printing.<sup>4,5</sup> This technique uses conventional lithography techniques to create a master, then mold a “stamp” that is then coated with an ink and used to mechanically deposit molecules onto a surface. Here, small features can be created with high-throughput and low-cost, however each new pattern requires the use of a new mold and a new stamp. Thus, the need for a new method of resist-free, mask-free nanolithography is present and significant. Because of the diversity in materials science and chemistry, this technique should be materials-generalizable. In other words, it should have compatibility with

most materials and substrates, like metals, semiconductors, polymers or gels, or even cells and proteins.

In another method called scanning probe lithography (SPL),<sup>6</sup> a nanoscale tip, or “probe”, is used to deposit materials onto a substrate by the transfer of either energy (i.e., photons, ions, or electrons) or materials (“inks”). This technique is often found to be advantageous due to its mask-less nature, as well as its lower cost and higher resolution. Also, in contrast with other techniques, SPL can pattern a seemingly limitless spectrum of materials onto a wide variety of substrates without significant added complexities, such as a vacuum or clean-room environment.

A substantial step forward in SPL technology occurred with the development of dip-pen nanolithography (DPN).<sup>7,8</sup> Established by the Mirkin group in 1999, DPN involves the coating of an atomic force microscopy (AFM) tip (or “pen”) with a desired molecule (or “ink”) that is transferred from the tip to the surface of a substrate. This typically occurs *via* capillary transport through a water meniscus that forms at the tip-substrate interface (**Figure 1.1**). One of the greatest advantages of DPN is its site-specific deposition capabilities. In addition, the technique does not rely on a resist, stamp, or other post-processing methods like similar methods, while still being high-resolution. The greatest limitation of DPN, however, is the low throughput caused by the use of a single tip at a time.

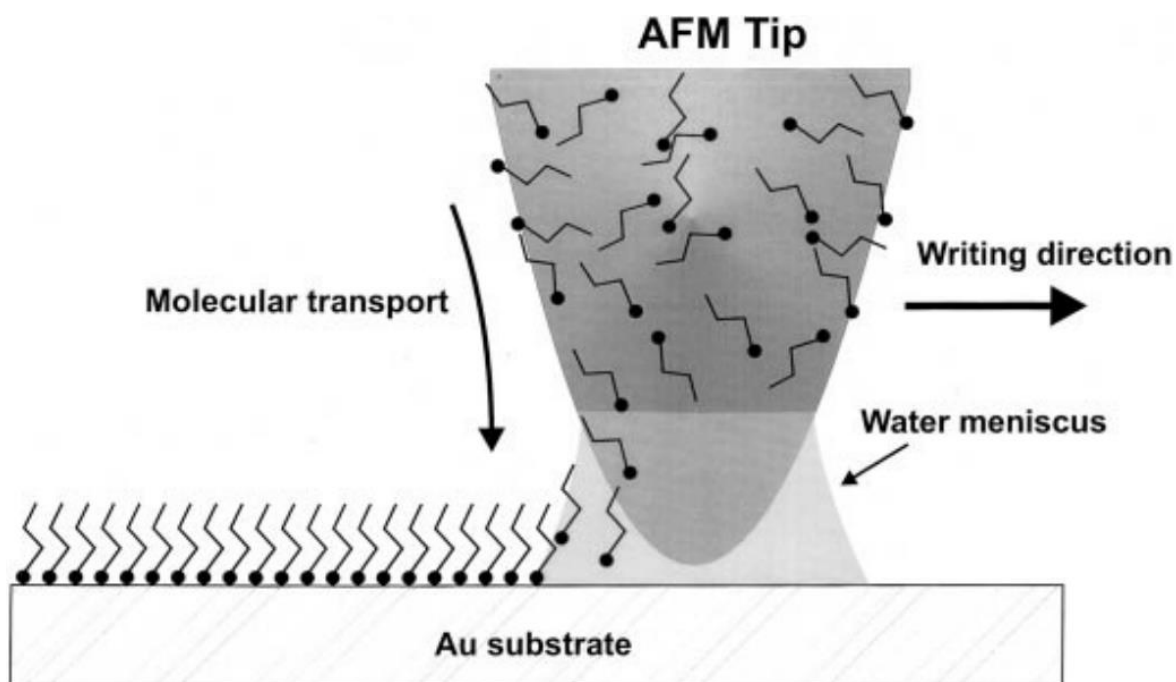


**Figure 1.1.** Schematic representation of dip-pen nanolithography (DPN). As an inked atomic force microscopy (AFM) tip comes into contact with a substrate, a water meniscus forms, which enables the transport of molecules from the tip to the substrate with high resolution.<sup>7</sup>

In order to address this shortcoming, several efforts have been made to expand the number of tips patterning in parallel. First to 11 pens, then 26, and eventually to 55,000 pens. However, the production of a 2D array of 55,000 cantilevers in a single substrate was time-consuming, very expensive, and the pens are fragile. So, nearly a decade later, polymer pen lithography (PPL) was developed as a high-throughput, cantilever-free version of this technique (**Figure 1.2**).<sup>9,10</sup> Using an array of elastomer tips on a glass backing layer, PPL allows for the parallel deposition of nanoscale features for high-throughput, large area patterning, while being inexpensive and relatively easy to fabricate. This paved way for an increasing number of applications from nanoscale studies of cell-surface interactions to high-throughput screening of

catalytic molecules. The technique allows for rapid and inexpensive, large-scale patterning of a wide variety of ink-substrate combinations. For these reasons, the development of PPL, which is inexpensive, high-throughput, and versatile, in conjunction with other cantilever-free scanning probe lithography (CF-SPL) techniques, has ushered in a new era of desktop nanofabrication.

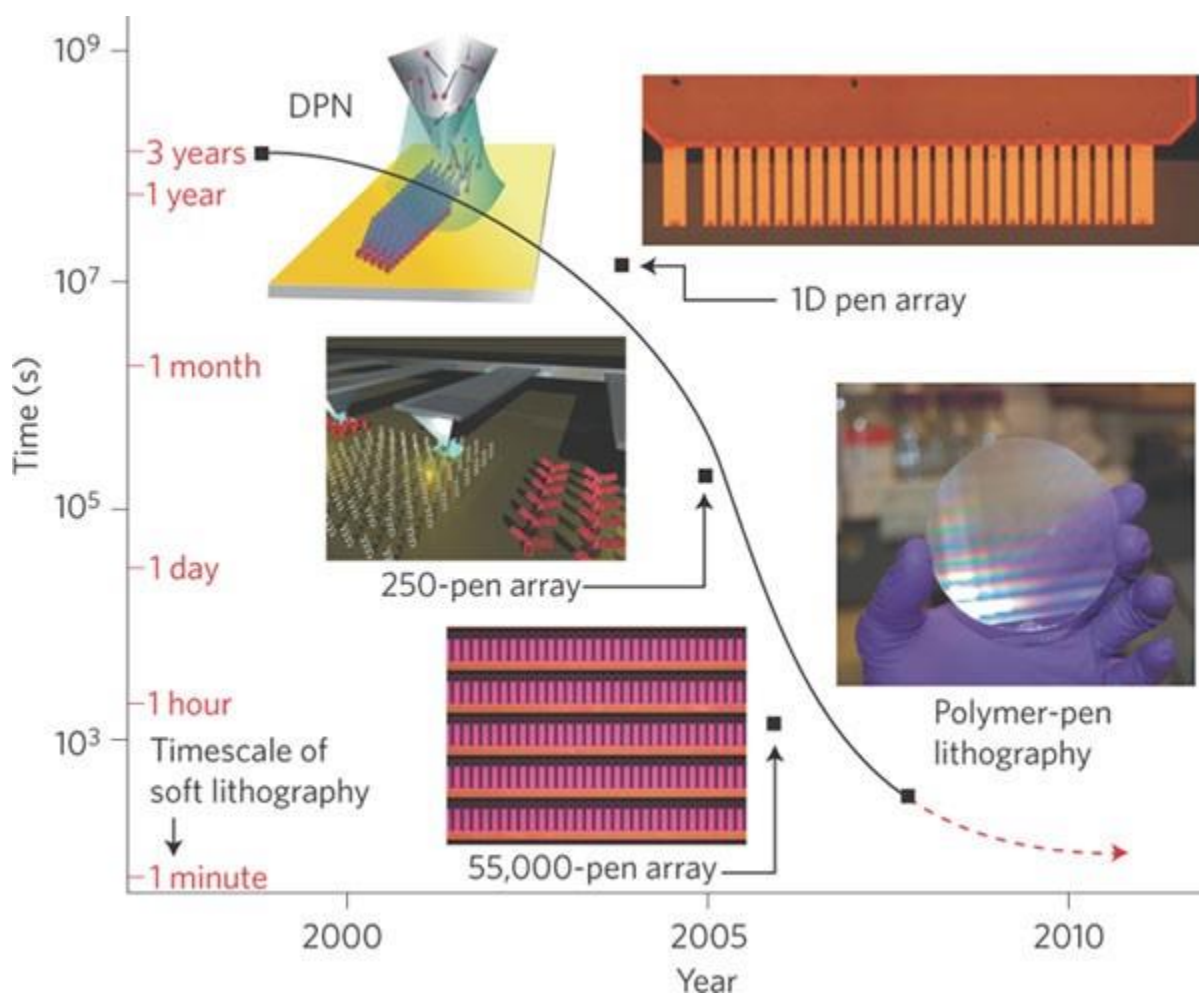


**Figure 1.2.** The rapid progression of DPN to polymer pen lithography (PPL) over nine years is shown, where throughput has increased by several orders of magnitude. The time needed to

pattern 1 cm<sup>2</sup> with 1 billion 100-nm dot features is plotted against the year of technology development.<sup>11</sup>

In 2008, the Mirkin group published the first report describing PPL (**Figure 1.3**).<sup>9</sup> PPL is similar to microcontact printing as it also utilizes an elastomer stamp molded from a master. However, it differs by use of its pyramidal, nanoscale tip array, which is cast onto a rigid glass slide and patterns using the mechanisms of scanning probe lithography. This cantilever-free scanning probe technique has increased the throughput of SPL to millions of pens on the centimeter-scale and lowered the cost of printing due to the relatively cheap materials and methods needed to produce each array and pattern. Each pen array in PPL has up to 11 million pens, with sharp (<100nm) tip diameters, writing simultaneously. When the pens are brought into contact with the surface, a meniscus forms, and colloidal molecules are deposited onto the substrate as the pens lift off. The feature sizes can be reliably controlled, as they are largely dependent on the amount of time pens spend in contact with the substrate (dwell time) and the contact pressure, or downward force of the z-piezo, on the substrate.

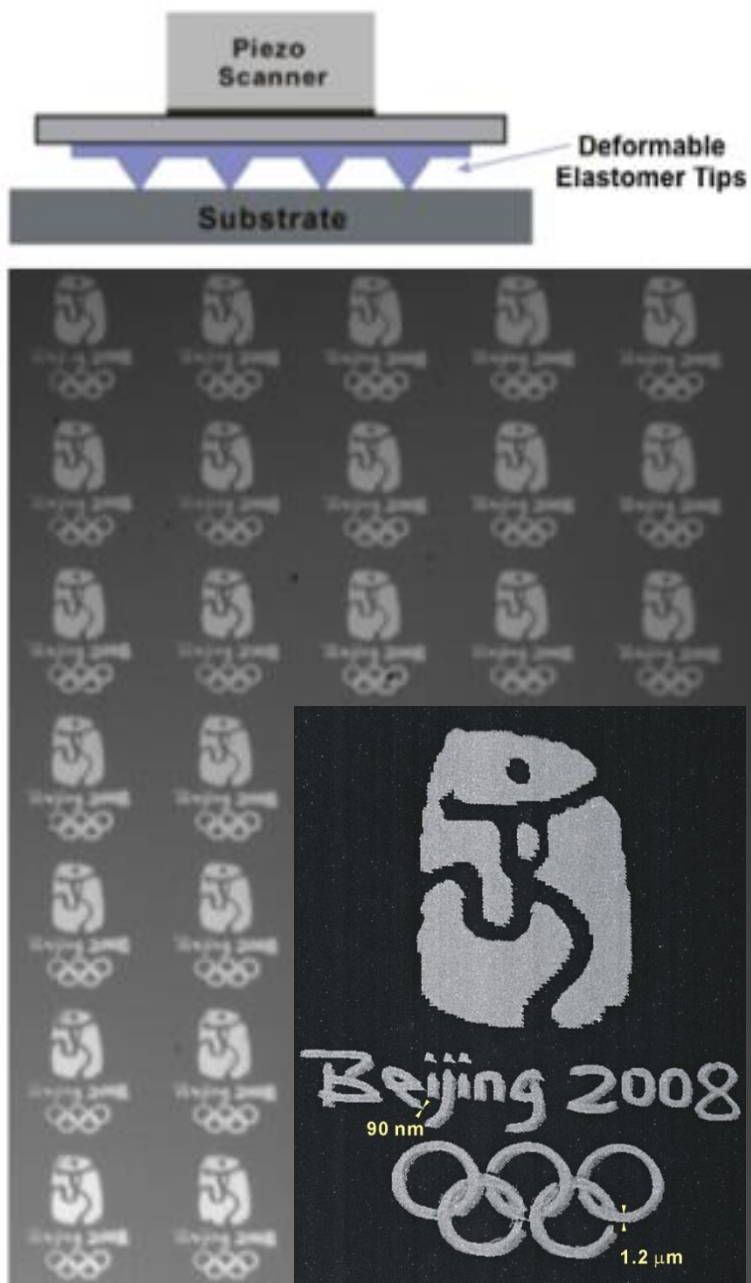


**Figure 1.3.** PPL uses deformable elastomer tips as the cantilever and piezo scanners to control the movement of the pen array. An example of a patterned array of 16-mercaptohexadecanoic acid (MHA) particles is shown, depicting the logo of the 2008 Beijing Olympics.<sup>9</sup>

The unique capabilities of PPL will enable it to fulfill a significant vacant role in the nanolithography field: desktop nanofabrication. The versatility and low-cost (each elastomer pen array is <\$1 in materials cost after a mask has been made) of each pattern allows researchers to quickly print new patterns one after another, with variable material composition and feature size ranging from sub-100-nm up to tens of microns. PPL allows for rapid prototyping of many materials, particularly for biological applications or for combinatorial materials screening.

Furthermore, the mask-free nature of PPL enables arbitrary patterning, and the ambient conditions enable a wide array of hydrophilic or hydrophobic materials to be deposited without the need for a cleanroom or complicated processing. One particular advantage of PPL is its capability for combinatorial synthesis, whereby millions of different materials (by simultaneously varying size and composition) can be patterned and analyzed for activity, such as catalytic reactivity or cell-binding affinity.<sup>12,13</sup> Techniques have been developed to predictably vary the feature size, such as tilting the array while printing to control contact pressure or spray coating the pen array at an angle to create a concentration gradient.<sup>12</sup>

Despite its potential, PPL has not yet become a standard lithography tool in the industry. The simplistic nature of elastomer arrays on a glass slide has only seen minor improvements since its conception, and it has remained a technique reminiscent of micro-contact printing, acting as a stamping tool rather than a versatile tool for arbitrary patterning. Furthermore, it cannot go beyond two-dimensional printing of materials. By introducing new modes of parallel printing, PPL can be advanced to function as a versatile desktop nanofabrication tool for arbitrary patterns or high-resolution three-dimensional structures. Pens could conceivably be used in an array to deliver heat, electrons, or ions to a substrate in order to make chemical

modifications at the tip. By adding electronically-active elements to the technique, PPL can become a multipurpose benchtop tool for all kinds of nanofabrication. Such versatility will allow for the study of new structures and materials that cannot be done at present. Herein lies the motivation for my dissertation. In this thesis, I will describe four methods of advancements of PPL towards arbitrary, materials-generalizable massively parallel nanolithography. First, by utilizing PPL architecture with aqueous biological systems, negative lithography may be performed. Second, the integration of a heating element into the PPL architecture enables localized thermo-chemistry at each tip. Third, by integrating electrochemical deposition into PPL, we can deposit metal locally at each tip and potentially scale the printing to a third dimension. And fourth, by optimizing a technique for localized Joule heating of the polydimethylsiloxane (PDMS) elastomer, thermal expansion of PPL will enable individual actuation of each tip within an array. All of these techniques will be used to develop a greater understanding of materials syntheses at the nanoscale, as well as the nanoscale effects that are at play in the system.

## **1.2 Ink and architectural advancements in CF-SPL**

One of the unique advantages of PPL is the ability to not only spatially encode features on a substrate with great precision, but also control both feature dimensions and composition, depending on patterning conditions and ink solutions used. In particular, many different inks have been used in conjunction with PPL, making it one of the most materials-versatile nanopatterning tools available. PPL pen arrays can be "inked" by drop-casting, spin-coating, or spray-coating. In particular, recent work has shown that by spray-coating two (or more) inks with separate spray guns across a pen array, a compositional gradient may be feasibly patterned using

PPL (**Figure 1.4**).<sup>12</sup> In addition, by varying the z-piezo extension of a pen array while patterning, thus varying the pressure across the array, feature size can be controlled with a gradient *via* a tilt of the array (**Figure 1.5**).<sup>14</sup> These techniques together introduced a novel method for the synthesis of large-area combinatorial megalibraries with variable size and composition, such that with the proper screening technique, optimal activity among millions of multi-compositional nanoparticles/molecules may be identified more rapidly than ever before. This presents a transformative tool for materials science as a platform for the rapid discovery of new ideal materials for catalysis, plasmonics, magnetics, and more.

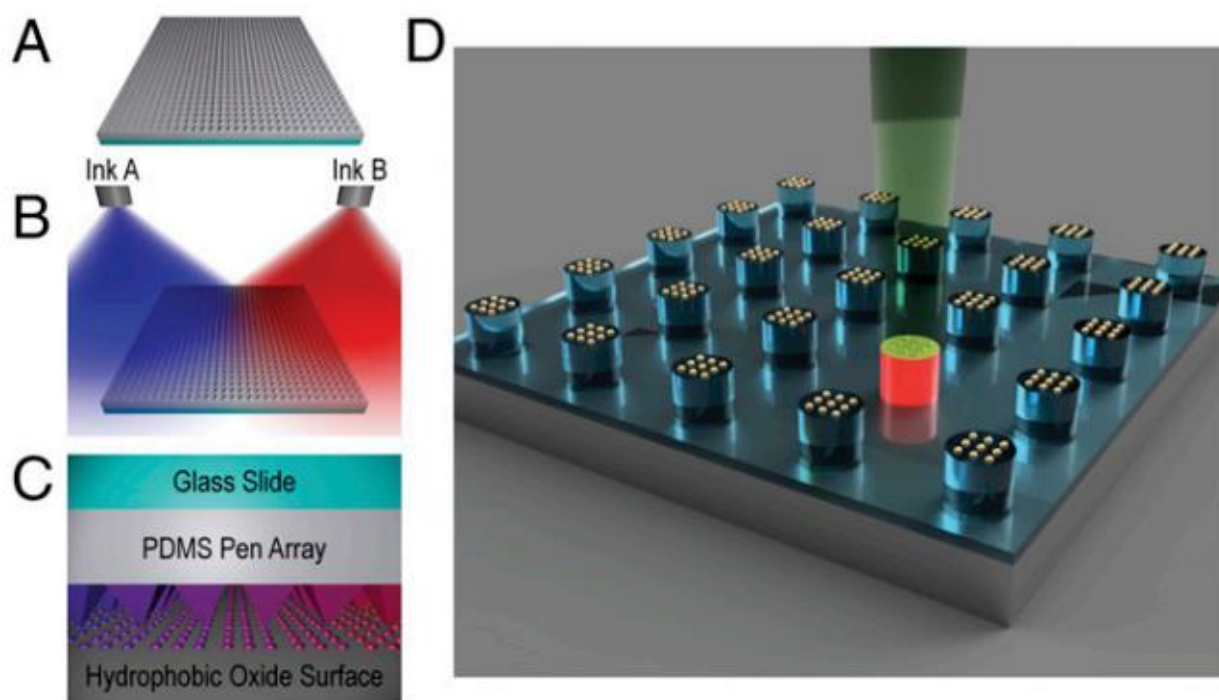


**Figure 1.4.** (a) A PPL array before inking is (b) inked using two spray guns delivering two different aqueous molecular inks. (c) By patterning using this coated array, a compositional gradient of particles is deposited onto a substrate. (d) By selective chemical vapor deposition (CVD) growth, in this case single-walled carbon nanotubes (SWCNTs) are grown and

simultaneously analyzed using Raman spectroscopy in order to identify the optimal catalyst for SWCNT growth.<sup>1</sup>

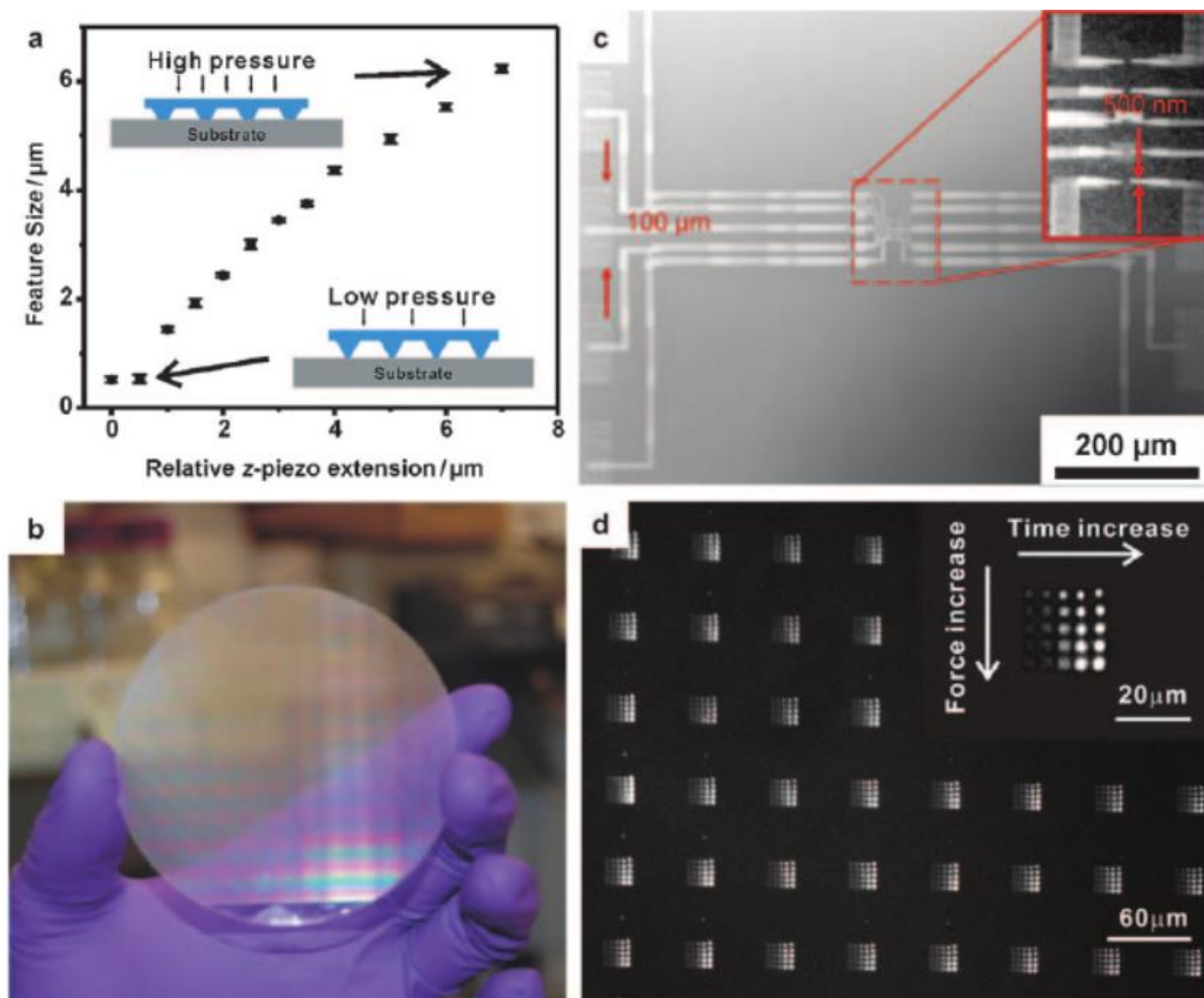


**Figure 1.5.** PPL provides precision control over resolution by varying z-piezo extension of the pen array or varying the deposition time. (a) Here, dot size of MHA features is plotted against relative z-piezo extension, using an array of 15,000 pens at room temperature with relative humidity of 40%. (b) Optical image of a 4-inch wafer containing 11 million polymer pens. (c) Shown is an optical micrograph of etched gold circuit patterns having both nanometer and

micrometer-sized patterns. (d) Periodic array of prostate specific antigen labeled with AlexaFluor antibodies is patterned, demonstrating the ability to control feature size based on both increased force (z-extension) and dwell time.<sup>14</sup>

Because PPL uniquely does not require any vacuum or high-temperature environment, nor any complicated post-processing steps, it is uniquely suited towards biological studies. Seeding cells over patterned fibronectin, DNA, or allergens enables scientists to study cell-cell and cell-environment interactions rapidly. Because of the high-throughput nature, these studies can be done rapidly and without the need for as many controls when working with a single substrate. Recently, varying shapes of fibronectin focal adhesions were patterned on a substrate, and the relationship between cell morphology, cytoskeletal architecture, and programmed cell behavior, in this case stem cell differentiation (**Figure 1.6**).<sup>15</sup>

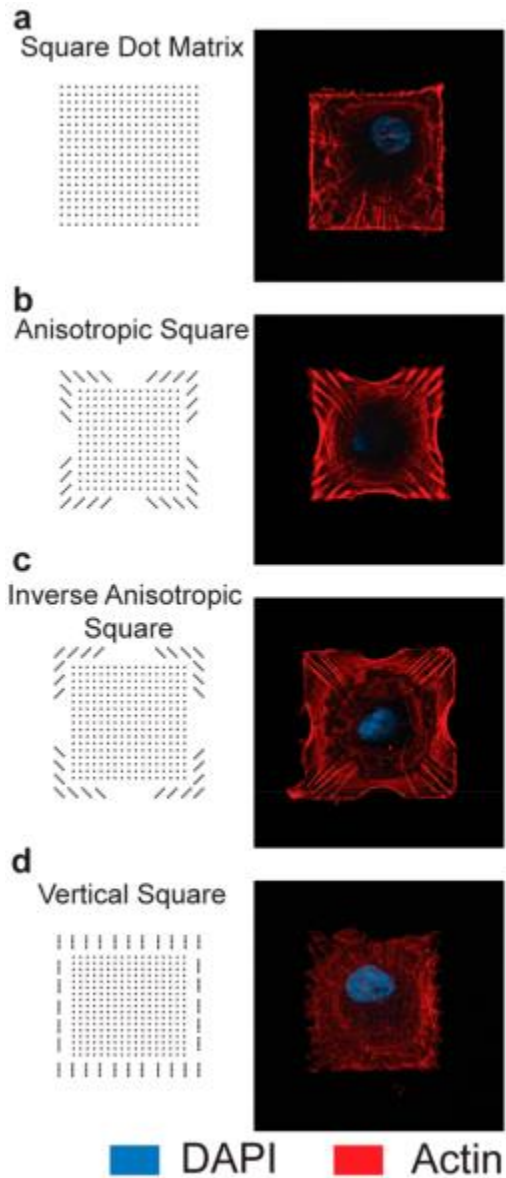


**Figure 1.6.** (a-d) MHA-fibronectin dot pattern designs on the left and representative fluorescence micrographs of the actin cytoskeleton in human mesenchymal stem cells seeded on each pattern (right).<sup>15</sup>

Another revolutionary ink to be used in CF-SPL was block copolymer-based inks, incorporating a method called scanning probe block copolymer lithography (SPBCL).<sup>16</sup> In this

case, for the first time polymers are used not solely as a viscous transport solution but as individual nanoreactors that can serve to synthesize inorganic nanoparticles. This work has been developed beyond only single nanoparticles, but has proven most interesting for patterning multi-metallic nanoparticles made of up to 10 distinct elements.<sup>17-19</sup> Using SPBCL in conjunction with a CF-SPL tool like PPL enables the rapid discovery of multimetallic nanoparticles for a wide variety of applications spanning electrocatalysis and plasmonics.

In the realm of architectural advancements of CF-SPL, which is the primary focus of this thesis, only limited progress has been made. In 2011, hard-tip, soft-spring lithography (HSL) was developed as a follow-up to PPL, in a major advancement towards increased resolution.<sup>20</sup> In this technique, the elastomer backing layer remains, but the pyramidal tips are replaced with hard silicon ones, in order to achieve consistently high resolution, but continue to take advantage of the elastomer backing layer as the deformable "cantilever." However, this method has very rarely been utilized because of the complex and difficult pen array fabrication process.

In order to compromise between fabrication complexity and feature size resolution, hard transparent arrays were developed for PPL in 2016.<sup>21</sup> In this work, a typical elastomeric PPL array is fabricated, and then it is coated with a thin (~175 nm) silica layer, in order to demonstrate a force-independent contact area with minimum feature sizes down to ~40 nm, and minimal pen-to-pen variation (**Figure 1.7**).

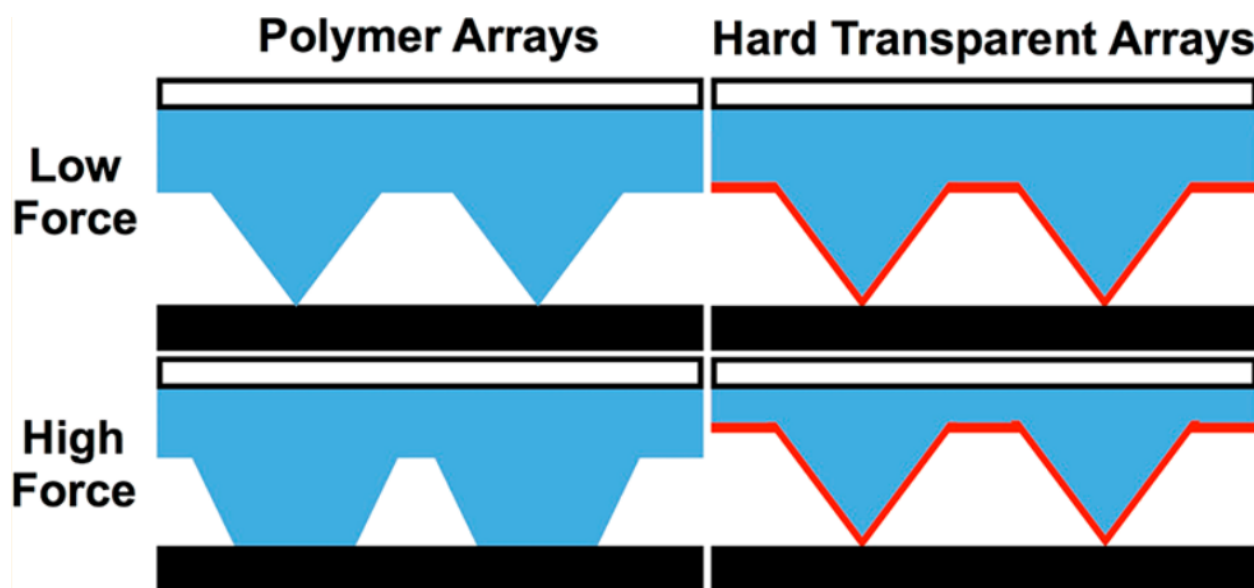


**Figure 1.7.** Hard transparent arrays use a thin silica coating in order to reduce minimum feature size and keep pen-to-pen variation minimal by redistributing the force to the backing layer rather than the tips.<sup>21</sup>

Other CF-SPL modifications and variations include changing the PDMS material to include PEG such that they absorb water better and patterning is not affected by environmental humidity. Also, other polymers besides PDMS have been explored, and often PPL has seen the use of two elastomers of different moduli, such that the pens are stiffer than the backing layer material. In this way, the dependence of feature size on force is minimized, especially among the pens. In 2012, a new method of CF-SPL was developed by coating the probe arrays with multilayer graphene.<sup>22</sup> In this way, the tips not only become more resistant to wear, but also bring about high electrical and thermal conductivities, potentially making way towards electrochemical or thermal CF-SPL. This method shows promise for novel CF-SPL patterning methods but requires complex fabrication and post-processing steps. In addition, a few methods

have been presented for independently actuated pen architectures, but they have not yet been fully realized, as will be described in Chapter 5.

Finally, perhaps the greatest architectural advancement thus far to CF-SPL is beam pen lithography (BPL).<sup>23,24</sup> This approach uses the very same elastomeric pen arrays as in PPL, but this time coated with an opaque, typically metal thin film with apertures etched out of the apex of each pyramidal pen (**Figure 1.8**). This pen array is then combined with a digital micromirror device (DMD) and a light source, such that photolithography can be performed through each individual aperture at each tip independently of one another. If the apertures are etched with a high enough degree of resolution, this may even lead to subwavelength patterning entering the near-field regime. This method is particularly powerful because it not only provides the potential for diffraction unlimited photolithography, but also arbitrary photo-patterning across a single substrate within environmental conditions. Some have also done this without an aperture, in particular by using a high-refractive index material.<sup>25</sup> One notable advancement in the BPL architecture has been observed using microfluidic channels to flow different chemical reagents onto a substrate without ever replacing the array, thus enabling multicomponent structural printing, such as for brush copolymers.<sup>26-28</sup>

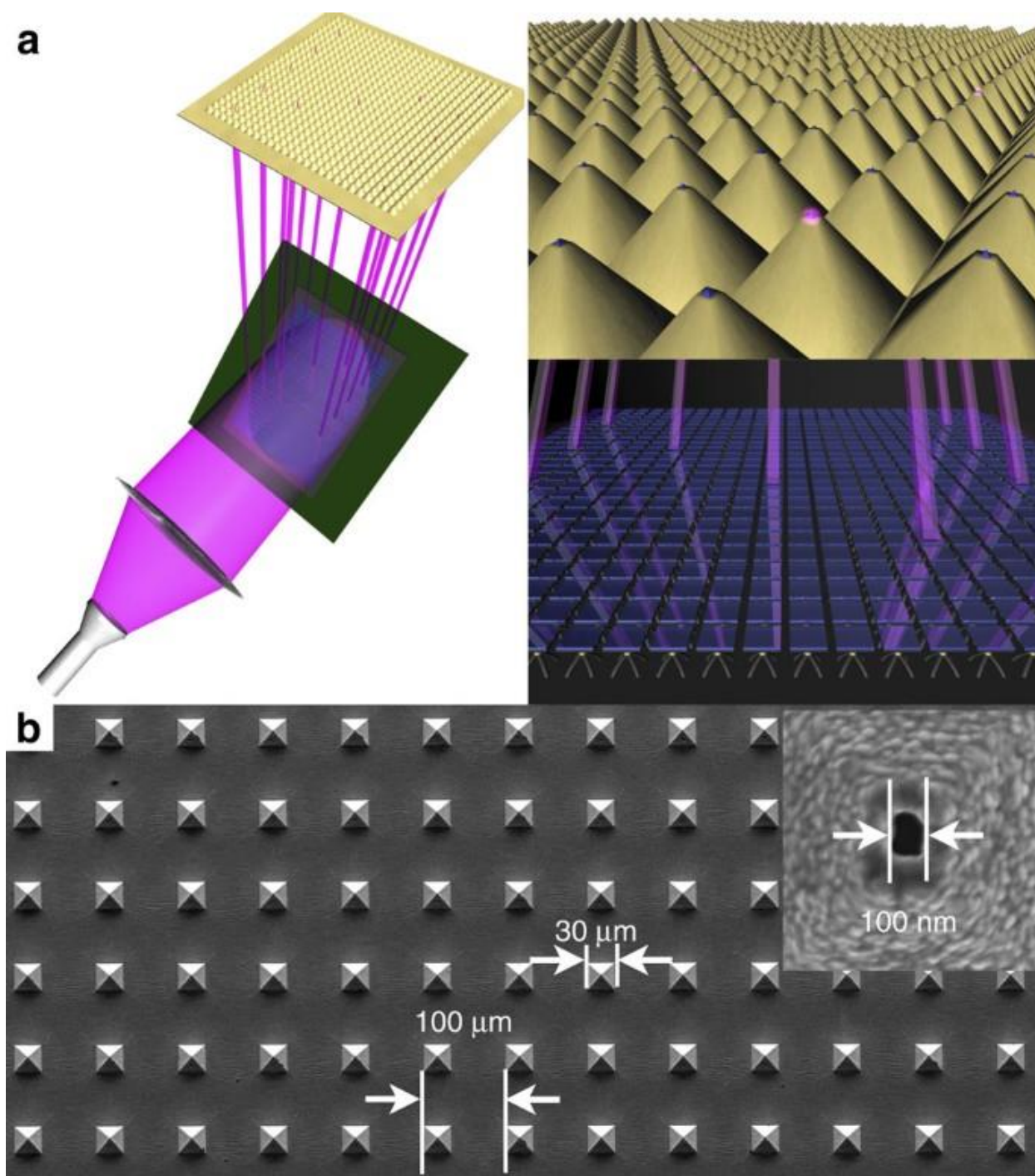


**Figure 1.8.** (a) Beam pen lithography (BPL) uses a digital micromirror device (DMD) to individually actuate pens in a pen array. (b) These pens are coated with an opaque (typically Au) thin film, and etched at each tip using either focused ion beam, photolithography, or mask-

enabled etching processes, such that small, subwavelength apertures allow light to penetrate to the material that is being patterned.<sup>24</sup>

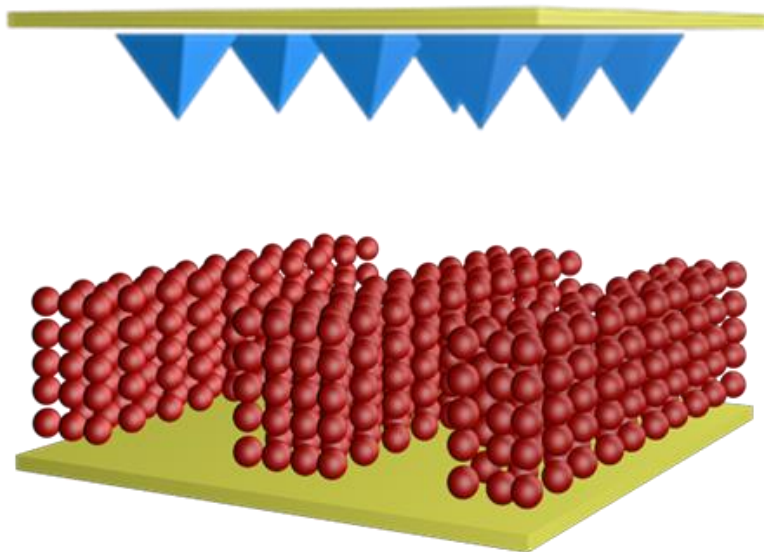
### **1.3 Future Outlook of CF-SPL**

CF-SPL shows promise in more ways than one. What remains is to fully develop the remaining technologies needed to maximize its usage and demonstrate that potential to the global scientific community. Not only does CF-SPL show promise in nanocombinatorics and materials discovery, which will perhaps be the most significant challenge to materials scientists over the next several decades, but also provides new ways to quickly prototype and manufacture nanoparticles, microstructures, cellular assays, and more from a desktop nanofabrication environment, in (typically) ambient conditions and with little to no post-processing required.

Developments like SPBCL will propel the use of CF-SPL as an essential tool for materials discovery of multimetallic nanoparticles, especially for catalysis and plasmonics. Meanwhile, architectural advancements like HSL and hard transparent arrays will continue to improve the tool. Pursuits of individual actuation are ongoing by several groups, including in this thesis, and with that next hurdle will come a wide avenue of opportunities for single-substrate analysis and highly flexible patterning, prototyping, and printing that is unparalleled by any other high-throughput lithography tool. At the same time, actuated BPL, while materials-limited by photo-sensitive materials, already provides this advantage and continues to be a projected route not only for rapid high-throughput near-field photolithography, but also nanoscale 3D printing by integrating the printing with an aqueous environment and using the tool in a manner similar to stereolithography.



**CHAPTER TWO:  
NEGATIVE POLYMER PEN LITHOGRAPHY**



## 2.1 Introduction

Colloidal nanomaterial assemblies are promising for applications in many fields including electronics, optics, catalysis, or magnetism due to their structure-induced unique optical, electronic, magnetic and catalytic properties.<sup>29,30</sup> Many different tools such as wet-chemistry methods and top-down lithography methods have been developed to synthesize and pattern these nanoscale building blocks with controlled size, shape and composition.<sup>29</sup> Bottom-up approaches, or the assembly of nano-sized building blocks into hierarchical structures have proven to be powerful tools in controlling the structural parameters of a final assembly. Well-developed assembly approaches include interface/template-assisted, field-induced, diffusion-controlled, and ligand-directed strategies.<sup>31-33</sup> Among them, DNA-mediated assembly is powerful because of independent control over the nanoparticle core and DNA bonds. Size, shape and composition of cores can be tuned to achieve different functionalities,<sup>34,35</sup> while DNA bonds can be adjusted to change length, strength and selectivity of colloidal crystals, making DNA-mediated assembly a truly versatile and highly valuable functional assembly technique.

New avenues for integration of colloidal crystals into functional devices were opened up upon the introduction of step-wise DNA-mediated assembly.<sup>36</sup> It has been demonstrated that DNA-mediated assembly combined with top-down e-beam lithography could enable DNA-density changes on a surface, otherwise using gold posts as the first layer, or trenches on the surface to build anisotropic hierarchical structures.<sup>37,38</sup> However, e-beam lithography is time-consuming and intrinsically low-throughput. DNA-mediated assembly can be also integrated with photopatterning approaches to achieve patterns *via* azoDNA-connected NP assemblies, where light-induced photoisomerization of azobenzene molecules can be used to control the

opening and closing of DNA bonds between nanoparticle building blocks to selectively remove unwanted nanoparticles. However, this approach requires specifically designed azobenzene-modified DNA rather than unmodified DNA with random sequences. Moreover, it is still challenging to achieve massive parallel patterning of colloidal nanomaterials on surfaces into pre-designed shapes.

CF-SPL provides us with a powerful approach to pattern nanoscale features on surface in a massive parallel manner.<sup>14</sup> PPL pen arrays were fabricated using conventional photolithography methods. Each pen array consists of thousands of tips which can be used to print nanomaterials on surfaces. Feature size is highly dependent on a few critical parameters including humidity, ink viscosity, applied force and dwelling time.<sup>9</sup> Although quite powerful, there are few reports of using polymer pen to remove, either chemically or physically, material from surfaces or to construct hierarchical structures, which can be powerful in integrating multi-compositional materials into one surface to achieve multi-functionality.

## 2.2 Results and Discussion

In this chapter, I describe a method for creating hierarchical patterns of colloidal nanomaterials by combining DNA-mediated surface assembly with the PPL architecture, which can be used to selectively remove unwanted nanoparticles post-assembly. This method is hereafter called “negative polymer pen lithography”, or n-PPL. Substrate preparation, DNA-NP stepwise growth preparation, and the broad patterning process are schematically represented in **Figure 2.1**. First, a commercially available centimeter-scale Si wafer is coated with a uniform thin film of 8 nm Au (with 2 nm Cr as an adhesion layer) using e-beam evaporation. Second, the as-prepared Au-Si substrate is immersed in an anchor DNA solution at 0.5 M NaCl overnight to

functionalize the surface with a dense layer of DNA strands *via* gold-thiol bonds. Third, programmable atom equivalents (PAEs) with DNA linkers complementary to the anchor DNA on substrate are added to the solution and gradually attach to the substrate *via* DNA hybridization. PAE solutions are prepared by first functionalizing spherical gold nanoparticles with thiol DNA strands and then attaching linker strands. Then, the PAE monolayer is agitatedly rinsed in buffer solutions for three rounds to remove physically adsorbed materials.

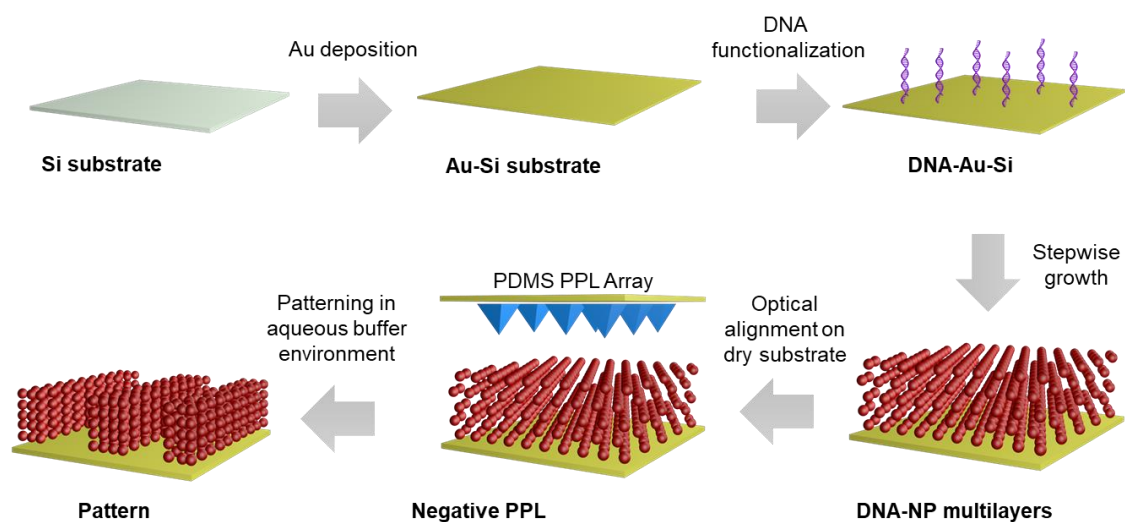


**Figure 2.1.** Substrate and nanoparticle multilayer preparation and patterning process are schematically illustrated.

Stepwise growth is applied to assemble PAEs into multi-layer assemblies on surfaces. The Au deposition and DNA functionalization of the substrate steps are similar to the aforementioned monolayer sample preparation. However, instead of using one type of PAE to generate a monolayer, two complementary PAEs (type A and B) are adopted to grow multiple layers on surfaces. The first layer is composed of type B PAEs since the DNA strands on the substrate are complementary to the type B linkers. The second layer can be grown by transferring the

monolayer sample into type A PAE solutions, since the type A PAEs can grow on top of the type B PAE monolayer. By alternating type A and type B PAE solutions, one can achieve multilayer PAE assemblies with highly controlled thickness. Throughout this work, a five-layer PAE assembly is adopted as a proof-of-concept.

A polymer pen array is optically aligned to a non-treated Si wafer in air. The heights and substrate features are ensured to be consistent between this sample wafer and the actual substrate. Once the stage and pen array are aligned, the dry wafer is replaced by the prepared substrate, and covered, immediately, with 0.5 M NaCl buffer solution. The pen arrays are brought into contact with the array as usual and patterning occurs within the aqueous environment. The major challenge here is to ensure that the pens are in contact with the substrate, but not too much. This is easily determined by using the z-extension distance of the aforementioned dry sample as a reference, then visualizing a slight color change at the tip of each polymer pen as soon as contact (and material removal) occurs. The array is rinsed with ethanol for three rounds and then dried in air before and after each use. The force applied by the piezo causes the PAEs to be disrupted and moved where there is contact. Moving the pen array across the substrate creates negative line features, and pressing once creates negative point features. In this way, one can easily “carve out” the desired pattern for the hierarchical structures.

The pen array used in these experiments is shown in **Figure 2.2a**. With it, cm-scale areas of DNA-mediated nanoparticle assemblies were negatively patterned and imaged, as shown in **Figures 2.2b** and **c**. Samples were embedded in silica using a sol-gel process to transfer into solid state prior to scanning electron microscope (SEM) characterization. High-resolution SEM images of the pattern reveal that PAE particles were pushed to the side of the feature, due to a

steric hindrance caused by the PDMS tip once in contact with the substrate (**Figure 2.2d**). The resulting feature size is tunable and can be as small as  $\sim 500$  nm.

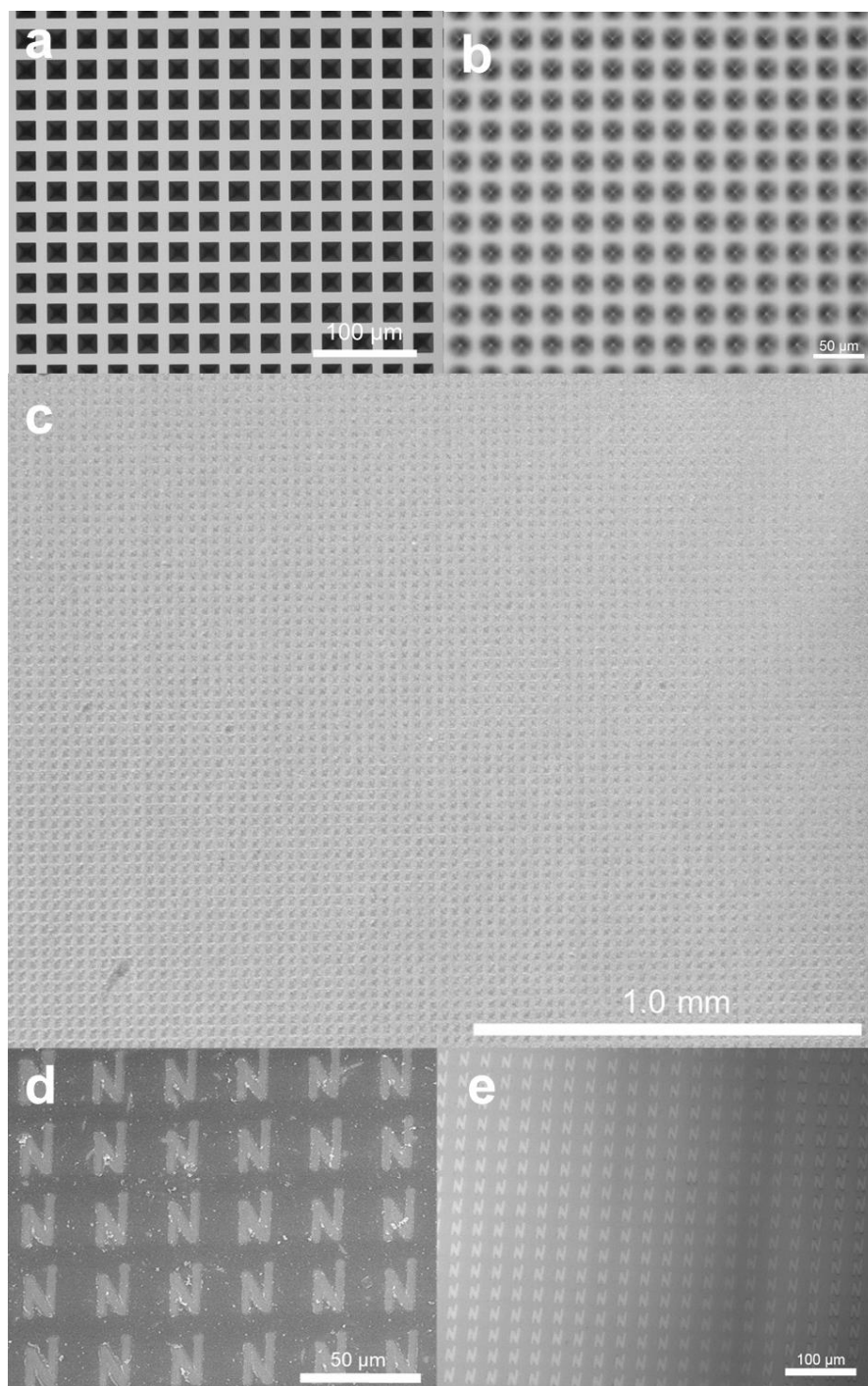


**Figure 2.2.** (a) A 30  $\mu\text{m}$ -pitch polydimethylsiloxane (PDMS) PPL array, as seen by optical microscope, with sharp tips, as observed in (b), was used to negatively pattern “N” shapes from a DNA-mediated nanoparticle assembly. The sample was then embedded in silica to observe in the solid state under a scanning electron microscope (SEM) (c, d), where the localized removal of programmable atom equivalents (PAEs) is apparent. The non-silica-embedded sample was imaged using optical microscopy in water as well (e).

One significant advantage of PPL is its ability to control feature dimensions with relative precision, as well as creating gradients of feature sizes and compositions over a single surface. Herein, we adapt the PPL technique to be a negative lithography method for DNA-mediated assemblies, and as such we must adapt the precision resolution and spatial control afforded to us by PPL. By aligning our substrate with the pen array, then tilting the patterning stage at various angles, we are able to create a gradient of variable z-piezo distances (and therefore variable applied force) across a single substrate. It was found that the piezo distance significantly affects feature size, as in PPL, and the feature dimensions can be plotted against z-distance in a linear fashion (**Figure 2.3a**). SEM images of silica-embedded patterned dot features of DNA assemblies are shown as a representation of each point on the plot. A unique advantage of n-PPL is its capability to move beyond single point features and create line features with ease, a task that has proven challenging with conventional PPL. The line features' width can also be precisely controlled by varying z-distance, which is shown in **Figure 2.3b** using a tilt pattern once again. Again, SEM images of silica-embedded patterned line features are highlighted within the plot. Feature dimensions can be controlled from 200 nm up to 4  $\mu\text{m}$ , as observed thus far.

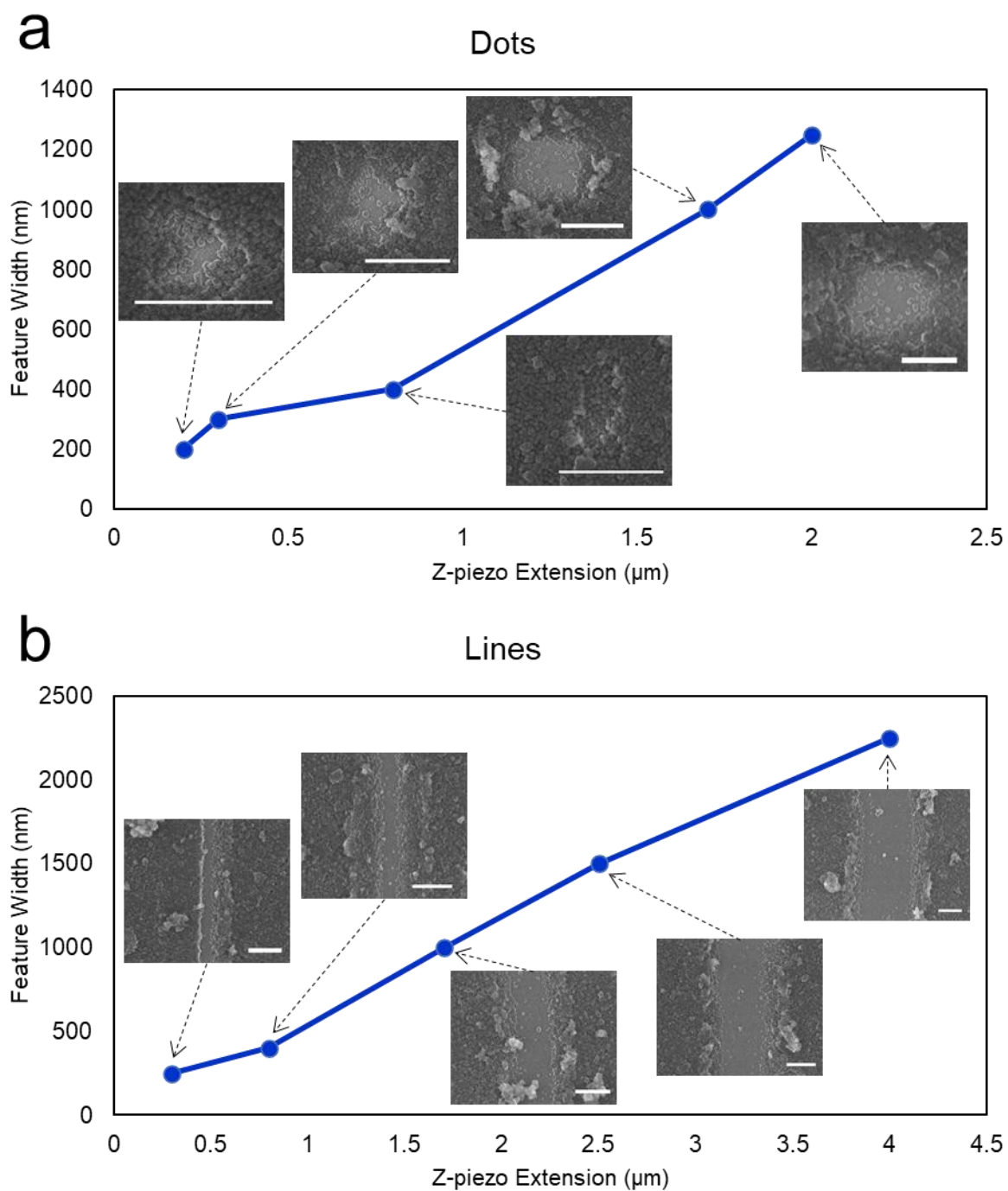


**Figure 2.3.** Tilting the stage during patterning creates a gradient feature size in both point (a) and line (b) features across a single substrate. These dimensions are plotted against calculated z-

distance in order to provide size control during patterning from 200 nm to 4  $\mu\text{m}$ . Scale bars = 1  $\mu\text{m}$ .

In order to fully understand how the nanoparticles are being removed at each patterning location, a series of experiments was performed where features were backfilled with different molecules to observe which would bond to the bare surface created by patterning. The results of these experiments can be seen in **Figure 2.4a-c**. First, a typical pattern was made without backfilling, then it was silica-embedded and imaged using SEM (**Figure 2.4a**). Then the same pattern was repeated on an identical substrate, this time backfilled with type A PAE alone, and it was again silica-embedded and image. And lastly the same pattern was repeated once more, but this time backfilled with type A linker along with type A PAE. It became apparent from these experiments that thiolated DNA and linker DNA remain intact on the substrate during the patterning process. What seems to be destroyed is the bond between the hybridized sticky ends between linkers, which is to be expected, as they have the weakest bonds within the system.

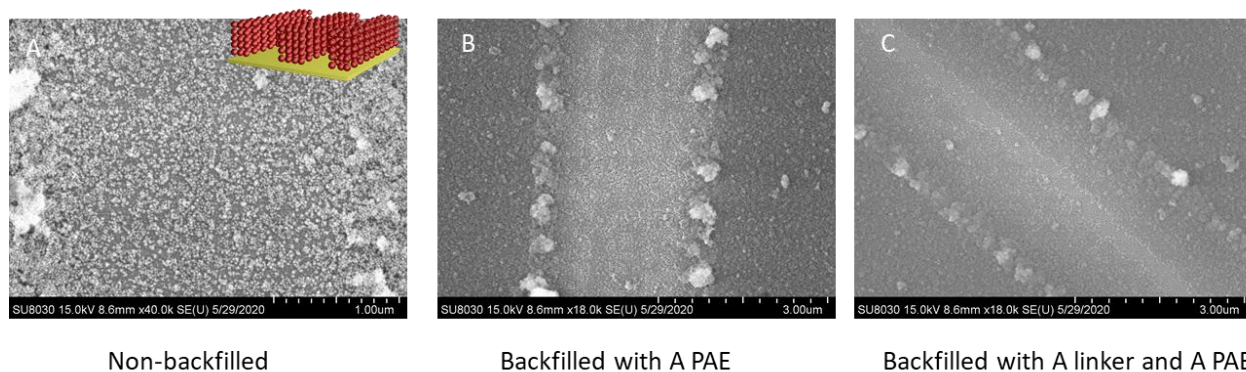


**Figure 2.4.** Patterns were successfully backfilled with new PAEs.

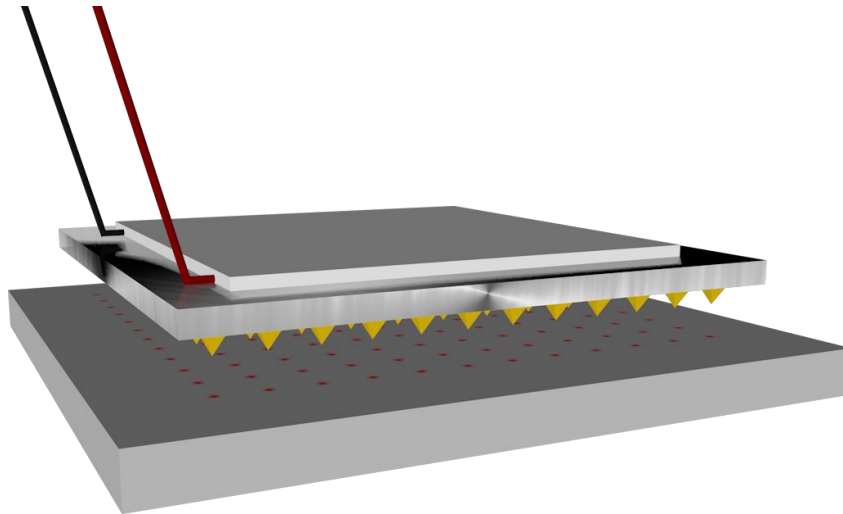
This set of experiments not only serves to better understand the bond-breaking that is occurring during n-PPL, but also demonstrates the potential for this technique to be used for multi-compositional hierarchical DNA-mediated lithography. By backfilling with complementary linkers attached to nanoparticles of different size or composition, one could feasibly create heterogeneous surfaces with relative ease. In fact, because the patterning is done in a fluid system, this could even be done in a single step, which is unprecedented. By flowing a new linker-NP solution across the substrate after each patterning step, several different NPs could be patterned in precise geometries across a single substrate, all in under a few hours, and done without any vacuum, high-temperature, or clean-room setup. Thus, complex, functionalized 3D nanostructures could be built within a few days with minimal laboratory requirements.

### 2.3 Conclusions

In summary, I have demonstrated a proof-of-concept example combining DNA-mediated assembly and polymer pen printing techniques to fabricate hierarchical structures out of colloidal nanomaterials on surfaces. In contrast to the conventional working principle of PPL where inks are coated onto the polymer tips and transferred to surfaces to form nanoscale features, we take advantages of the mechanical forces induced by polymer pen arrays to selectively remove unwanted DNA-functionalized nanoparticles on surfaces. Remarkably, centimeter scale patterns of colloidal assemblies with nanoscale features were successfully achieved using this approach. In fact, it was remarkably facile to reproduce different images, especially with line features, as shown in the "N" pattern in **Figure 2.2**. Since DNA-mediated assembly is expandable to many hard and soft colloidal nanomaterials, this approach opens up new avenues for generating

complex structures with both high-throughput and nanoscale resolution, and can be applied to build next-generation optical, catalytic and biological functional devices.

**CHAPTER THREE:**  
**THERMAL POLYMER PEN LITHOGRAPHY**



### 3.1 Introduction

Thermal energy is a universal stimulus for material conversion, being used to trigger chemical or physical reactions in virtually any material. When this concept is brought to nanoscale volumes of material, only very short bursts (nano to microseconds) of heat are required. These qualities have lent materials heating to be used in conjunction with scanning probe lithography to rapidly cure, evaporate, melt, or otherwise change material at the nanoscale.<sup>39,40</sup> By heating a scanning probe tip (typically through resistive heating), highly precise patterning may be achieved with resolution otherwise unseen. This technique is called thermal scanning probe lithography, or t-SPL (**Figure 3.1**).<sup>41</sup>

t-SPL was first introduced in 1992 by the IBM Research Laboratories, where a typical AFM cantilever was heated using a laser in order to create indents in a polymeric thin film.<sup>42</sup> The resistive heaters came soon after that, where a voltage bias is applied across a cantilever in order to induce heat. These resistive heaters are typically incorporated just above the tip of the cantilever, and they enable ultra-fast heating and cooling due to their small size. At this point, t-SPL can be broadly divided into two patterning methods: energy deposition or materials deposition. In energy deposition, heat is transferred to an existing inked substrate, such that the material is being locally modified, either physically (melting, evaporating) or chemically. In materials deposition, the ink is pre-existing either on the tip or in the patterning chamber as a gas. The heated tip is typically then used to melt the material from the tip to the substrate or *via* CVD from a precursor material.<sup>39,40</sup>

One of the most significant challenges to the broad, commercial usage of t-SPL is its limited throughput. Efforts have been made to increase this throughput, with 10 probes in a row,

or the "Millipede project" at IBM, where parallel arrays of up to 4096 independently -controlled thermal cantilevers were developed for the use of reading/writing data.<sup>43,44</sup> In addition, the Mirkin group demonstrated one architectural advancement of PPL that turned it into a thermal heating array using a graphene coating (see Chapter 1), but this technique is complex and has inconsistencies when patterning.<sup>22</sup>

In order to broaden the capabilities of t-SPL, here I have developed a simple to fabricate, inexpensive, and easily reproducible massively parallel cantilever-free thermal scanning probe lithography tool called thermal polymer pen lithography, or t-PPL. This method uses the existing elastomer array and architectural platform of PPL in conjunction with conductive metal backing layer and coating, as well as a commercially available ceramic heater in order to induce localized thermal transfer over the scale of millions of pens at a time.

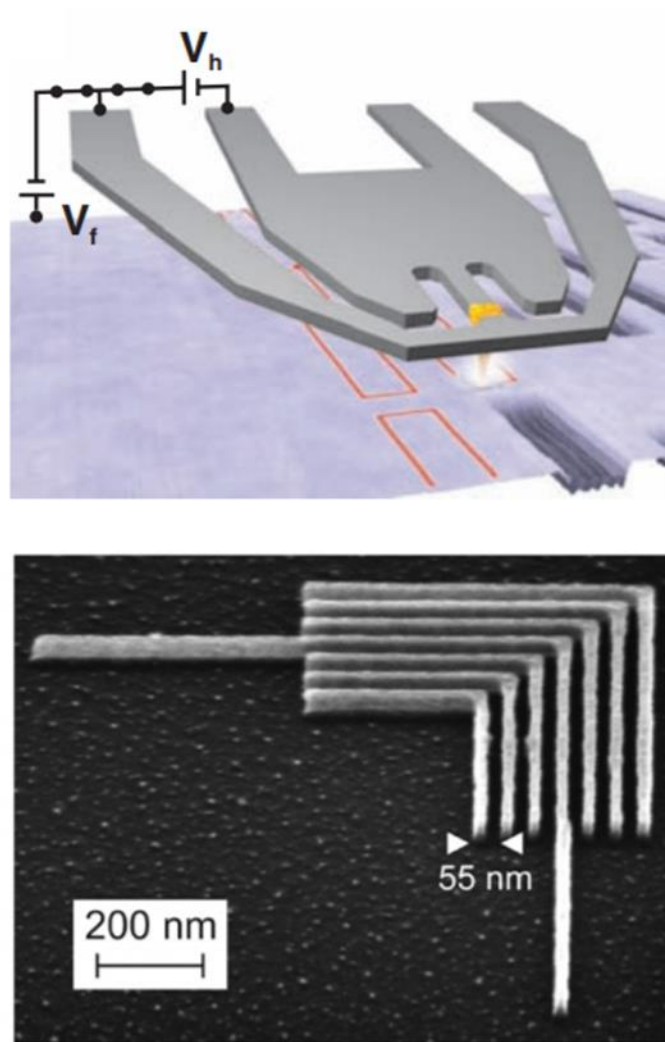


**Figure 3.1.** Schematic of thermal scanning probe lithography (above) and its capability (below) for ultra-high-resolution, spatially-precise patterning of silicon using a thermal resist (poly(phthalaldehyde)).<sup>41</sup>

### 3.2 t-PPL Development and Technology

In order to make the technology easy to fabricate, compatible with existing commercially-available CF-SPL platforms, and inexpensive, only straight-forward design changes were made to the PPL architecture to develop t-PPL (**Figure 3.2**). This includes the use

of a 24 W ceramic heater that operates on a simple applied voltage, with temperature control up to 400 °C. The pen array was fabricated using the common photolithography fabrication methods described elsewhere, using PDMS,<sup>10</sup> but using an aluminum plate as the backing layer, rather than glass. The aluminum plate is thoroughly polished and cleaned with ethanol and water, then plasma-cleaned in order to increase oxide presence for PDMS-adhesion. The aluminum plate enables rapid thermal transfer from the heater to the pen array. The PDMS array is then cured onto the aluminum plate and coated with 100 nm Au using an e-beam evaporator. This coating will not only sharpen the tips and provide higher resolution patterns with more consistent pen-to-pen variation, but it also provides a thermally conductive layer for rapid heat transfer. The coating is deposited with a mask that is compatible with TERA-print instruments for electrical alignment. Finally, the ceramic heater is adhered to the backing layer directly using polyimide tape. The tape is placed over the heater and plate such that it also thermally insulates the piezos and pen array holder from the direct heat of the heater. Electrical leads from the heater are connected to a power source with alligator clips.

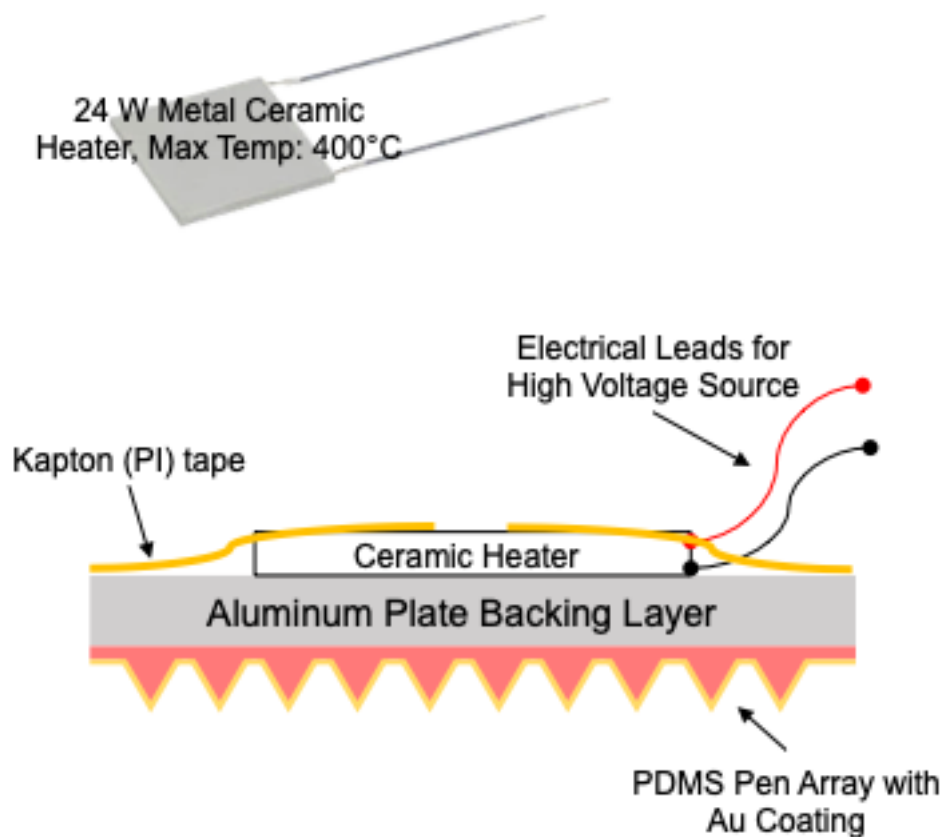


**Figure 3.2.** Schematic of thermal PPL (t-PPL) pen array. The PDMS PPL array is affixed to an aluminum plate, serving as the backing layer, then coated with a thin film of Au in order to provide more efficient thermal conduction while also enhancing resolution consistency. A ceramic heater is adhered to a PPL array using polyimide tape (thermally resistant) for easy replacement while also providing insulation for instrument safety.

This pen array is finally loaded into a TERA-fab M-series instrument used for CF-SPL (**Figure 3.3**), where the array holder is made from PEEK (polyether ether ketone), which has a high melting point and glass transition temperature (343 and 143 °C, respectively), such that the

radiative and conductive heat from the array does not affect it. The pen arrays are then brought into contact with the surface of a sample substrate (not the desired substrate) that is either electrically conductive or has been given a deposited border of Au for electrical conductivity. In this way, the Au coating of the pen array can be used alongside the metal of the substrate to perform alignment by electrical contact, as well as contact point detection. The substrate is often placed atop a thermal sink in order to minimize thermal damage to the instrument while also improving the cooling speed.

Alignment and contact point detection is performed after the pen array has reached the desired temperature, largely because of thermal expansion of the PDMS. As has been well-documented, PDMS expands significantly with heat. However, rather than attempt to fight against that, I chose to embrace that expansion and make sure any and all expansion has been allowed to occur by leaving the hot (or warm) pen array to equilibrate its size before performing levelling. One drawback of this method is that because heating is slightly uneven between the center and edges of the pen array, there tends to be a bowing effect. This can be mitigated in the future by re-arranging the heaters into four smaller heaters working in parallel. In order to determine the damage to the Au coating after heating and PDMS expansion, the pen arrays were imaged in SEM both before and after patterning, and it was found that while some cracks occurred after very high temperature ( $>250$  °C), the thin film remained largely intact.

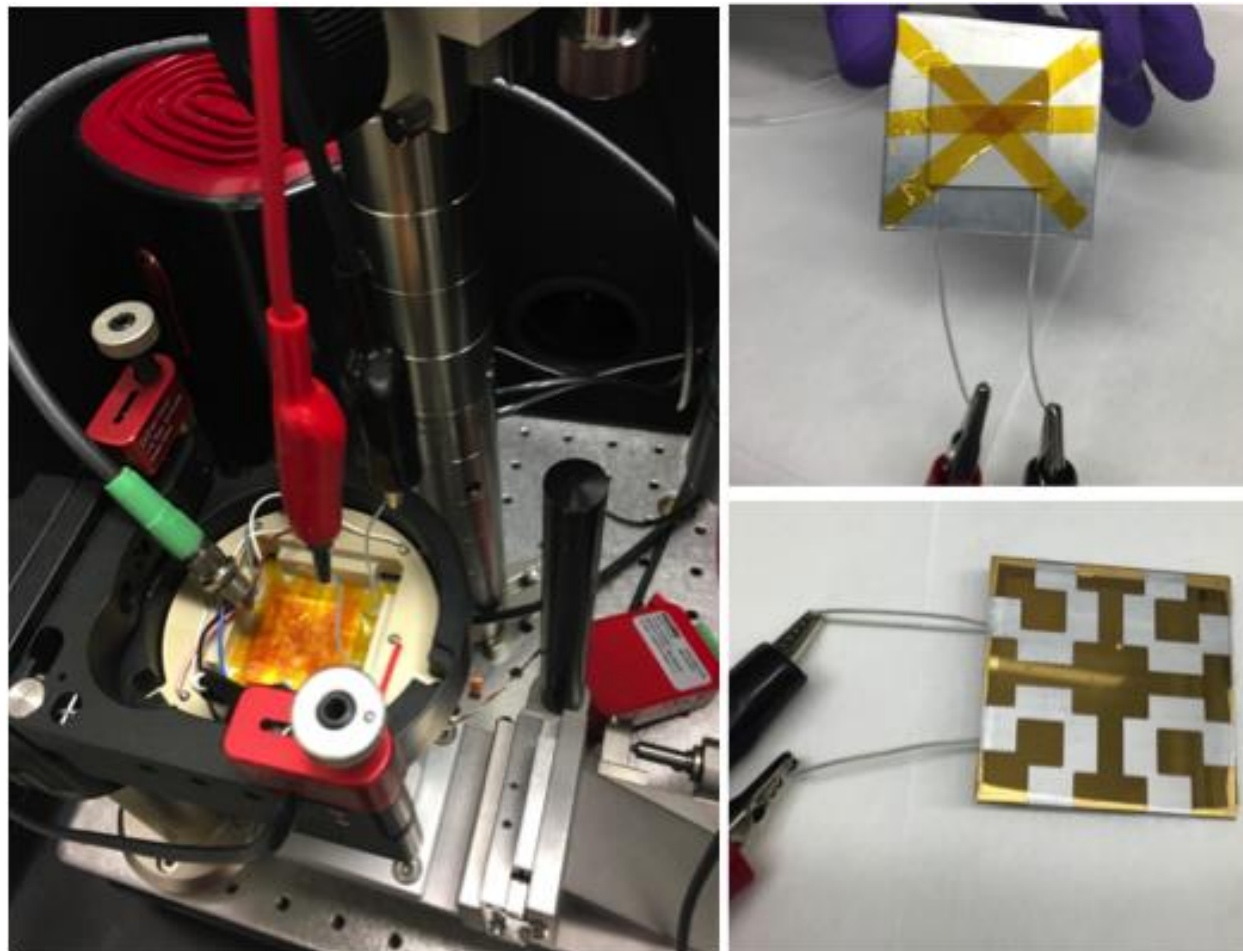


**Figure 3.3.** Images of pen array loaded into TERA-fab M-series instrument for patterning (left) and t-PPL pen array (right).

Alignment and contact point detection is done using the TERA-fab software, which uses applied bias and current detection to determine contact between the gold coating and the conductive edges of the substrate. After this has been performed with a sample (in order to mitigate levelling marks on the final substrate), the sample is replaced with the final substrate, and patterning occurs. The pen array is brought down into contact with the substrate, and when done, it is lifted off above the substrate a few inches. This step should be done quickly such that

radiative heating does not affect the patterning process, especially when dealing with an energy - transfer mode of t-PPL.

Much like t-SPL, t-PPL can be used in either energy-transfer mode or materials-transfer mode. In order to demonstrate both uses, first energy transfer was performed using an image-reversal photoresist (AZ 5214E). The processing of this photoresist importantly includes a crucial heating step at 110 °C, where after UV-exposure, the resist is crosslinked. Without the heating step, the crosslinking does not occur. So, a Si wafer was spin-coated with this photoresist, and flood-exposed with the requisite UV light. The exposed resist was then patterned with t-PPL to locally crosslink the resist. The entire wafer was then washed thoroughly with acetone to remove the un-crosslinked resist. The resultant features were imaged with optical microscopy (**Figure 3.4**), and measured with a profilometer, and determined to be ~10 μm tall features with ~5 μm width. These preliminary experiments demonstrate the ability of this technique to locally affect the thermal chemistry of a material with ultra-high-throughput that is unprecedented.

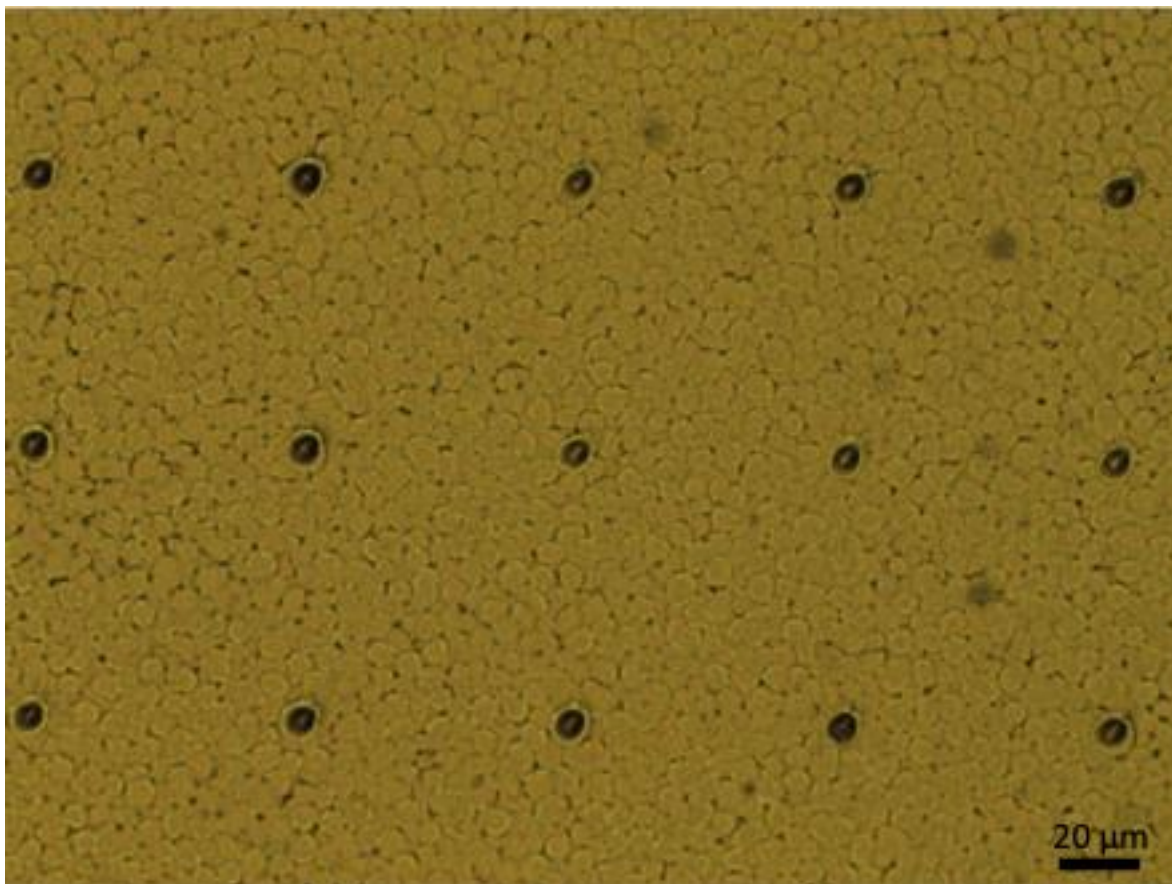


**Figure 3.4.** t-PPL delivers localized heat at each tip location. Using an image-reversal photoresist (AZ 5214E), where a crosslinking agent in the resist formulation activates at temperatures above 110 °C, areas of a photoresist were selectively crosslinked using t-PPL.

The energy-transfer mode presents a unique potential for high-throughput nanoscale 3D printing of metals, semiconductors, or polymeric resists. An arguably more interesting method of printing is by so-called materials-transfer or melt printing. In order to investigate this further, gelatin methacryloyl (gelMA) was used due to its reversible thermal gelation that can be thermally crosslinked through photopolymerization. This material has been widely used for 3D printing of tissue constructs and cell adhesion. Due to its high water content, small molecule

permeability, biocompatible nature, and its integrin-binding sites, gelMA adheres encapsulates and adheres to cells exceptionally well. Thus, developing a way to rapidly 3D print gelMA for tissue engineering and cell assays over large areas with high-throughput will enable many avenues of research to be explored more rapidly than ever before.

To that end, warm (60 °C) gelMA is spin-coated onto a t-PPL array in order to coat the pens, and then it is allowed to cool to room temperature (**Figure 3.5**). These pens are then warmed to 60 °C and brought into contact with a Si substrate in order to pattern small features.

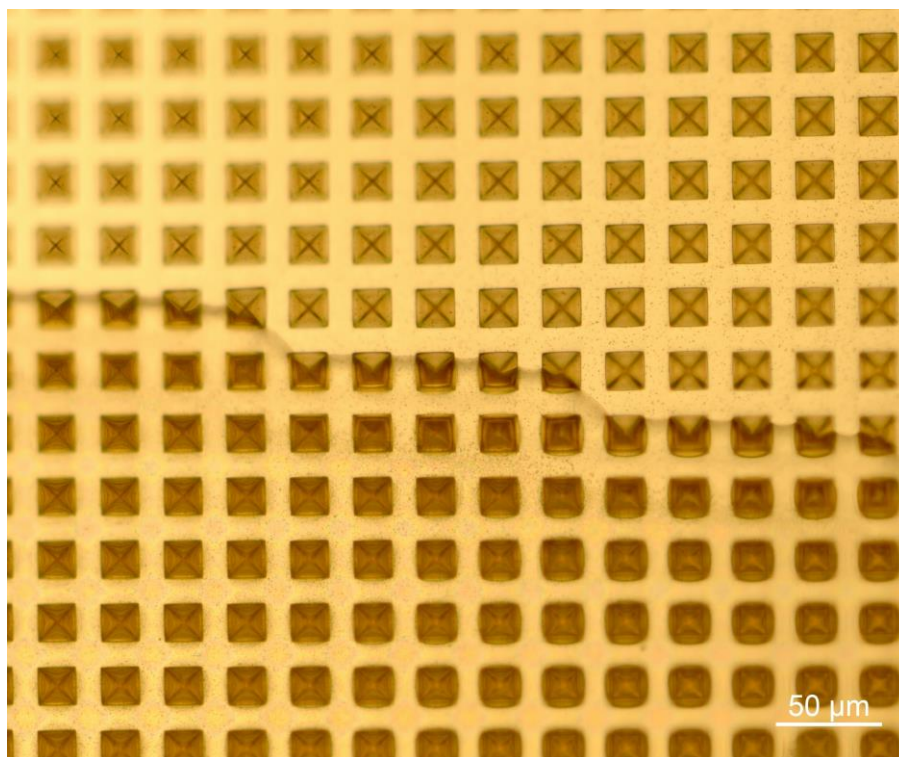


**Figure 3.5.** t-PPL tips coated (top half) with gelatin methacryloyl (GelMA), ready to be patterned.

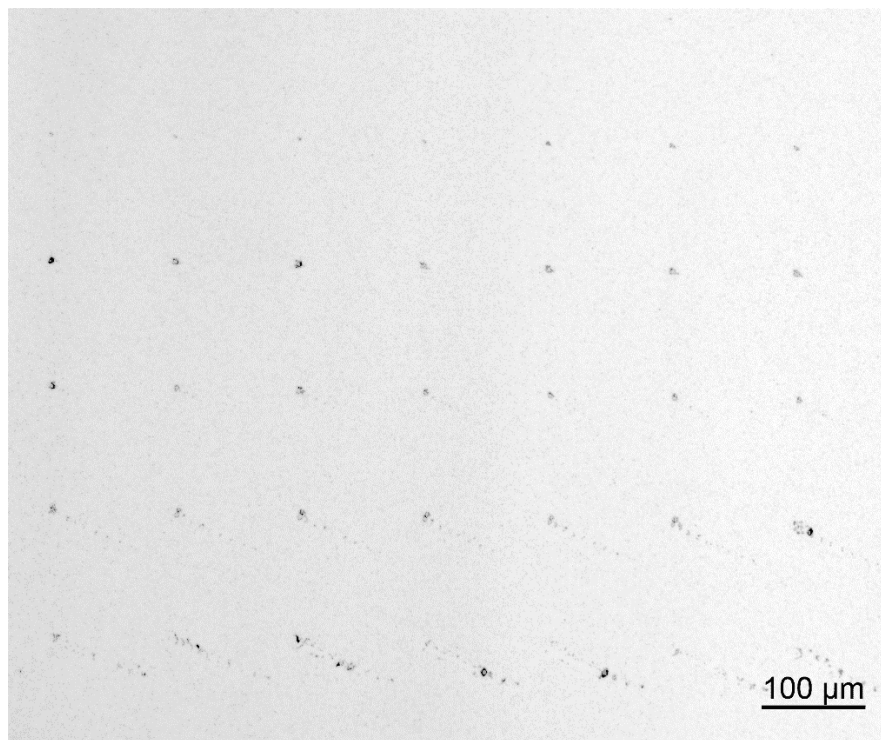


**Figure 3.6.** Patterned GelMA features on an Si substrate, as seen under an optical microscope.

After lift-off, the resulting pattern was imaged using an optical microscope (**Figure 3.6**). This especially took trial-and-error, due to the finicky nature of precision viscosity of the gelMA. It must be just warmed enough to flow off the pens, while not being so warm that pools of hydrogel are deposited onto the substrate. This hydrogel can be combined with a photoinitiator and flood-exposed after patterning in order to permanently crosslink the gel into the desired morphology. Then, the patterned hydrogel may be used for cell assays and tissue engineering with high-throughput.

### 3.3 Conclusions and Future Outlook

To summarize, t-PPL has been developed in such a way that ultra-high-throughput patterns may be synthesized with the precision and resolution and unique materials-versatility of

t-SPL, while also opening avenues for high-throughput nanoscale 3D printing. The pen array fabrication process is inexpensive and facile, and the patterning method uses the commercially - available TERA-fab instrument, providing the technology another head-start. Here, I have described two methods of patterning with these pen arrays, energy-transfer: patterning a deposited thermally-activated resist with hot probes, and materials-transfer: flowing a viscous hydrogel off the tips by reducing viscosity with heated (or warmed) probes.

The technology not only offers exciting potential for high-throughput 3D nanoprining and even tissue engineering and cell-assays, but also could be used to deposit nanoparticles. In one work, for example, the materials-transfer mode of t-SPL was used to flow a polymer-nanoparticle (PMMA and  $\text{Fe}_3\text{O}_4$ ) composite off of heated tips onto a substrate, then etching the polymer off with an additional plasma cleaning step (**Figure 3.7**).<sup>45</sup> This method enables the printing of single nanoparticles as well as arbitrary lines and morphologies of clustered nanoparticles, making it an ideal method for printing in electronics, especially in circuit design or repair. This can be theoretically expanded to many pre-prepared polymer-nanoparticle composite inks as well, and it may even be expanded to perform in the z-direction, such that 3-dimensional nanoparticle colloidal structures can be generated with ease and high-throughput.

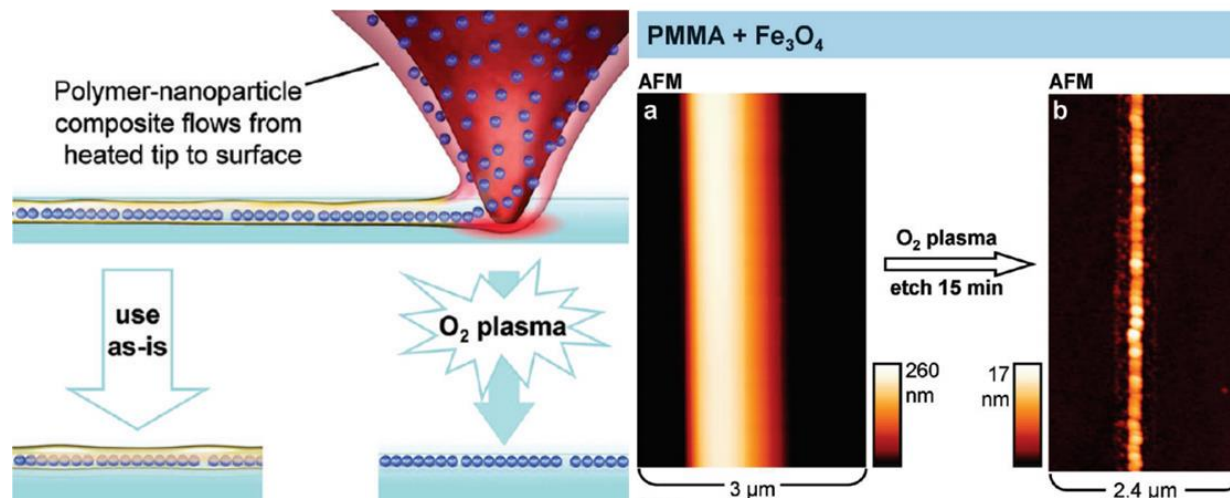
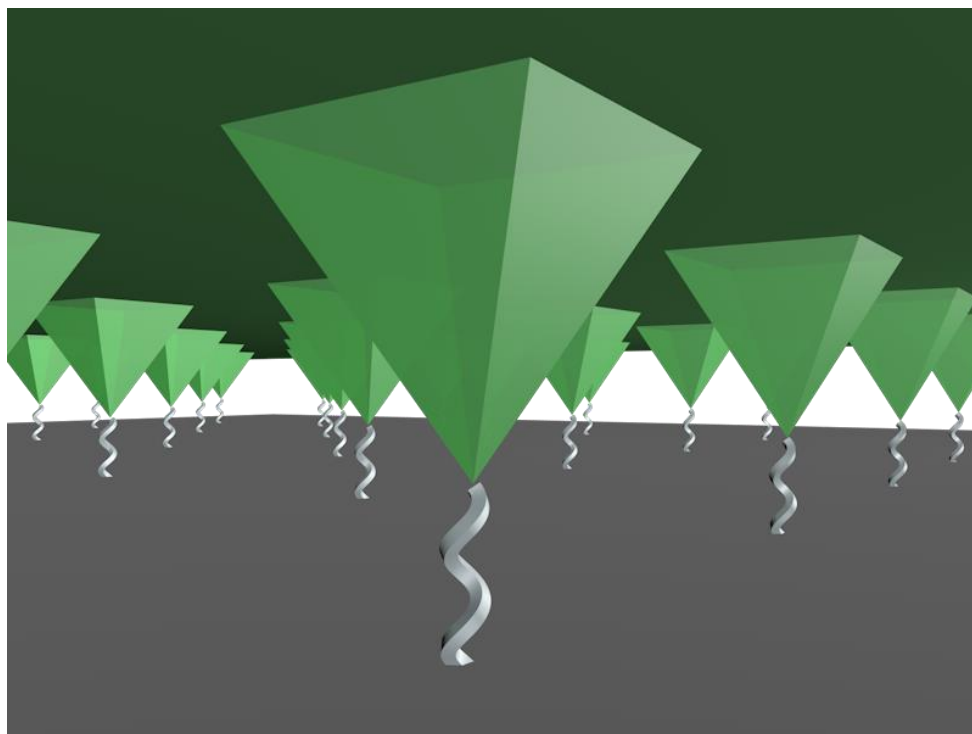


**Figure 3.7.** Example of thermal dip-pen nanolithography being used to pattern nanoparticles with high resolution and in a straight line for potential use in electronics for circuit building and repair.<sup>45</sup>

Finally, this iteration of t-PPL may be seen as the precursor to more precise, optimized patterning tools that may use individual pen actuation by optoelectronic heating or laser irradiation, such that this can also be a more arbitrary patterning technique. Other modifications may include incorporation of a thermoelectric heater under the substrate for more controlled heat flow, as well as a thermocouple integrated such that pen array temperature can be more easily measured and changed in real-time. This work represents the beginning of t-PPL, and while there are improvements to be made, I have herein demonstrated the potential and capabilities for the technique in this thesis.

**CHAPTER FOUR:**  
**ELECTROCHEMICAL POLYMER PEN LITHOGRAPHY**



## 4.1 Introduction

Metal micro- and nano-structures have widespread applications in the fields of electrocatalysis, electronics, plasmonics, and magnetism.<sup>46-49</sup> In order to synthesize, prototype, and discover structures with enhanced activity, methods for printing libraries of materials with control over their size, composition, and location on a single substrate are required.<sup>12,49,50</sup> Bottom-up syntheses, compared to the often-used top-down methods, present a potential solution to this challenge, as metal features may be patterned arbitrarily with defined placement and size control. One commonly used bottom-up technique, electrochemical deposition, possesses many benefits wherein both the volume and composition of deposited metal features can be tuned by controlling precursor composition, applied potential, and contact area.<sup>51-53</sup> While it is a fast, inexpensive, and highly versatile technique, it has typically been limited to conventional thin-film electroplating or more recently, serial single nanostructure deposition.<sup>54,55</sup>

Scanning probe techniques have shown promise for site-specific nanoscale metal printing *via* the electrochemical deposition of metals onto a conducting substrate.<sup>54-66</sup> One such method used a nanopipette or AFM tip loaded with a metal salt solution to reduce a metal directly onto a cathodic surface for 3D printing of metallic structures.<sup>54,56,57,59,60,62</sup> In another technique, a metal ion-embedded hydrogel was molded into a pyramidal shape and used for electrodeposition *via* the diffusion of metal ions through the hydrogel and reduction on a surface.<sup>63,64</sup> However, in all cases, the use of a single tip makes patterning large-areas cost- and time- prohibitive, thus limiting their application in the preparation of single-substrate libraries. A scalable approach may be possible through an existing large-area patterning technology: PPL. The architecture of PPL allows millions of pens to act in parallel, and has been shown to enable the formation of single -

substrate libraries with tens of thousands of spatially encoded features, or megalibraries.<sup>12</sup> The PPL platform is thus ideal for the high-area, high-throughput generation of libraries of electrochemically deposited nanomaterials.

Here, we describe a method of massively parallel, localized electrodeposition using a hydrogel pen array, termed electrochemical polymer pen lithography, or ePPL. ePPL combines the scanning probe capabilities of PPL with the flexibility of electrochemical deposition by integrating a metal salt-loaded hydrogel pen array with a three-electrode electrochemical cell. This architecture allows for the parallel deposition of a variety of metals with control in the x, y, and z directions using >10,000 pens over cm-scale areas. An illustration of this technique is provided in **Figure 4.1**. In addition, ePPL eliminates the need for solution-phase surfactants, cleanrooms, or vacuum environments. Importantly, this all-in-one lithography tool has the capacity to generate megalibraries of mono- or multi-metallic nanomaterials, enabling vast investigations in materials properties, as well as the ability to rapidly prototype 2D/3D metallic structures.

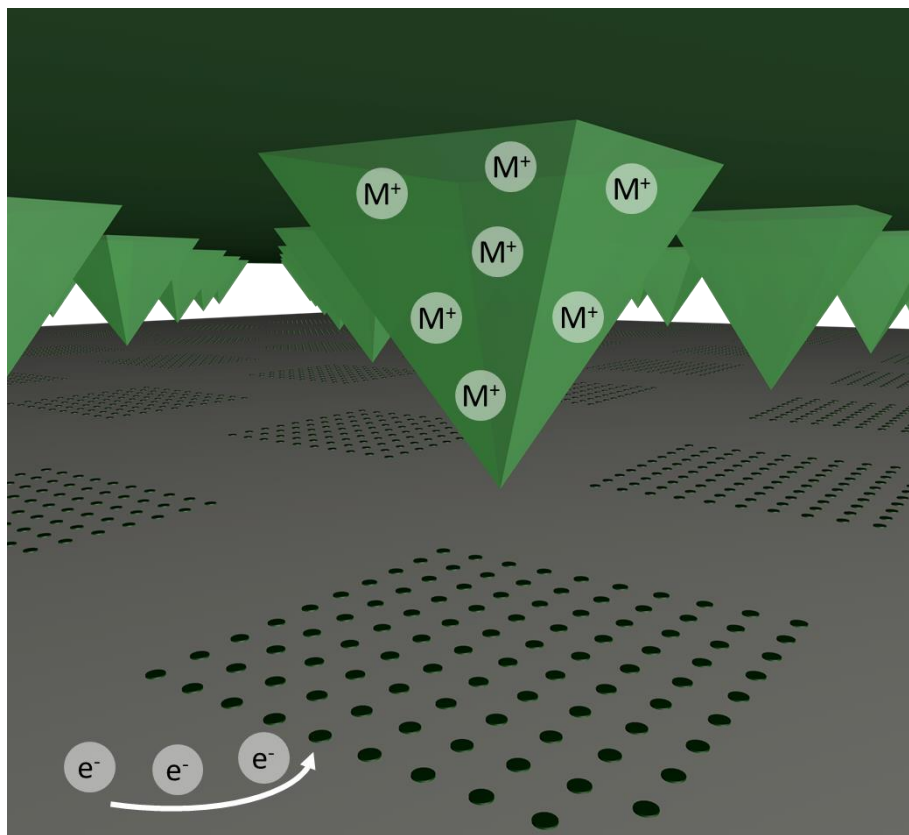


**Figure 4.1.** Exaggerated 3D rendering of electrochemical PPL (ePPL) procedure. As a metal salt-embedded hydrogel is brought into contact with a cathodic surface repeatedly using a piezo, metal micro/nano-structures are reduced sequentially.

## 4.2 Experimental Section

### *Fabrication of pen array masters*

Masters were fabricated following procedures outlined in prior reports.<sup>10</sup> In brief, a photoresist, Shipley S1805, was spin-coated on a silicon <100> wafer with a 5000 Å thermal oxide layer (NOVA Electronic Materials, LLC.). The wafer was soft baked at 115 °C for 80 s and cooled to room temperature. Using a mask aligner (Suss MJB4; Suss MicroTec), the wafer

was UV-exposed to pattern  $15 \times 15 \mu\text{m}^2$  squares with a  $30 \mu\text{m}$  pitch;  $30 \mu\text{m}$  was used for all the data shown here, but arbitrary pitch distances up to  $120 \mu\text{m}$  have been successfully used as well. The patterns were developed in MF-319 developer for 60 s and rinsed with water. To remove the oxide layer before the etching step, the patterned Si wafer was immersed in a buffered HF solution. The patterns were then selectively etched in potassium hydroxide, which results in an array of inverted pyramids. Pyramids form due to an anisotropic etch which etches the  $\langle 100 \rangle$  face of silicon  $\sim 74$  times faster than the  $\langle 111 \rangle$  face. The surface of the Si wafer was coated with fluorinated silane to facilitate the lift-off process of the hydrogels by making it superhydrophobic. Masters were cleaned periodically by sonicating for  $\sim 10$  min in methanol, then rinsed with DI water and dried.

#### *Metal Deposition Solutions*

Ni, Pt, and Ag electroplating solutions were purchased from Technic, Inc. Ni-Co electrolyte solution was prepared by combining 22 g  $\text{Ni}(\text{NO}_3)_2 \cdot 6\text{H}_2\text{O}$  and 2.2 g  $\text{Co}(\text{NO}_3)_2 \cdot 6\text{H}_2\text{O}$  in 40 mL DI water for a 10:1 molar solution, and 22 g of both  $\text{Ni}(\text{NO}_3)_2 \cdot 6\text{H}_2\text{O}$  and  $\text{Co}(\text{NO}_3)_2 \cdot 6\text{H}_2\text{O}$  for a 1:1 molar solution.

#### *Preparation of Polyacrylamide Hydrogel Solution*

A gel stock solution was prepared by dissolving 2.38 g acrylamide and 0.25 g bis-acrylamide powders in 100 mL DI water, which is enough to fabricate 1-2 pen arrays. The curing process was initiated by adding 880  $\mu\text{L}$  of 10 wt% ammonium persulfate (APS) and 88  $\mu\text{L}$  of tetramethylethylenediamine (TEMED) to the stock solution. All chemicals were purchased from Sigma-Aldrich, Inc.

### *Assembly of an Electrochemical Cell*

The setup of the three-electrode cell is shown in **Figure 4.2b**. The custom 3D electrochemical cell was designed using AutoCAD, and printed by Protolabs, Inc. In order to attach the acrylamide hydrogel to an indium tin oxide (ITO)-coated glass slide (Nanocs Inc.), the surface was functionalized with 3-(trimethoxysilyl)propyl methacrylate (Sigma-Aldrich) in toluene (1:3 by volume) *via* vaporization in a sealed chamber. The functionalized ITO glass slide was attached to the top of the cell using double-sided tape. The cell was then placed directly onto an Si master, and the gel solution was poured into and around the cell through the reference electrode well at the corner of the cell. The gel was cured for no longer than 20 min at room temperature. The molded gel was removed from the master and soaked in a Ni, Pt, Ag, or Ni-Co metal deposition solution for at least 3 h or overnight in order for the metal salts to diffuse into the hydrogel. The entire cell was mounted to an AFM head for patterning, and the ITO substrate was clipped to a long wire, which served as the counter electrode. To create a functional working electrode (or a substrate), a long wire was connected *via* a flat alligator clip to a gold-coated glass slide. An Ag/AgCl electrode in 3 M NaCl (BASi, Inc.) was used as a reference electrode and inserted gently into the well at the corner of the cell, along with additional metal deposition solution.

### *Patterning Procedure*

Before patterning, the pen arrays were aligned to the substrate using the optical alignment method described previously.<sup>9</sup> Controlled potential electrolysis (CPE) was performed to generate each feature. Once the tips were in contact with the substrate, a constant voltage was applied using a potentiostat (BASi EC Epsilon) for a given amount of time, depending on the metal used

and thickness desired (**Table 4.1**). The speed of the piezo in the x-y and z directions was set to 0.1  $\mu\text{m/s}$ , allowing each pen tip to be replenished with metal ions before patterning the next feature.

**Table 4.1.** Applied voltages and minimum deposition times used for each metal deposition.

Metal	Applied Voltage (mV)	Minimum Deposition Time (s)
Ni	-950	20
Ag	-950	10
Pt	-500	10
Ni-Co	-550	60

### *Characterization of Patterns*

The patterned images were observed using optical microscopy (Zeiss Axio Imager.M2m) and scanning electron microscopy (SEM; Hitachi SU8030). The height and surface roughness of the patterned features were analyzed using atomic force microscopy (AFM; Dimension Icon; Bruker). Using NCHR-50 cantilevers (Nanoworld), images were acquired in tapping mode at a scan rate between 0.10 – 0.99 Hz with a spring constant of 42 N/m. The imaging was performed at room temperature, and the collected data was analyzed using NanoScope Analysis software. Elemental analysis was performed *via* energy dispersive spectroscopy, fitted onto SEM (Hitachi SU8030) and X-ray photoelectron spectroscopy (XPS, Thermo Scientific EscaLab 250 Xi) to characterize the composition of the patterned features.

### 4.3 Single Metal Patterning

In order to use the existing PPL platform and architecture for electrochemical deposition, a pen array that can be embedded with metal ions while still retaining its fidelity (i.e., stiffness and sharp tips) is needed. Here, we chose a polyacrylamide hydrogel to support the localized electrochemical deposition of metal "inks" because it is easily cured into a mold, can be chemically affixed to a stiff conductive substrate by way of an acrylate monolayer, and absorbs and transmits aqueous solutions through its polymer network. A pre-polymer solution was poured into a silicon master and covered with an acrylated ITO-coated glass slide. As the hydrogel cured into the form of a cm-scale pen array, it also adhered to the surface of the ITO, which serves as the counter electrode. The ITO slide also maintains the planarity of the array, allowing the user to uniformly engage the pens that comprise the array with the substrate during the patterning process. Its optical transparency makes levelling straightforward. The pen arrays were then loaded with metal salt solution, which functions as both the metal source and the electrolyte. To perform precise and consistent electrodeposition, this hydrogel was incorporated into a three-electrode fluid cell (**Figure 4.2a,c**). An Ag/AgCl reference electrode is used to monitor the applied voltage and current, and a conductive substrate (i.e., Au-coated Si-wafer) serves as the working electrode. In a typical experiment, the pen array is brought into contact with a conductive substrate using an AFM (**Figure 4.2b**), and a voltage is applied, which reduces metal ions at each pen location.

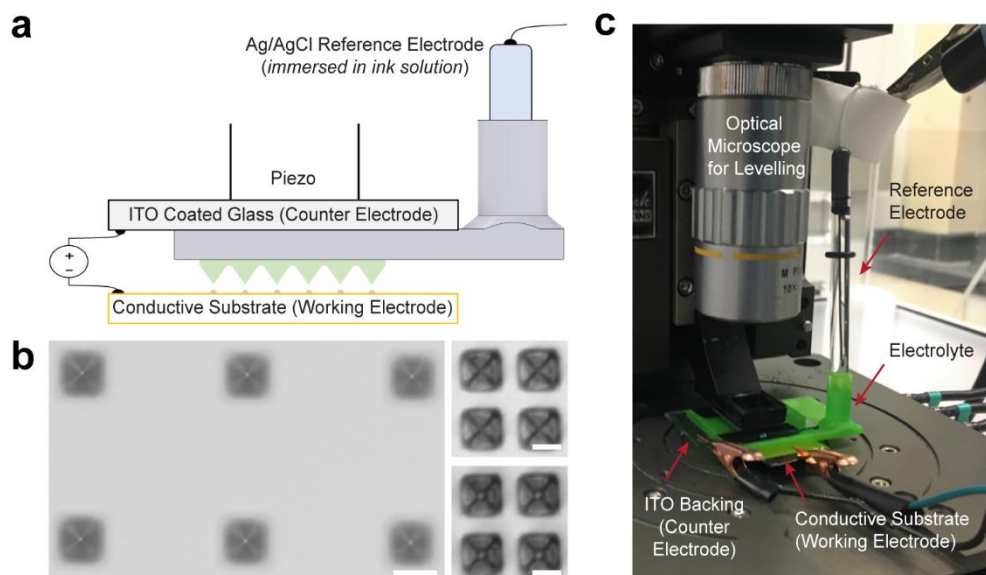


**Figure 4.2.** Experimental setup of ePPL. (a) Schematic of a three-electrode cell designed to hold the hydrogel array, electrolyte, and reference and counter electrodes in place during patterning. (b) Optical image of fabricated polyacrylamide hydrogel pen arrays, which were prepared by curing the hydrogel within a silicon master (scale bar = 30  $\mu\text{m}$ ). Images on the right show a pen array during the patterning process, highlighting how contact was determined: pens (top) out-of-contact and (bottom) in-contact with the substrate (working electrode) (scale bars = 15  $\mu\text{m}$ ). (c) Photograph of the experimental setup in a Park AFM, showing the cell, electrodes, electrical leads, and optical microscope used for leveling.

In order to determine the potential required to affect electrodeposition, cyclic voltammetry (CV) experiments were performed. Both reduction and oxidation peaks are observed at three different scan rates (**Figure 4.3**), indicating that the ePPL system behaves similarly to a general diffusion-limited system. The experimentally determined  $E_{1/2}$  is  $-0.453 \pm$

0.004 V (vs. Ag/AgCl), consistent with the reduction potential of  $\text{Ni}^{2+}$  to  $\text{Ni(s)}$ , which is -0.459 V (vs. Ag/AgCl) for a 1.32 M solution. While -0.453 V is sufficient to deposit Ni, the rate of deposition at this potential is low. Therefore, a higher potential (-0.95 V) was used, while taking care to avoid potentials ( $< -1.0$  V) at which point the onset of gaseous hydrogen evolution occurs and bubbles disrupt the deposition process.

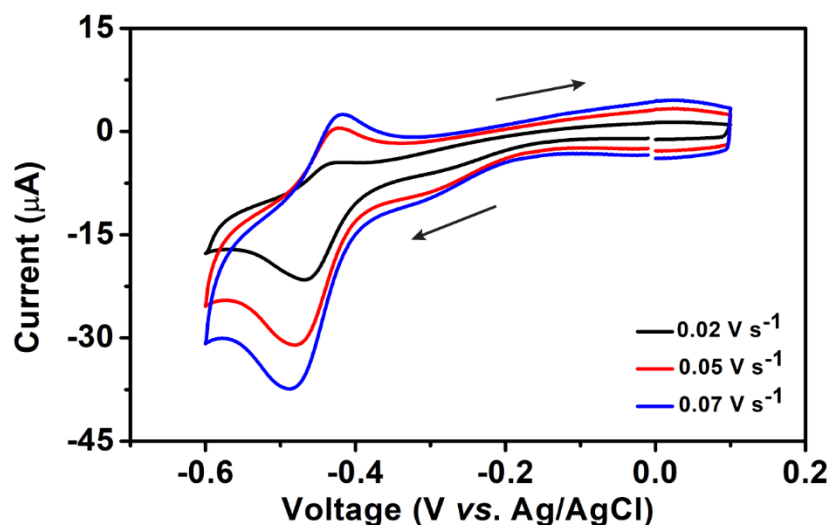


**Figure 4.3.** CV scans for a Ni-embedded hydrogel 3-electrode cell at three different scan rates, indicating both reduction and oxidation potential peaks.

To verify the consistency of patterning with the three-electrode cell, a proof-of-concept experiment was performed using a hydrogel pen array loaded with a nickel electroplating solution ( $\sim 1.32$  M) and an Au-coated Si-wafer as the substrate (or working electrode). The hydrogel with the counter and reference electrodes was loaded onto an AFM, and the contact point of each tip across the array with the substrate was determined optically as the center of the

pyramidal tip changes from black to white upon contact (**Figure 4.2b**). To deposit a pattern of three Ni features in a line, a reduction potential of -950 mV was applied for 30 s at the point of contact for each pen in a single array (**Figure 4.4a**). The resulting features had an average width of  $4.5 \pm 0.1 \mu\text{m}$  (SE), indicating the relative uniformity of the patterning across the substrate.

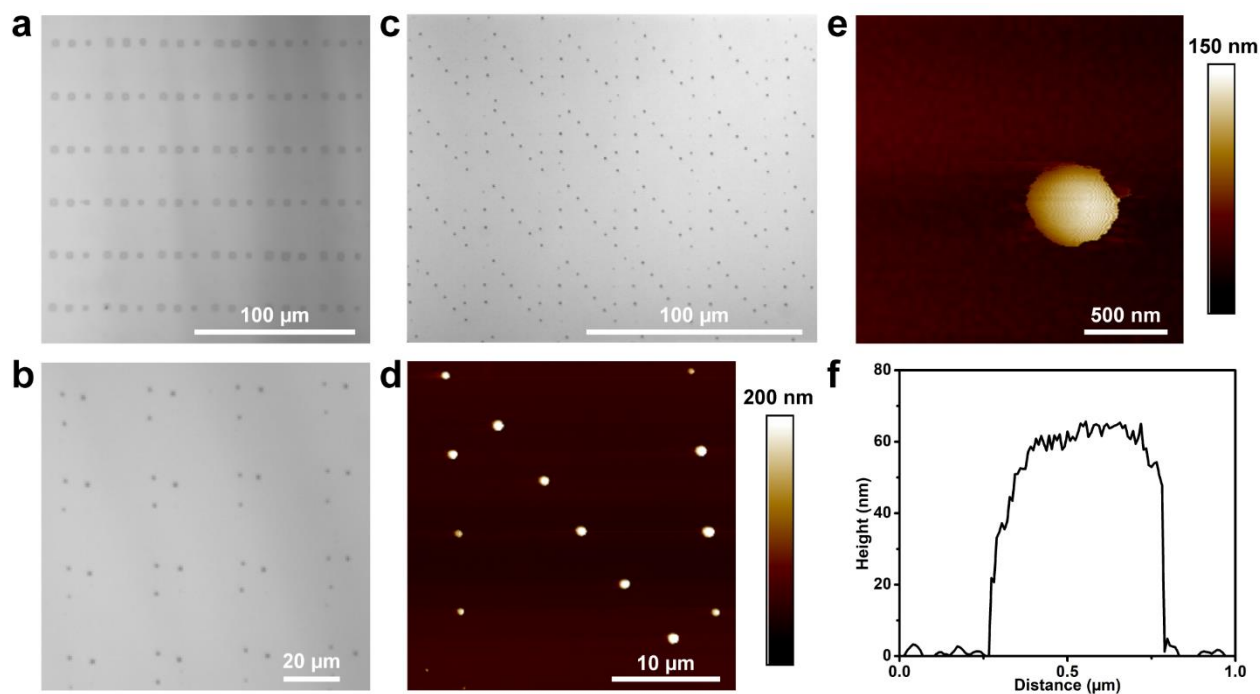


**Figure 4.4.** Patterning capabilities of ePPL. Optical micrographs of patterns of (a) Ni on an Au substrate (scale bar =  $100 \mu\text{m}$ ), (b) Ag on an indium tin oxide (ITO) substrate (scale bar =  $20 \mu\text{m}$ ), and (c) Pt on an Au substrate (scale bar =  $100 \mu\text{m}$ ). The Pt pattern consists of an array of 13 dots arranged as the letter “N” at each pen location. AFM images of (d) a single “N” (scale bar =  $10 \mu\text{m}$ ) and (e) a single Pt particle (scale bar =  $500 \text{ nm}$ ). (f) The associated line scan of the particle in panel (e).

To confirm that the observed metal features were electrochemically deposited rather than physically transferred from the hydrogel, two sets of control experiments were carried out. In the first, no features were observed when Ni patterning was performed without an applied voltage (Figure 4.5). In the second test, a patterned sample was thoroughly rinsed with water and then sonicated to remove any residual salt from the substrate (Figure 4.6). Even after this aggressive washing, the patterns remained, indicating that the observed features are not remnant salt or liquid residues from the hydrogel, but rather metallic features adhered to the substrate.

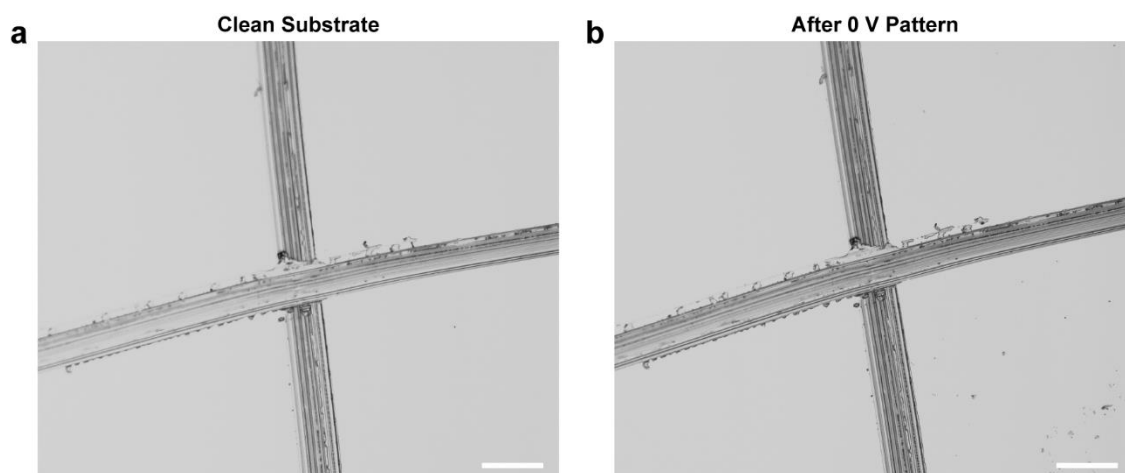


**Figure 4.5.** Control patterning experiment shows that an applied voltage is needed for metal deposition to occur. An Au-coated Si wafer was scratched with a cross and imaged before (a) and after (b) typical Ni patterning with 0 V applied. No patterned features are observed. Scale bars = 50  $\mu$ m.

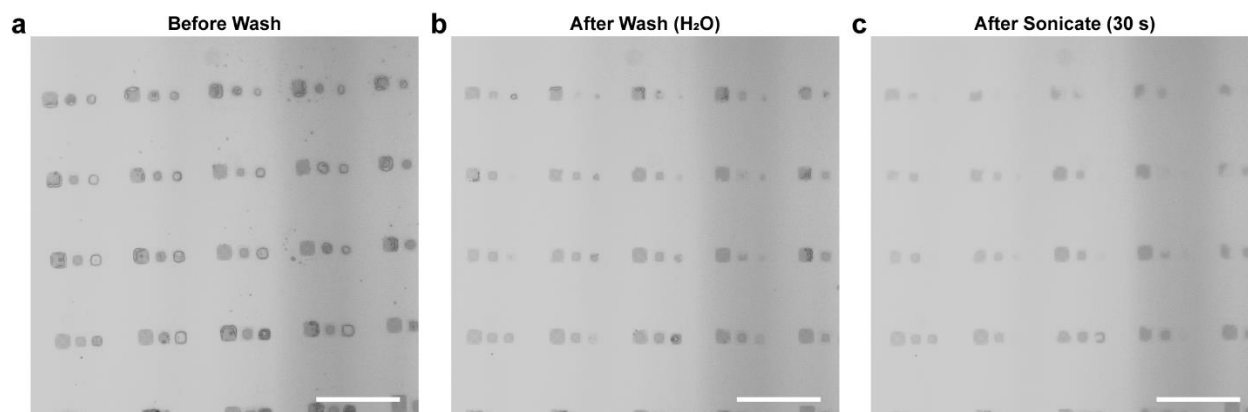


**Figure 4.6.** Optical images of a substrate with Ni features before and after extensive rinsing indicate the presence of reduced metal. (a) An Au-coated Si wafer was patterned with an array of 3 Ni features from each tip (b) washed thoroughly with water, and then (c) sonicated for 30 s in water. While the features faded after agitation, this experiment shows that the patterned features are reduced metal on the substrate and not salt residue. Scale bars = 30  $\mu\text{m}$ .

To test the versatility of this lithographic tool, arbitrary patterns were generated using various metal inks such as Pt and Ag in addition to Ni, as well as a different substrate (ITO). The resulting patterns were characterized *via* AFM and XPS (**Figures 4.4b-d, 4.7**). For instance, the letter “N” was printed on an Au-coated Si-wafer using Pt where a reduction potential of -500 mV was applied for 10 s. This resulted in a pattern comprised of 13 features per pen with an average diameter and height of  $777 \pm 81$  nm and  $166 \pm 7$  nm, respectively, as determined *via* AFM (**Figure 4.4e,f**).

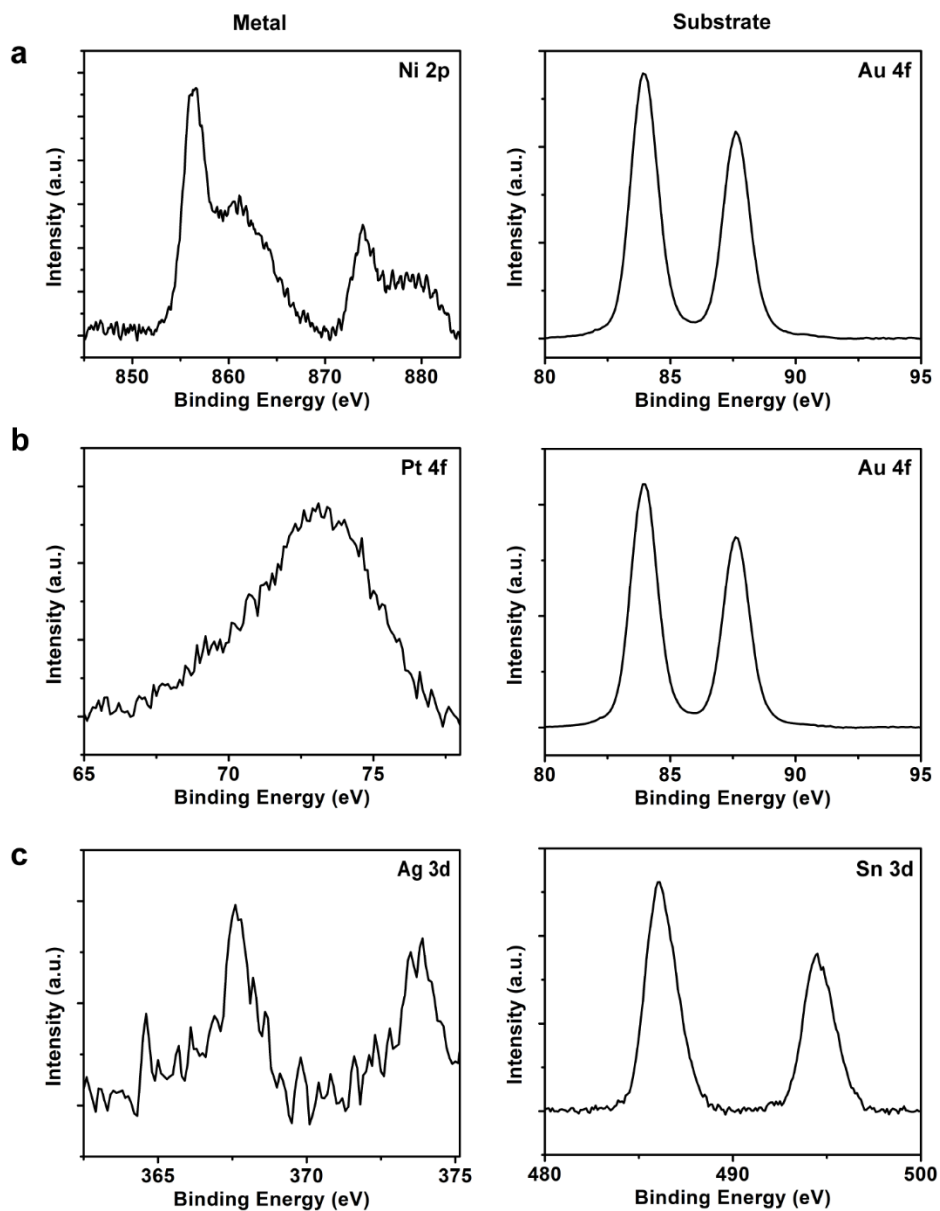


**Figure 4.7.** X-ray photoelectron spectroscopy (XPS) patterns of the patterned samples confirm the presence of metal on the respective substrates. (a) Ni features on an Au-coated Si wafer. The peaks at 856 eV and 873 eV (left) are expected Ni 2p peaks. Au 4f peaks are observed at 84 eV and 87.7 eV (right). (b) The peak at 73 eV (left) indicates Pt on Au-coated Si substrate with Au 4f peak at 84 eV (right). (c) The presence of the Ag is confirmed by the peaks at 367 eV and 373.6 eV (left), and the peaks at 486 eV and 494.5 eV (right) are assigned to Sn 3d from the

ITO-coated glass slide. The main peaks in the deposited features are all oxides due to rapid oxidation upon exposure to ambient conditions.

Additionally, with this technique, the dimensions of printed features can be controlled, demonstrating the potential of ePPL for high-throughput printing of 3-dimensional metallic structures. The width of each feature depends largely on pen-substrate contact area, where the smallest diameter achieved was ~210 nm (**Figure 4.8**), which corresponds approximately with the sharpness of each tip. Two methods were used to control feature height: (i) varying the deposition time and (ii) layer-by-layer deposition. In the first case, we found that, as expected, the height of a Ni feature increased with deposition time (**Figure 4.9a**). It is important to note that a thin base layer was observed for all deposition times; this is particularly obvious at 5 and 20 s. We hypothesize that as with Dip-pen Nanolithography,<sup>7,67,68</sup> an electrolyte meniscus initially forms as the pens come into contact with the substrate, and ions in this meniscus are reduced first, resulting in a thin layer (**Figure 4.10**). As the ions in the meniscus are depleted, however, reduction occurs directly from the hydrogel. Because the hydrogel contact area is smaller than that of the meniscus, the following layers are smaller in width as well, as evident at later time points.

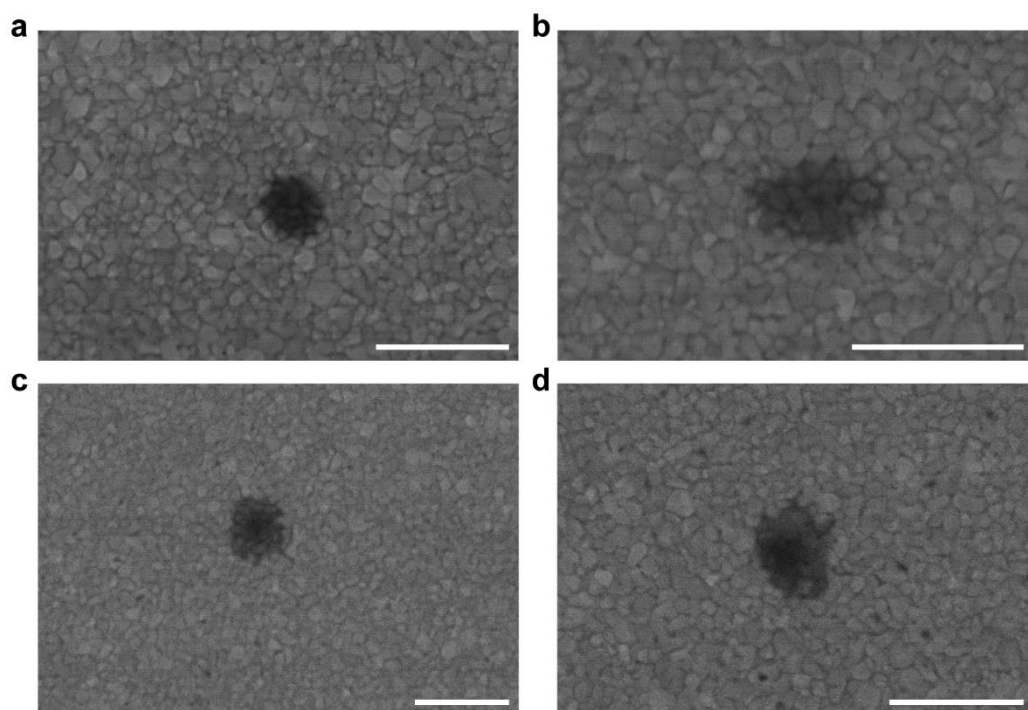


**Figure 4.8.** Scanning electron micrographs of patterned Pt features on Au-coated Si wafer, highlighting the high-resolution capability of ePPL. The black features indicate Pt particles with diameters ranging from ~210 nm to 280 nm. Scale bars = 500 nm.

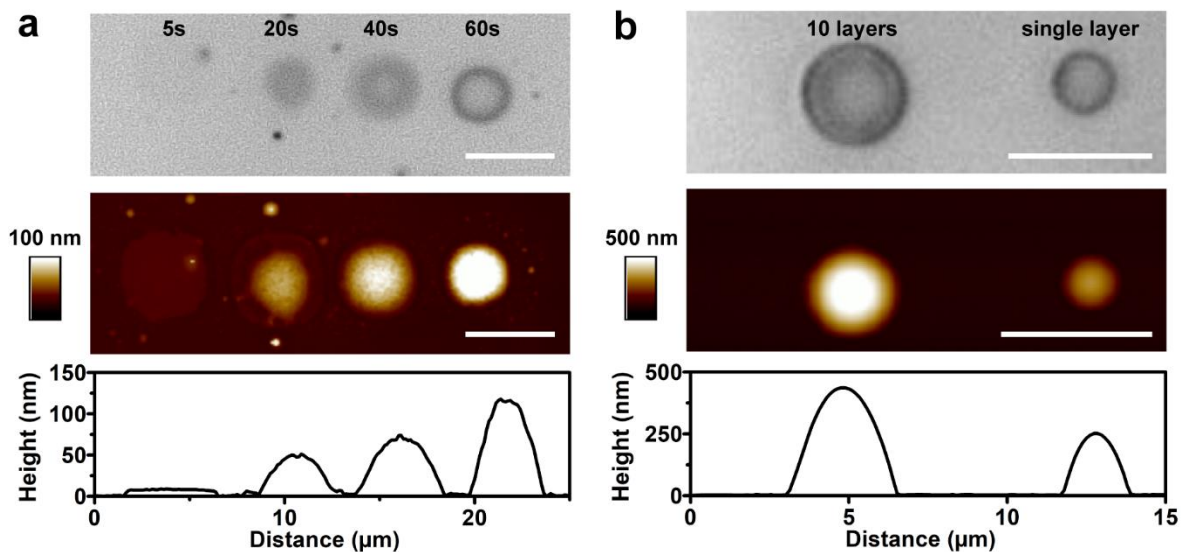


**Figure 4.9.** Feature dimensions are controlled by deposition time and layering. (a) Optical and AFM images of a pattern consisting of 4 Ni features where height was controlled by varying the deposition time. (b) Optical and AFM images of a pattern with 2 Ni features where size is controlled by depositing multiple layers of Ni, 60 s at a time. Features shown are 10 vs. 1 layer. Scale bars = 5  $\mu\text{m}$ .

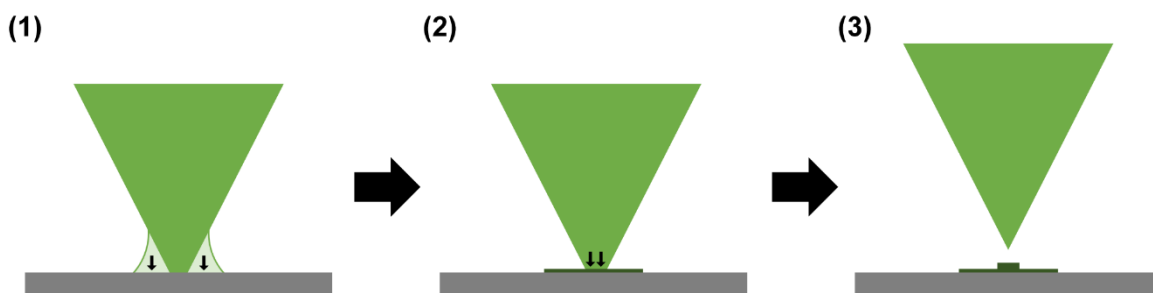


**Figure 4.10.** Schematic depicting the hypothesized mechanism of ePPL deposition. (1) First, metal reduction occurs preferentially from the meniscus that forms between the tip and the substrate upon contact. (2) Once ions are depleted from the meniscus, reduction occurs directly from the hydrogel, at the tip-substrate interface. (3) When the tip is lifted, the shape and size of

the resulting structure corresponds to the shape of the tip-substrate interface, along with a very thin layer from the meniscus.

Feature height can also be controlled by depositing metals in a layer-by-layer fashion. A nearly two-fold increase in height was observed for a feature with 10 layers versus that of a single layer (**Figure 4.9b**). Here, growth occurred in both the height and width of the features as deposition occurs outwards over time, likely due to the hydrogel pen acting as a physical barrier to increasing feature height. This may be overcome by more precise tuning of each layer height with corresponding z-movement. Therefore, using this layer-by-layer method in combination with control over the deposition time, this technique can be used to generate 3D metallic structures of various sizes in a high-throughput manner.

#### **4.4 Multimetallic Patterning**

Because this technique is diffusion-based, multiple metals may be absorbed by the hydrogel at once, such that multimetallic features can be patterned as long as they have comparable reduction potentials. To test this, a hydrogel pen array was saturated with a 10:1 nickel-cobalt salt solution and used to pattern Ni-Co alloys, one of the known hydrogel evolution reaction (HER) catalysts, onto an Au-coated silicon wafer at -550 mV. In order to understand the composition of the deposited features, a surface characterization tool like XPS is needed. Because this is a surface-sensitive technique, larger features were patterned in order to generate sufficient signal (**Figure 4.11a**), although smaller features are possible (**Figure 4.12**). These large features were patterned with fully extended pen tips resulting in a pyramidal structure that corresponds to the shape of the pen tip (**Figure 4.11a inset**). AFM analysis shows that these

patterned features are  $\sim 80$  nm tall, with a base layer of  $\sim 12.5 \times 12 \mu\text{m}^2$  and 10 nm in height (Figure 4.13).

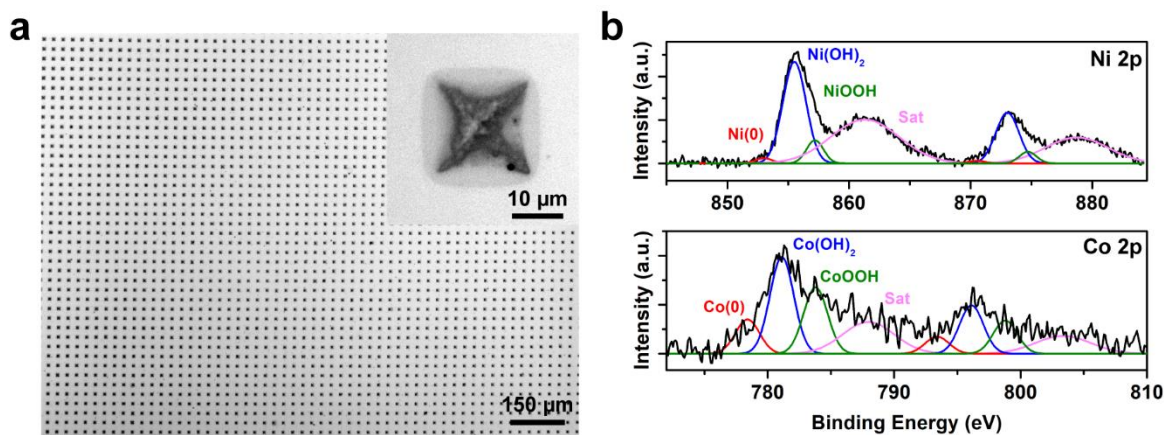


**Figure 4.11.** Deposition of Ni-Co alloys. (a) Optical micrograph of a large-area pattern of  $>10 \mu\text{m}$  Ni-Co features. The large feature size enables accurate elemental characterization. Inset shows a single feature. (b) XPS characterization of these patterns indicates that both the Ni and Co are present mainly as oxides. Auger peaks have been subtracted for clarity.

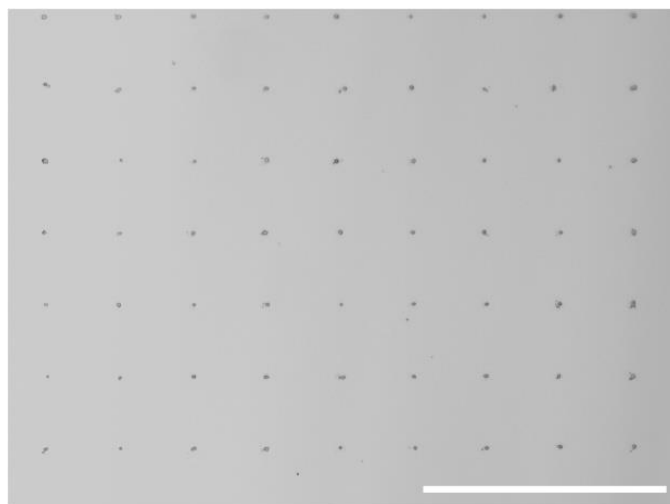


**Figure 4.12.** Optical micrograph of Ni-Co particles patterned on an Au substrate. Scale bar = 50  $\mu\text{m}$ .

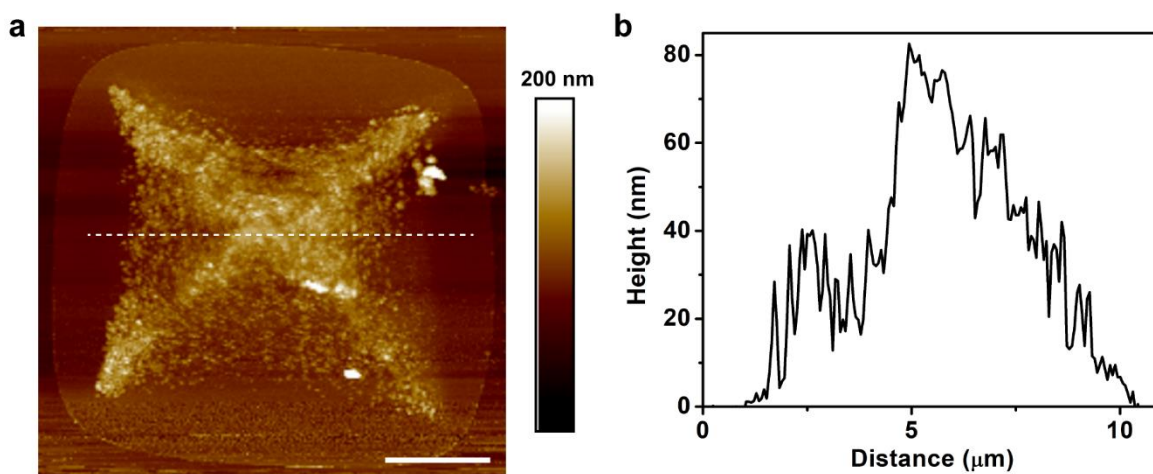


**Figure 4.13.** (a) AFM height profile of a large Ni-Co feature, and (b) AFM line scan across the large feature in (a), location indicated by dashed line. Scale bar = 3  $\mu\text{m}$ .

To confirm the presence of reduced Ni and Co, XPS analysis was performed. The Ni 2p and Co 2p spectra show two major peaks corresponding to the  $2p_{3/2}$  and  $2p_{1/2}$ , each followed by a satellite peak. As shown in **Figure 4.11b**, the 2p peaks are best fit with three Gaussian curves for both Ni and Co suggesting the presence of three different chemical environments. For Ni, the appearance of a peak at 852.6 eV suggests that some of the patterned Ni is in a metal-like environment. The major peak is at 855.6 eV, however, indicating that most of the Ni exists as  $\text{Ni(OH)}_2$ . This oxidation is expected since the patterning was performed under ambient conditions and the ink solution contained  $\text{H}_2\text{O}$ . Also,  $\text{Ni(OH)}_2$  is easily oxidized to oxyhydroxide ( $\text{NiOOH}$ ) in the presence of water, thus explaining the minor peak at 857.2 eV.<sup>69</sup> Similar behavior is expected for Co, and this explains the peak at 783.7 eV which can be attributed to  $\text{CoOOH}$ .<sup>70</sup> Additionally, the Co exists in a metal-like environment as evidenced by the peak at 778.4 eV, however, the majority is in hydroxide form as suggested by the main peak at 781.1 eV.

The composition ratio of Ni-Co was analyzed using energy-dispersive X-ray spectroscopy (EDS) and XPS. EDS data reveals a 3.56:1 ratio of Ni:Co (atomic wt%) in the printed structures (**Figure 4.14**) while XPS analysis based on the area of the  $2p_{3/2}$  peaks results in a similar Ni:Co ratio of 3.86:1. Due to the different reduction potentials of Ni and Co, the composition ratio can be tuned by changing the applied voltage (**Table 4.2**). An increase in Ni content is observed as a more negative potential is applied. Another approach to control composition of deposited materials is to inject a gradient of inks across a single hydrogel pen array. With either of these methods, ePPL can be used to create a compositional variation of alloys across a single substrate.

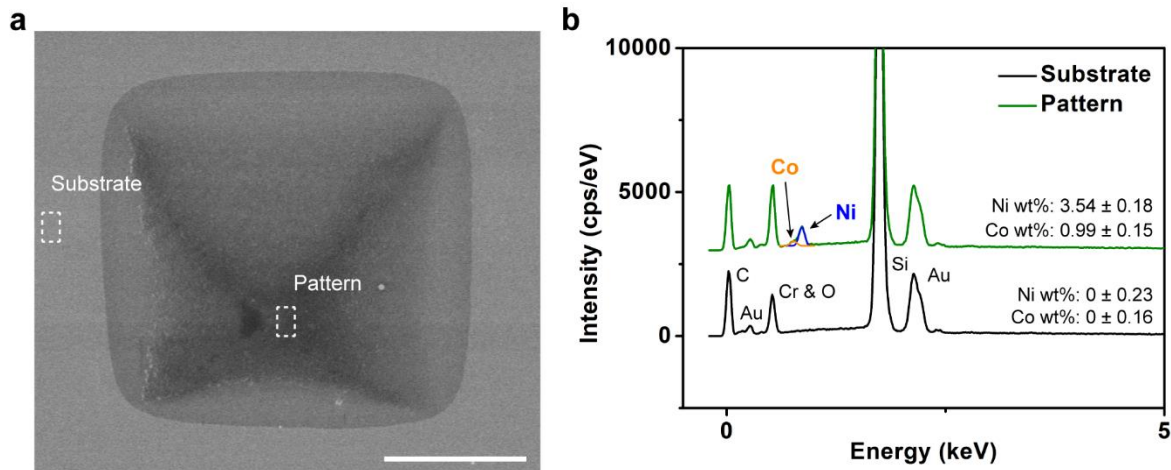


**Figure 4.14.** Energy-dispersive X-ray spectroscopy (EDS) characterization of a Ni-Co feature indicates the presence of both Ni and Co in the deposited region. Ni-Co was patterned on an Au-coated  $\text{SiO}_2$  wafer with a chromium adhesion layer. Corresponding metal peaks are labeled. Scale bar = 5  $\mu\text{m}$ .

**Table 4.2.** Chemical composition of Ni–Co deposited alloys as obtained by X-ray photoelectron spectroscopy (XPS).

Ratio	Applied	Ni%	Co%
Ni:Co	Potential	at/at	at/at
	(mV)		
10:1	-525	77.3	22.7
10:1	-550	79.4	20.6
10:1	-575	81.1	18.9

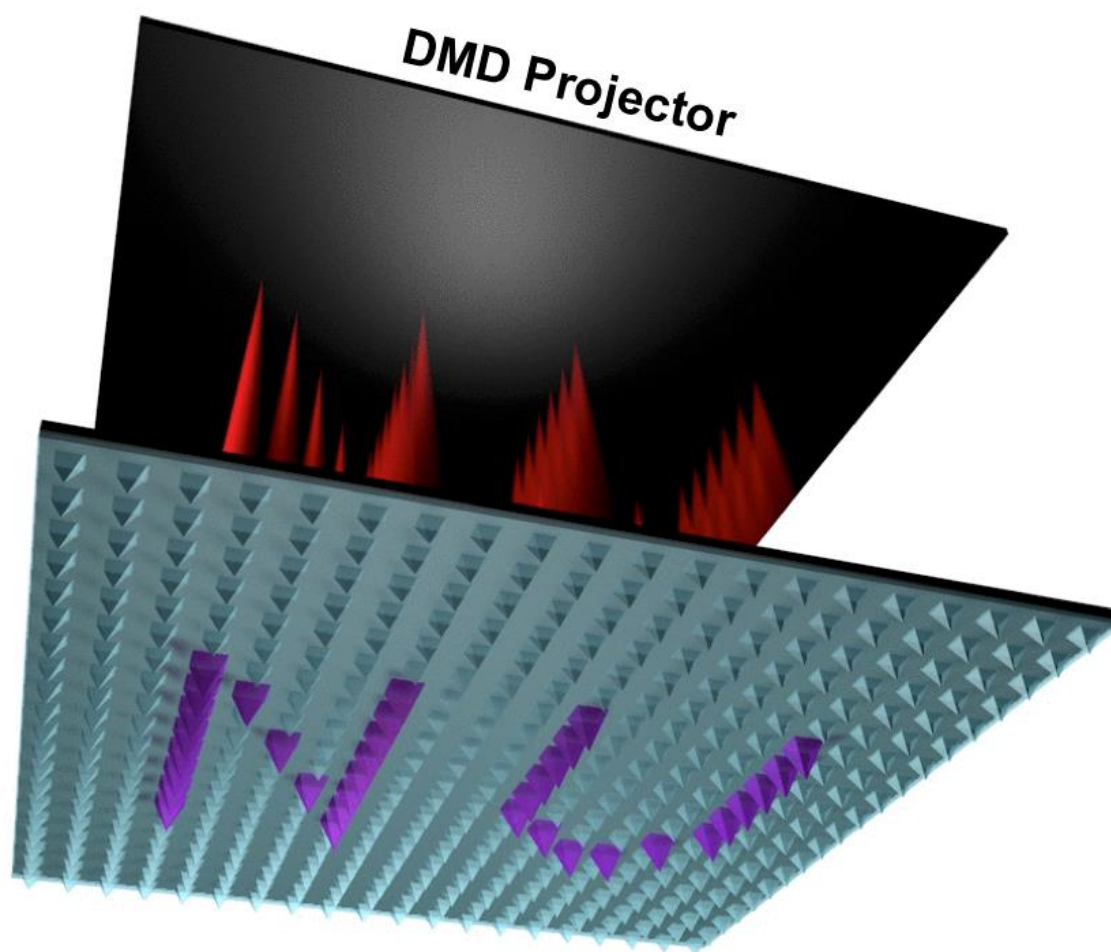
1:1	-525	38.5	61.5
1:1	-550	40.9	59.1
1:1	-575	41.7	58.3

---

#### 4.5 Conclusion

In conclusion, we report a new cantilever-free electrochemical patterning approach based upon the concept of ePPL. While we present the proof-of-concept ability to synthesize mono- and bi-metallic features, this approach should be extendable for patterning other alloy materials with control over size and composition across a single substrate. The high-throughput materials generality of the approach, combined with its ease of use, make it attractive for many purposes. For example, such a tool could be used to create combinatorial megalibraries.<sup>12,50</sup> in order to systematically study and discover ideal catalyst materials for applications spanning the chemical and energy fields. Finally, it may be possible to expand the scope of ePPL to other charged ink compositions, including conductive organic molecules, such as diazoniums, peptides, oligonucleotides, or conducting polymer materials.

**CHAPTER FIVE:**  
**ACTIVE POLYMER PEN LITHOGRAPHY**



## 5.1 Introduction

The past few decades have seen a surge in research and development of nanolithography techniques brought about by the need to precisely control the size, position, and composition of nanoscale features.<sup>8-10</sup> Highly driven by the microelectronics industry, these advancements have unfortunately left a gap in technology for the nanoscale patterning of soft materials, such as biomaterials. Uniquely suited to address this issue, PPL enables nanoscale patterning of soft or hard materials over virtually any large-area substrate. However, while high in throughput, PPL at its current state is a “stamping” tool, meaning that images must be repeated at each pen location, typically 60-200  $\mu\text{m}$  apart. This becomes most problematic in research that uses nanoscale features to investigate effects over a larger area, such as in studies of cell adhesion or migration.

Cellular migration is fundamental to many biological processes as well as technological advancements such as tissue engineering.<sup>71</sup> As they move, cells interact with extracellular matrix proteins with nanoscale surface topographies and geometries, making it crucial to understand the effects of nanoscale cues.<sup>13,72,73</sup> However, in order to observe cell movement over a large area, new technology will be required. Advancing PPL from a stamping tool to an active patterning technology with individually actuated pens would allow complex, non-symmetric patterning of soft materials over a large area to observe cell adhesion and migration. Thus, this project aims to develop a new method of patterning, called active PPL, to pattern many complex nanoscale migration pathways in order to better understand how cells respond to directional cues over long distances.

In order to achieve active PPL, we begin by considering the challenge of addressing each individual pen within an array. Established mechanisms such as DMD arrays enable efficient

illumination of an image at the microscale. Using this technology, we must then consider photo-responsive materials which can actuate the PDMS pens within the device. These include photo-active hydrogels, liquid crystalline elastomers, materials with a photo-thermal response, or photoconductive materials. Photo-active hydrogels are ones which are crosslinked with a photo-responsive molecule such that the polymer network contracts/expands upon light exposure and water is released and re-absorbed.<sup>74</sup> However, one can eliminate photo-active hydrogels due to the reported slow response times (up to 20 minutes) as well as the high levels of humidity required in order to repeatedly re-hydrate the gel, which is incompatible with the electronics of the DMD. Liquid crystal elastomers can produce significant expansion upon light exposure and do not require any particular atmospheric conditions.<sup>75</sup> However, the azobenzene isomerization required for light-activated expansion is a relatively slow process through a micron-scale film, which makes this a nonideal candidate for efficient large-scale patterning.

In nanolithography, many methods have been developed for patterning in one of two broad mechanisms: serial or parallel printing. Serial printing can be thought of as analogous to one pen writing on paper, and includes methods such as electron beam lithography, laser writing, or DPN. This method is fundamentally slow and low in throughput, but it is amendable to arbitrary patterning. Parallel printing, as in photolithography, microcontact lithography, or PPL, is analogous to woodblock printing, where each new pattern requires the fabrication of a new mask or mold. These techniques are very high-throughput but have low flexibility in patterning. A major goal of this work is to develop a technique, active PPL, that bridges serial and parallel nanolithography methods and acts as a high-throughput and flexible nano-scale printing tool.

Before thoroughly discussing active PPL, it is important to note that significant work was done to actuate arrays of DPN cantilevers. Prior to the complete development of PPL, parallel DPN was used for higher throughput scanning probe nanolithography.<sup>76</sup> At this stage, cantilevers were fabricated from using silicon micromachining processes. To achieve active cantilevers capable of individual actuation, metal films were deposited onto the cantilevers to create thermal bimorphs, wherein the different thermal expansion constants of the two materials were used to induce downward motion of the cantilevers when current is applied (**Figure 5.1**). While this method proved interesting and effective, due to the difficulty of scaling such fragile and expensive DPN cantilevers, the technique is less relevant to the nano-patterning field today.<sup>77-79</sup>

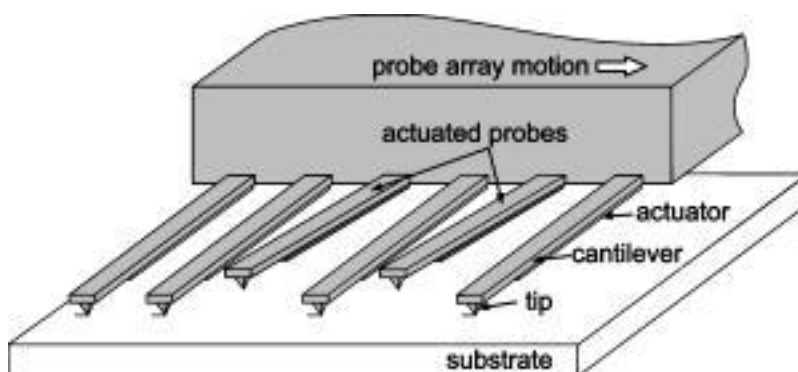


**Figure 5.1.** Illustration of actuated DPN using thermal bimorphs. This method is difficult to scale up, fragile, and expensive to manufacture.<sup>78</sup>

After PPL was developed, the question of active pen arrays was again brought up in order to increase the complexity of patterns made with this architecture. Here, to address each individual elastomeric tip, pneumatic chambers were fabricated behind each tip, and the air pressure within the chambers was individually controlled using an external pneumatic controller (**Figure 5.2**). This method was not optimized beyond its proof-of-concept demonstration for two

pens at a pitch distance of 250  $\mu\text{m}$ , due to the impracticality of large-scale pneumatic control necessary for arrays with tens of thousands or millions of chambers and pens.<sup>80</sup>

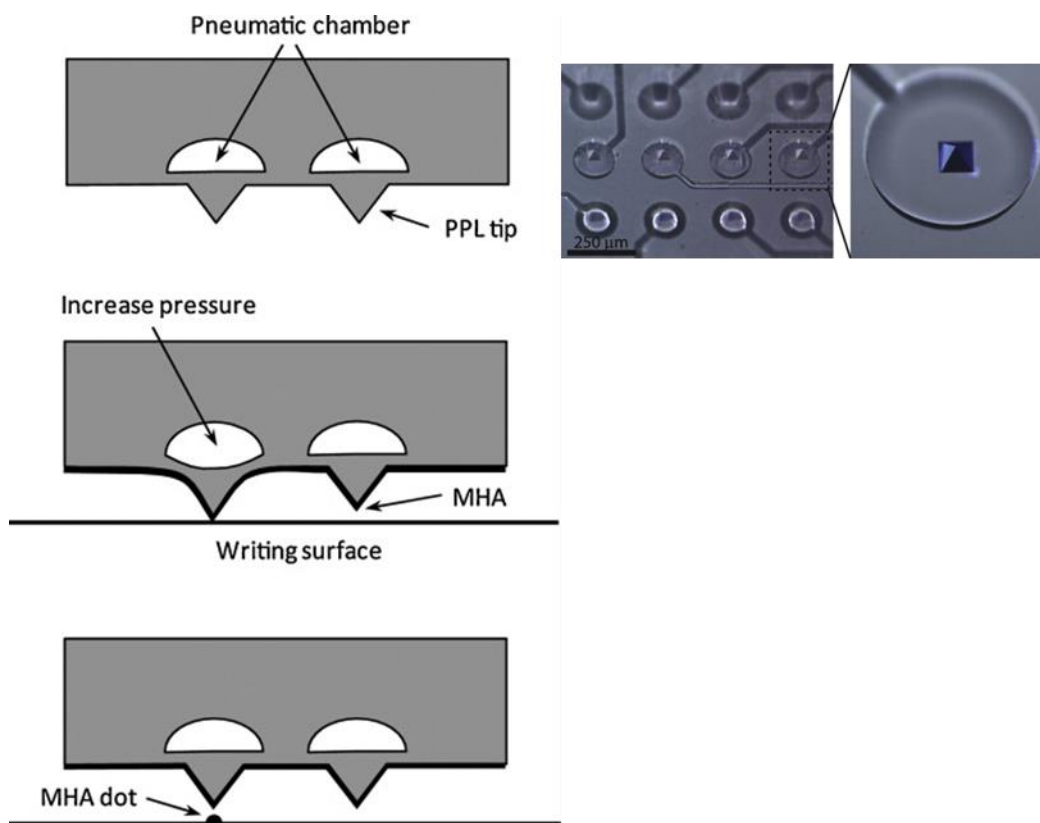


**Figure 5.2.** Schematic of pneumatic chambers and optical image of fabricated chambers behind PPL tips. The air pressure inside the chambers expands to “push” each tip towards the substrate for patterning.<sup>80</sup>

The second attempt to achieve active PPL provided more reliable actuation and demonstrated actuation using 16 pens. In 2013, the Mirkin group demonstrated a technique for actuation by thermal expansion of each PDMS elastomer pen *via* electrical heaters fabricated on the glass layer beneath each polymer pen tip (**Figure 5.3**).<sup>81</sup> Upon heating, the PDMS pens were shown to expand without significant cross-talk between pens or degradation in performance. In

this design, the heaters were made of ITO as a transparent conducting element where resistive heating was induced through an ITO coil by sending a current across each heater. The heat was transferred to the elastomer, which locally expanded both substantially and quickly. This demonstrated that heat is a reliable mechanism for significant expansion and rapid actuation (response times on the order of milliseconds). However, as with the pneumatic chambers, this technique failed in scalability to the level of thousands, or even millions of pens—as the electronic circuitry that would be involved in creating thousands of individually addressable heaters is complex and expensive.

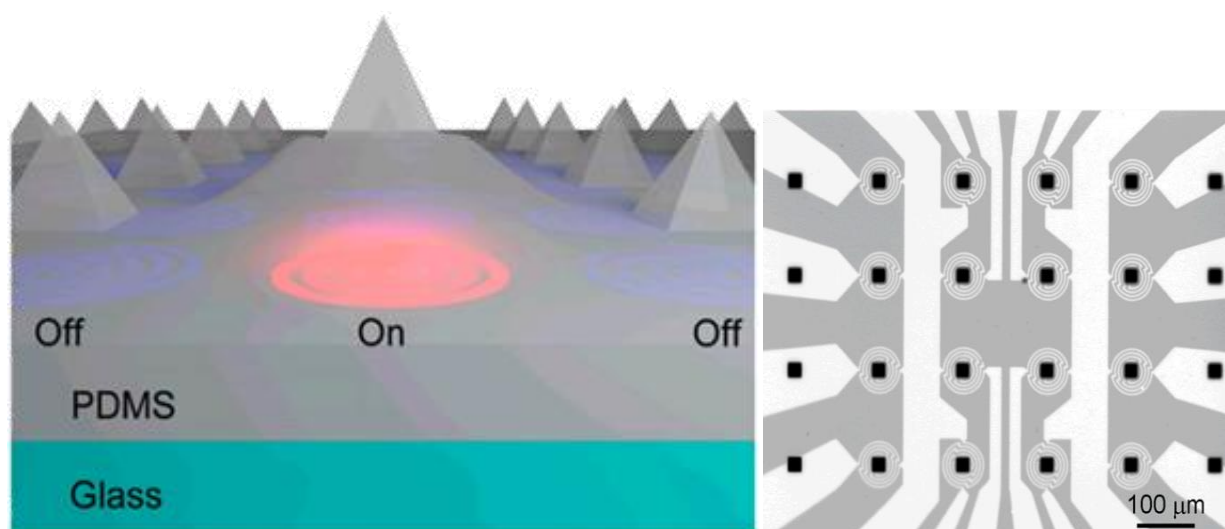


**Figure 5.3.** Illustration and image of actuated PPL using patterned resistive heaters.<sup>81</sup>

To create an easily scalable system, the most efficient method to address each pen at a large scale would be to use light. When coupled with a digital micromirror device (DMD), light can easily address each tip. This is well studied and, in fact, is used for actuated BPL where large-scale arbitrary patterning using an array of apertures bore from a gold-coated PPL array has been demonstrated (**Figure 5.4**).<sup>23,24</sup> Here, light from the DMD shines through the apertures onto

a photoresist to induce a photochemical reaction. Each pen in this apparatus is aligned to a patterned array of light from an LED directed by a DMD. Images can be arbitrarily loaded into the software of the DMD to project light in a pattern, and the timing can be corrected in order to sequentially display certain light images once pens are in contact. While this was a significant leap forward in the field of desktop nanofabrication, this tool is limited to patterning onto photochemical materials such as photoresist. By extending large-area arbitrary patterning to PPL, the capability of nanoscale patterning will become highly generalizable and unspecific to feature or substrate materials.

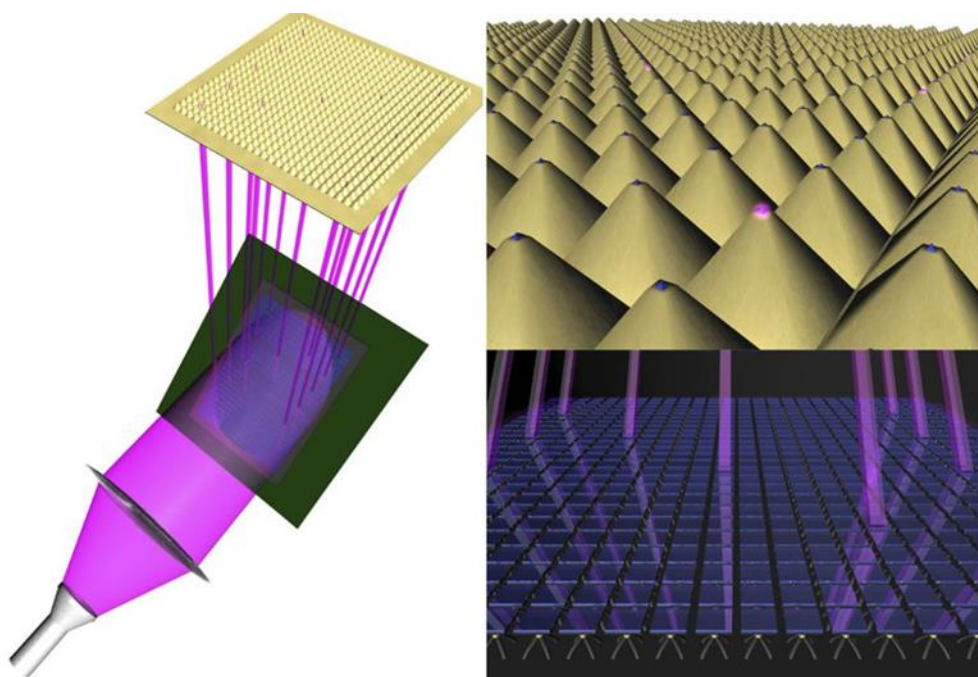


**Figure 5.4.** Depiction of actuated BPL. A DMD array is used to program and control the light output through the aperture at the apex of each pen and onto the substrate for large area arbitrary nanoscale light patterning.<sup>24</sup>

When considering light activation of a PPL array, it becomes important to consider which light responsive materials may be viable candidates. Such materials include photo-active hydrogels, liquid crystalline elastomers, opaque materials with a photothermal response, or photoconductive materials. Photo-active hydrogels are ones which are crosslinked with a photo-responsive molecule such that the polymer network contracts/expands upon light exposure and water is released and re-absorbed.<sup>74</sup> However, one can eliminate photo-active hydrogels due to the reported slow response times (up to 20 minutes) as well as the high levels of humidity required in order to repeatedly re-hydrate the gel, which is incompatible with the electronics of the DMD. Liquid crystal elastomers can produce significant expansion upon light exposure and do not require any particular atmospheric conditions.<sup>75</sup> However, the azobenzene isomerization required for light-activated expansion is a relatively slow process through a micron-scale film, which makes this a nonideal candidate for efficient large-scale patterning. Another approach is to consider using the energy from the light source directly as thermal energy. Recent work showed this using a PDMS pen array embedded with light-absorbing carbon nanotubes.<sup>82</sup> By irradiating the opaque elastomer with light, the excitation of absorbed photons induces heat, which thermally expands the polymer similarly to that observed with resistive heaters. Because the amount of heat generated is directly dependent on the number of photons absorbed, there is a fundamental limit to the expansion that can be generated per milliwatt (mW) of light per unit area. This limit also depends on the amount of power that can be transmitted through a DMD per unit area. Due to this limitation and the lack of a high-power addressable light source, the direct photothermal approach is not realizable in practice. This leaves photoconductive materials as the most promising light active material. Specifically, hydrogenated amorphous silicon (a-

Si:H) has the ability to rapidly increase its conductivity when irradiated with low-power light,<sup>83</sup> and by integrating this capability into a device architecture with thermal radiation, one may be able to utilize a-Si:H as a microscopic switch for thermal expansion.

In order to conceive of such a device architecture, one may look towards existing methods of light actuation. One widely used device is optical tweezers, which relies on high-power light to trap and move particles at the nanoscale. More recently, a new device technology has been investigated called optoelectronic tweezers (OET), where instead of directly using one high-powered light beam to control particles, large-area, directed low-powered light images, integrated with dielectrophoresis, are used to manipulate many objects at once.<sup>84-87</sup> This technique uses a photoconductive material to locally direct conductivity. Here, a moving projected image is displayed onto the substrate to manipulate particles using the opto-dielectrophoretic effect. Consequently, OET is an efficient and large area particle manipulation technique, requiring only one hundred thousandth of the light power needed for optical tweezers. Using inspiration from these methods of light-addressable conductivity, combined with resistive heating, a so-called optoelectronic heating device is proposed for localized micron-scale heating over large areas.

Use of the photo-thermal effect should be investigated thoroughly. A material would be needed, in this case, that can absorb enough energy from the light source to achieve substantial thermal expansion. Upon further investigation, volumetric thermal expansion in solids is insufficient for active PPL, which would require at least three micrometers of linear expansion for patterning. Even when making the material opaque for optimal light absorption, state-of-the-art DMD arrays cannot deliver enough energy at each mirror location to cause sufficient

expansion. Gases and liquids observe significant thermal expansion, and in theory could be integrated into the PPL polymer architecture to act as an expansion mechanism for each pen. This is an option moving forward in our studies, but because it would require complex engineering, microfabrication, and optimization, a more straightforward route was taken in this project to deliver localized heat to each polymer pen: an optoelectronic heater.

In this device, a-Si:H is a promising candidate. It has not only been used as the principle component for optoelectronic tweezers and an optoelectronic heating device from the literature,<sup>88,89</sup> but it is common in the semiconductor industry where it is an alternative thin film solar cell material in low-energy applications such as in solar-powered calculators and watches. An inexpensive, thin-film alternative to crystalline silicon, a-Si:H has a higher band gap and higher absorption coefficient. Due to the high presence of dangling bonds in amorphous silicon, largely passivated by hydrogen in a-Si:H, there is a higher defect density and lower diffusion lengths. When integrated into a device structure, the conductivity of amorphous silicon increases locally and rapidly upon exposure to light. Localized Joule heating can be induced in a-Si:H when illuminated because in the dark a-Si:H acts as an insulator, but when irradiated electrons can flow through a circuit with a resistance that generates heat. Effectively, this scheme enables conversion of low-power illumination to a high-power electronic response from an external power source, subsequently generating heat. The idea is illustrated in **Figure 5.5**.

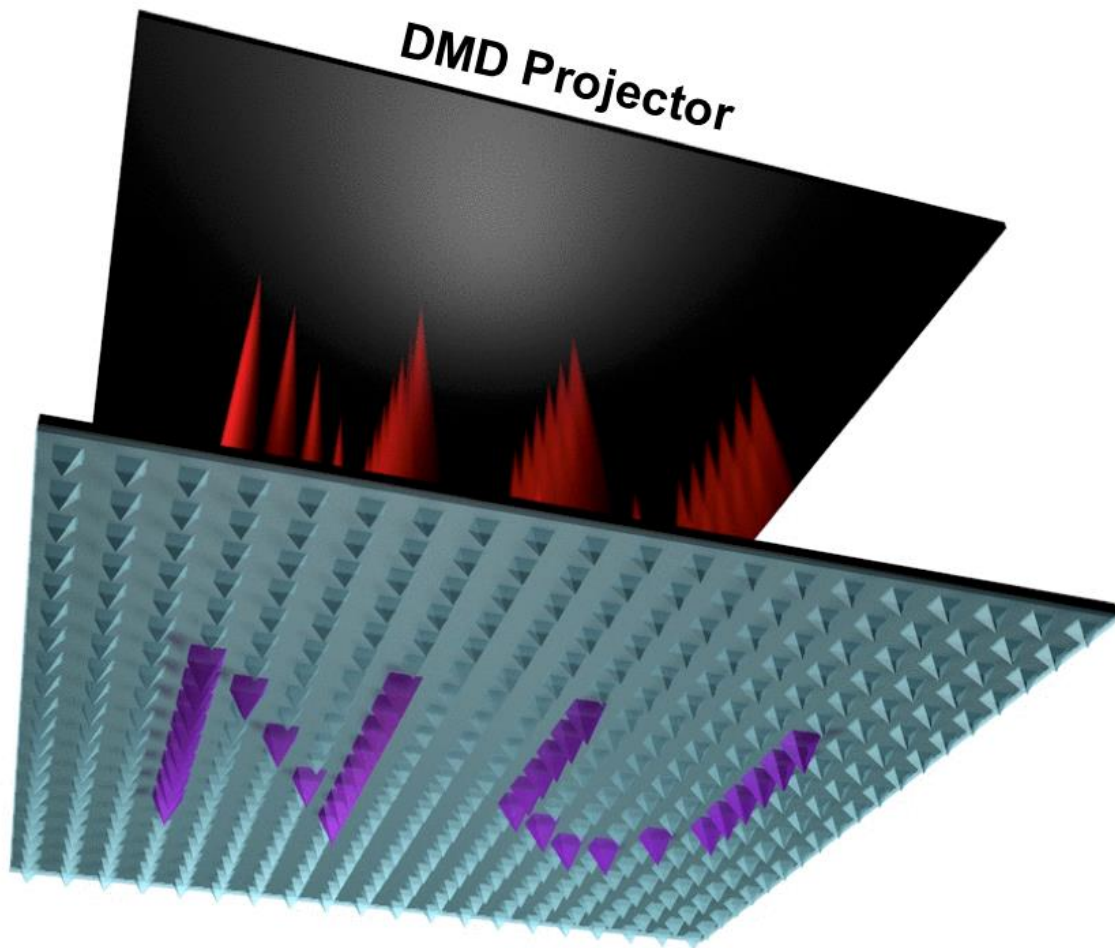


**Figure 5.5.** Conceptualization for active PPL. A DMD projector will illuminate the area behind select pens within an array which will thermally expand and selectively deposit material onto the substrate.

## 5.2 Conceptualization of Photo-actuation

In order to develop an optoelectronic heating (OEH) device for local heating and conductivity control, optimal fabrication procedures were determined both computationally and experimentally. The basic structure of the device can be drawn from solar cell technology and

prior literature in OET, OEH, and demonstration of active PPL using resistive heaters. A schematic of the structure and conceptual description is shown in **Figure 5.6**. The active layer in the structure is a-Si:H. It is photoconductive and responds to light in order to create conductivity in an otherwise effectively insulating material. When electrons are conducted through an illuminated region of the a-Si:H, this acts as a resistor in the circuit. We can thus expect that Joule heating will be produced in the area of illumination. With sufficient heating and a fast heat-transfer mechanism, a layer of PDMS adhered to the device should then thermally expand. This is the basic concept behind the proposed OEH device, which can be applied to use in active PPL.

To fabricate the device layers for sufficient thermal response, careful optimization and development was required. Material deposition used conventional photolithography methods using a positive tone photoresist and a UV mask aligner, electron beam evaporation for SiO<sub>2</sub>, Cr, Pt, Ag, and Au deposition, Buffer HF to wet-etch SiO<sub>2</sub>, and RIE etching for dry etching of the a-Si:H. The efficacy of the device was first measured using an electrometer and probe station combined with an LED light source (**Figure 5.7**). Because amorphous silicon absorbs best at 629 nm (red), a red LED was integrated with the DMD projector as the light source. After electrometer measurements, a thin film (100 μm) of un-cured Slygard 184 PDMS was spin-coated onto the device for uniform thickness, and then thermally cured. Portions of PDMS were very carefully removed from the device using a razor blade in order to provide access to the electrical contact pads. The heating capability of the device was then characterized using an infrared (IR) camera equipped with a high-resolution lens for micron-scale imaging. Finally, the expansion of the PDMS under light-illumination was measured by placing the illuminated,

biased device underneath an AFM cantilever and measuring the deflection of the cantilever as a function of time.

In order to demonstrate effective active PPL patterning, continued optimization of the device will need to be done. To improve response times of the PDMS, a PPL array must be deposited onto the device and measured to correct for the shape when measuring volumetric expansion. Once appropriate volumetric expansion response magnitudes and times is exhibited, then the device must be integrated with an existing BPL tool such as the TERA-fab E-Series instrument. The DMD and scanning probe platform, along with a functionality for alignment of the pen array with a substrate via determination of electrical contact points, will enable full realization of arbitrary high-throughput nanoscale patterning of hard or soft materials, as has been shown in actuated BPL.

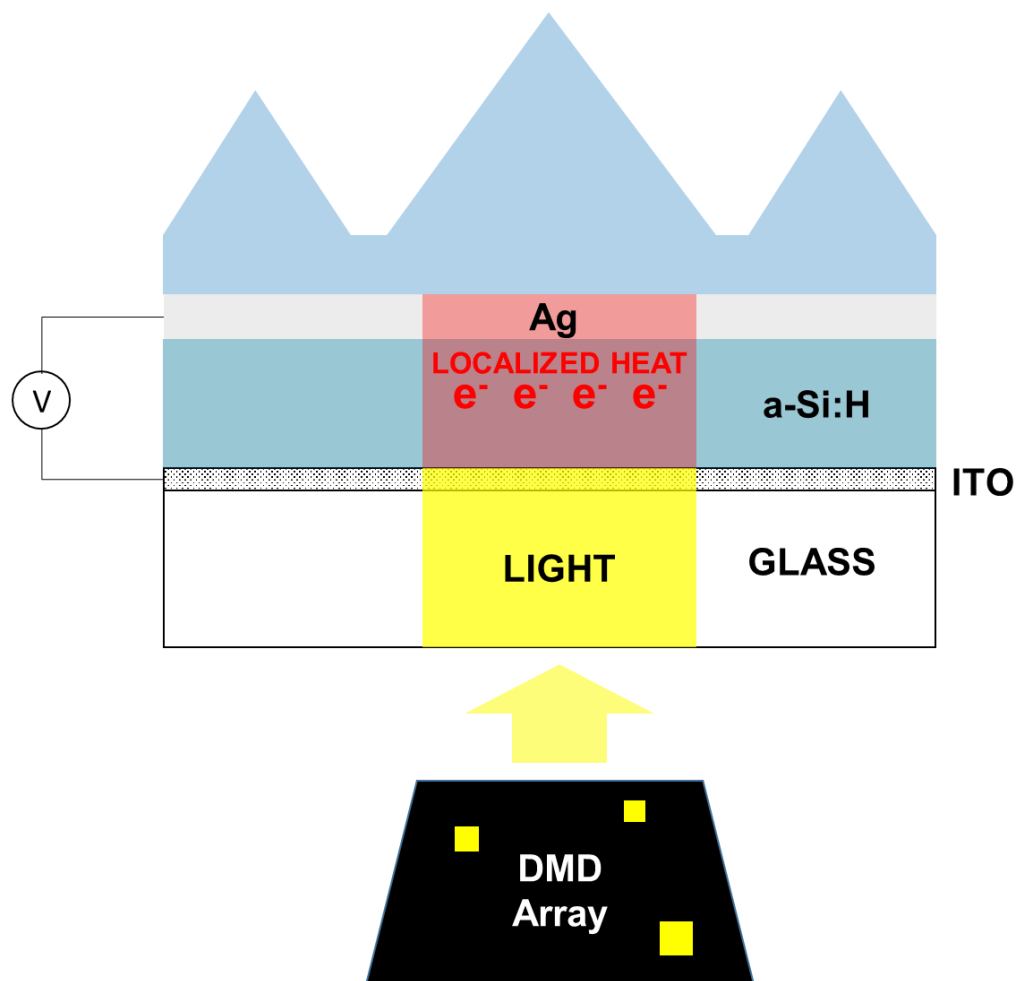


**Figure 5.6.** Schematic of active PPL design. A potential is applied across a transparent conducting oxide layer (i.e., ITO) and a reflective metal layer (i.e., Ag), with a mostly insulating layer of photoconductive hydrogenated amorphous silicon (a-Si:H) in between. By guiding the flow of electrons through the a-Si:H layer, the resistive heating can be localized to micron-scale regions, thereby thermally expanding each PDMS pen sitting atop that region.

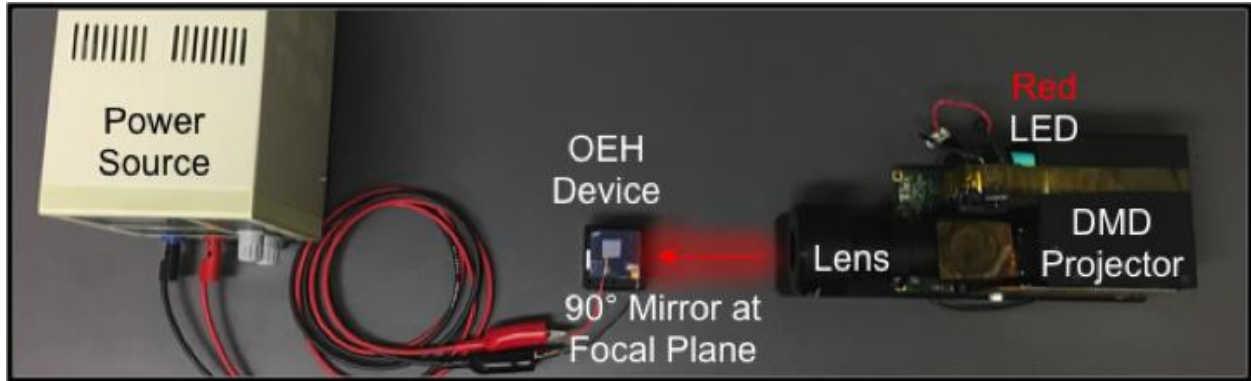


**Figure 5.7.** The setup used for characterization of the optoelectronic heating (OEH) device is shown where an external power source applies a potential to the contact pads of the two electrodes; meanwhile, a DMD projects light from a red LED orthogonal to the device in order to illuminate the amorphous silicon. Measurements from an AFM cantilever, infrared (IR) camera, or probe station would be collected from above the device.

### 5.3 Optoelectronic Heating Device

To successfully achieve high-resolution heating and conductivity control using low-power light from a DMD, inspiration was drawn from work in amorphous silicon thin film solar cells, optoelectronic tweezer devices, and an optoelectronic heating device made in a prior work showing micron-scale heating control for melting of a layer of hexadecane, which melts at 18 °C.<sup>88</sup> These devices tend to use a “sandwich” structure of two thin film electrodes above and below an a-Si:H light absorbing layer. The bottom electrode is a transparent conductor such as ITO, which enables direct illumination of the a-Si:H, and the top electrode is highly reflective, such as Ag or Au, effectively doubling the number of photons absorbed by the device. A potential bias is applied between the electrodes, inducing an electric field across the photoconducting a-Si:H. Localized light will then create charge carriers (higher conductivity) in the semiconductor layer that are accelerated by the electric field. These charge carriers produce heat by the Joule effect, so power for heating draws upon the electric field rather than the light itself.

Due to the possibility of lateral heat transfer and area crosstalk, the thermal conductivity of a-Si:H is important, which is low and reportedly between  $0.1 \text{ Wm}^{-1}\text{K}^{-1}$  and  $2.6 \text{ Wm}^{-1}\text{K}^{-1}$ .<sup>83,90</sup> a-Si:H can also absorb light efficiently so that low thicknesses can be used. One-micron films have been shown to have high absorption of  $10^{-4} \text{ cm}^{-1}$  at 630 nm.<sup>83</sup> In contrast, crystalline Si would need 30  $\mu\text{m}$  thickness for efficient light absorption, and it has much higher thermal conductivity at  $140 \text{ Wm}^{-1}\text{K}^{-1}$  as well.

Because heat in the device is generated by the Joule effect, heating power is dependent on the electrical current and voltage bias, as  $P=IV$ . Therefore, when measuring the device's I-V

curve, we can also get an understanding for the expected heat differential. The key in this case is a high contrast between light and dark currents. As such, when fabricating the device, a 5 nm layer of n<sup>+</sup>-doped a-Si:H is added between the ITO and intrinsic semiconductor layers, in order to provide better Ohmic contact. However, a rectifying junction is still necessary in order to provide high photocurrent contrast. This comes from the Schottky contact between the semiconductor and the Ag/Au electrode,<sup>91</sup> and it has been reported for a-Si:H photo-sensitive applications many times. The reason there is one ohmic contact and one Schottky contact is that dark currents will be greatly influenced by the Schottky barrier and photocurrents less -so. High forward bias tends to reduce such barriers since the depletion region tends to decrease at higher potentials. Also, at high potentials the current becomes series-resistance limited,<sup>91</sup> and that signifies high heat generation in the device.

The next greatest challenge when fabricating the layers of the device involves shunt currents. Because of the relatively low-quality PECVD deposition of a-Si:H, pinholes which create shunt currents are possible. By depositing 500 nm SiO<sub>2</sub>, then wet-etching it with Buffered HF, the shunt currents are effectively filled in. This can later be combined with the addition of a thin (~50 nm) SiO<sub>2</sub> barrier between pen areas for further thermal/electrical isolation. Furthermore, the top electrode includes a 10 nm layer of Cr for adhesion and 50 nm layer of Pt as an atomic diffusion barrier to the Ag, at 100 nm thickness. After electrode deposition, an area of the chip is etched using RIE, and Au metal contacts with a Cr adhesive layer are deposited as well. These steps are shown in **Figure 5.8**.

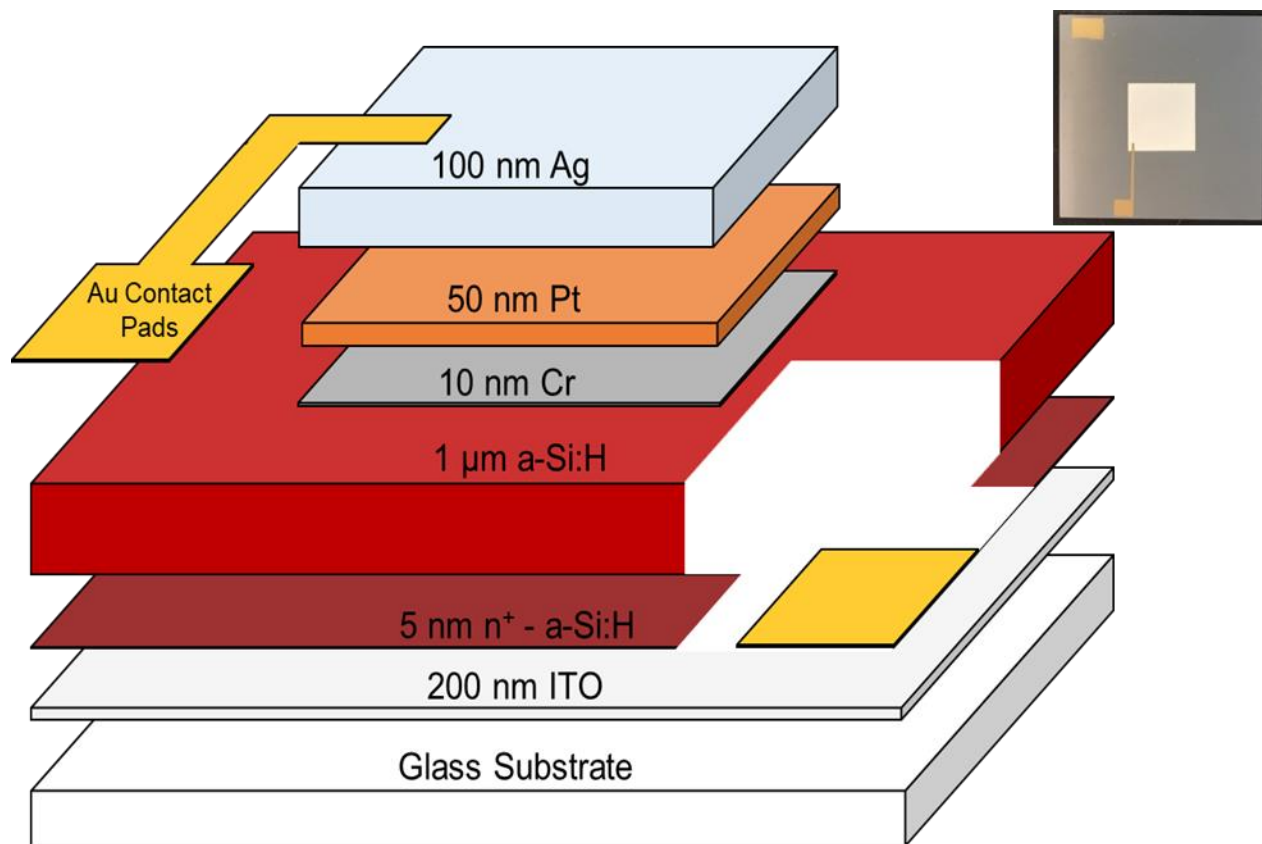


**Figure 5.8.** Layers of thin film deposition are shown for OEH device fabrication. An example of a completed device is shown in the corner of the figure.

The I-V characteristics of the device were measured using a Keithley Source Meter and probe station, shown in **Figure 5.9** along with the characteristic from the device used in the literature. It is important to notice the rectifying behavior shown in the dark current and the large difference in contrast between light and dark currents, which will induce proper high-resolution heating effects. In **Figure 5.10**, more electronic measurements are shown, including a variable light source intensity as well as a time-response study. It is clear that we are operating near saturation and that there is precision control of the conductivity based on light. Also, the time

response was measured to be less than 10 ms, which indicates that the photo-response of the device will not be a time-limiting factor when applying the device to an actuating pen array.

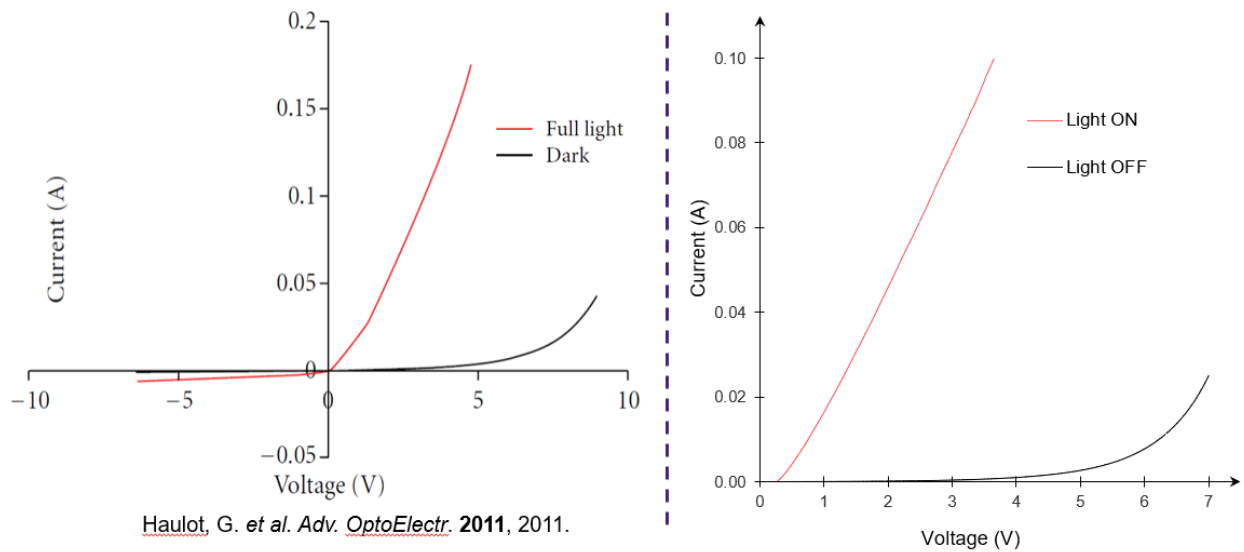


**Figure 5.9.** I-V profile of OEH device was measured on the right, and the literature result is shown on the left for visual comparison.

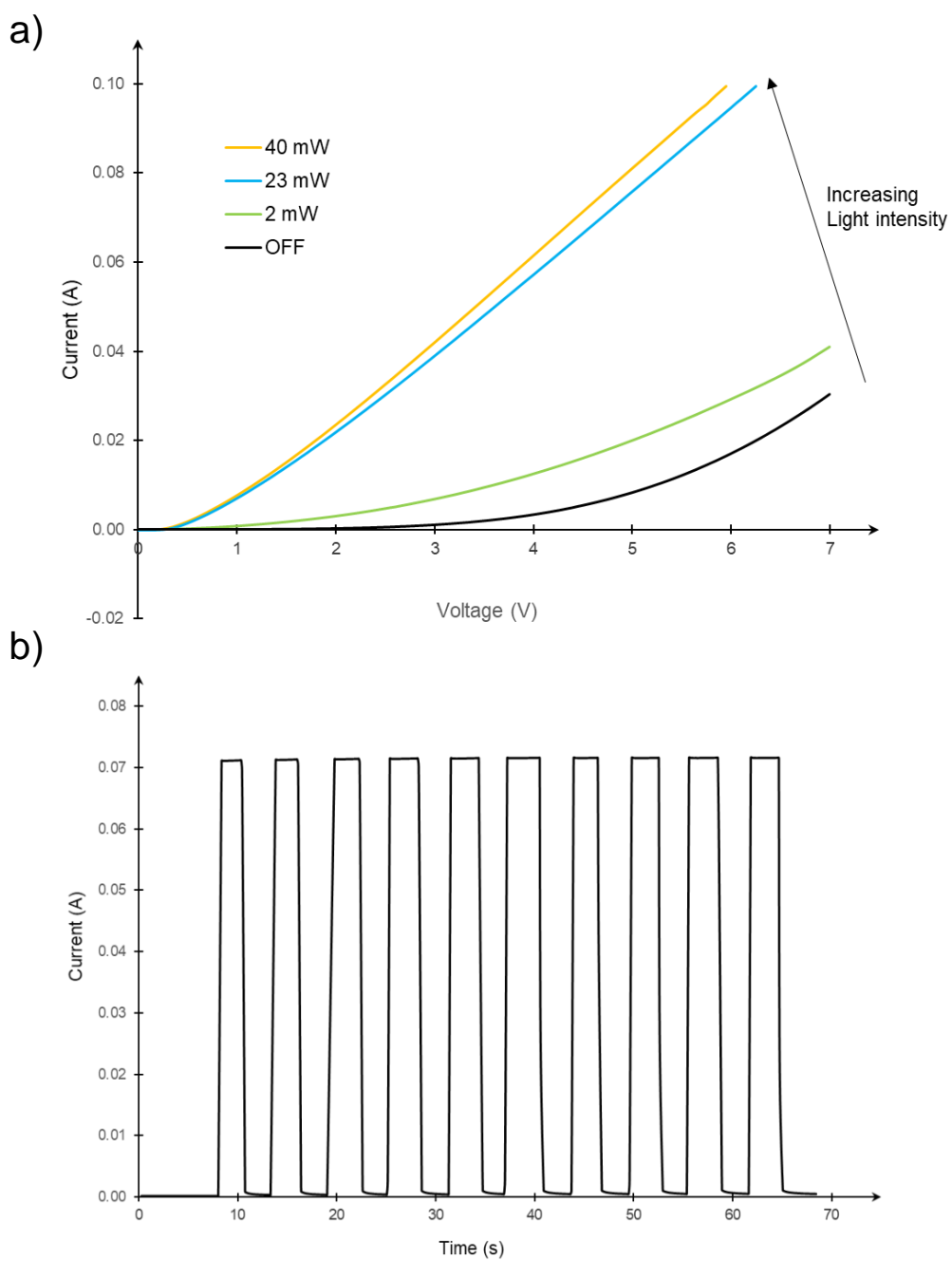


**Figure 5.10.** More electronic properties of the OEH device were measured, including a) response to different light intensities, and b) time-response of the photocurrent.

In order to use the device for active PPL, it should generate enough heat to thermally expand PDMS. This effect was measured using a thin film (100  $\mu\text{m}$ ) of PDMS spin-coated onto the device. This thickness is what is typically used as a backing layer in PPL, though it can be adjusted. The expansion was measured using contact-mode AFM, shown in **Figure 5.11**. The time response can be improved still, but this can be expected to decrease dramatically once the geometry of the PDMS is changed and the thickness is optimized.

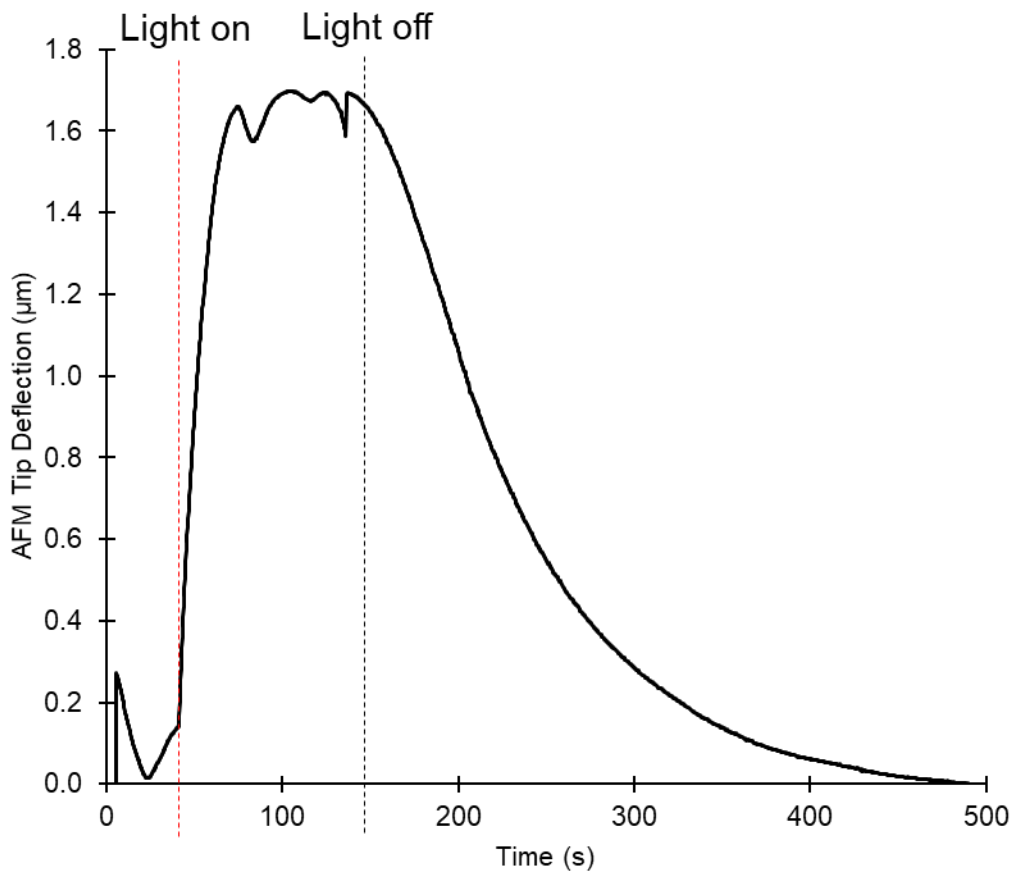


**Figure 5.11.** The AFM tip deflection over a layer of expanding PDMS is shown over time. The markers indicate when light is turned on (red) and off (black).

## 5.4 Future prospects

The design of the optoelectronic heater discussed in this proposal was inspired by the literature, including the development of optoelectronic tweezers, and optimized for the active PPL system.<sup>84,86,88</sup> Using a photo-conductive material and an applied voltage bias, the joule heating effect is triggered in illuminated regions of the material. To achieve this effect, several different photoconductors were investigated, such as CdS or conductive polymers like polyvinylcarbazole. Hydrogenated amorphous silicon is unique among these because of its highly tunable, disparate light and dark conductivities, which enable its function as an insulator in the dark and as a heat-producing resistor in the light. In order to model this system and the thermal dissipation across the active PPL device, finite element modeling can be used. Simulation software will enable modeling of the electrical properties, thermal conductivity, and thermal expansion of every layer within the device architecture.

Further improvement of this device may incorporate insulation between tips such that crosstalk is minimized, for example by patterning SiO<sub>2</sub> between each pen through photolithography. In addition, a thermoelectric cooler may be integrated into the system as the backing layer of the ITO (or sapphire), such that the retraction time may be quickened, and enabling improved precision control of the temperature of the pens over time. Both of these concepts are illustrated in **Figure 5.12**.

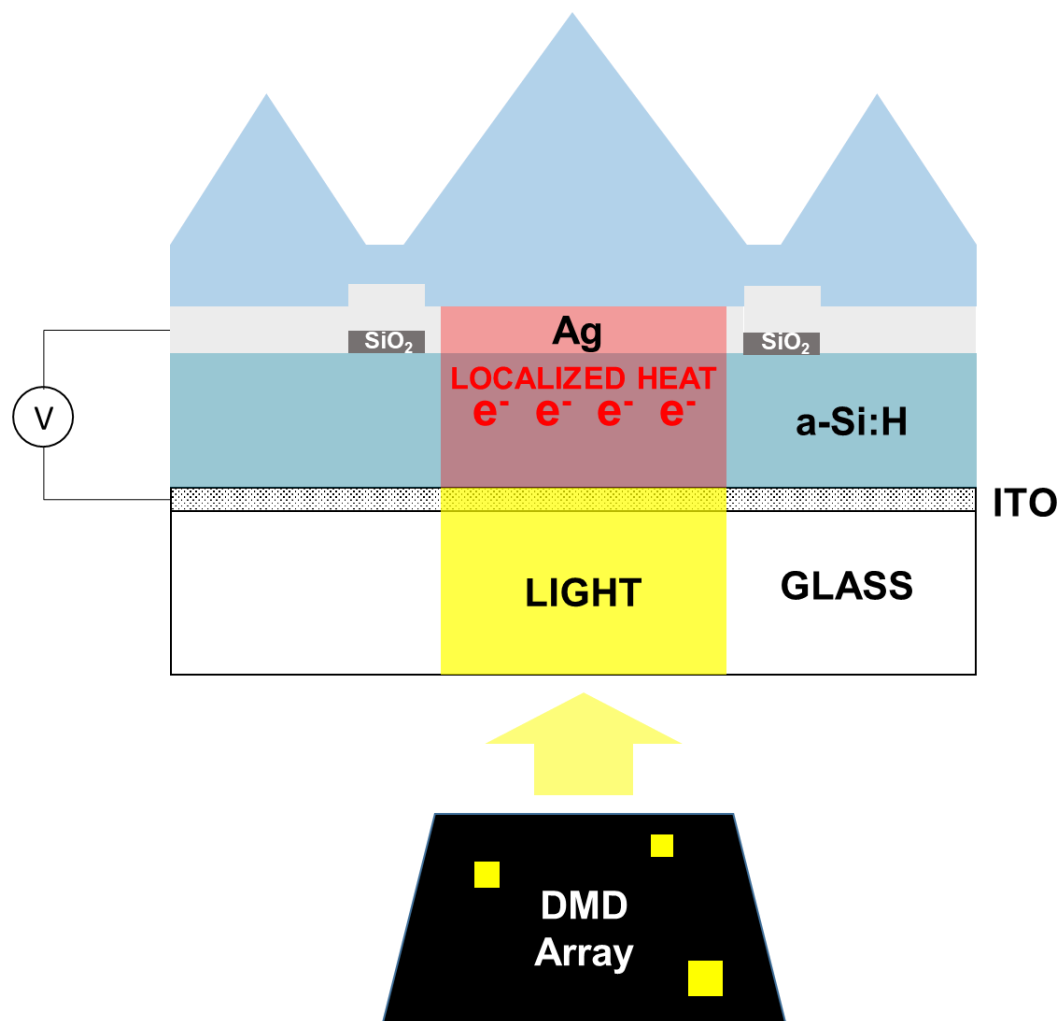


**Figure 5.12.** Schematic depicting how insulating features may be patterned between pens on the Ag backing layer, and a thermoelectric cooler may be integrated for improved reaction time and overall temperature control.

Upon successful demonstration of an OEH device that can control conductivity microscopically, this mechanism can be combined with ePPL (Chapter 4) or t-PPL (Chapter 3) to develop active ePPL or t-PPL. In theory, the previously described OEH device can serve as the substrate/working electrode, where bias is applied to the ITO and only conducts electrons and reduces metal in localized regions defined by a DMD (in ePPL), or locally heats a substrate such

that thermosensitive inks only pattern at each individual location. This concept for ePPL is shown in **Figure 5.13**.

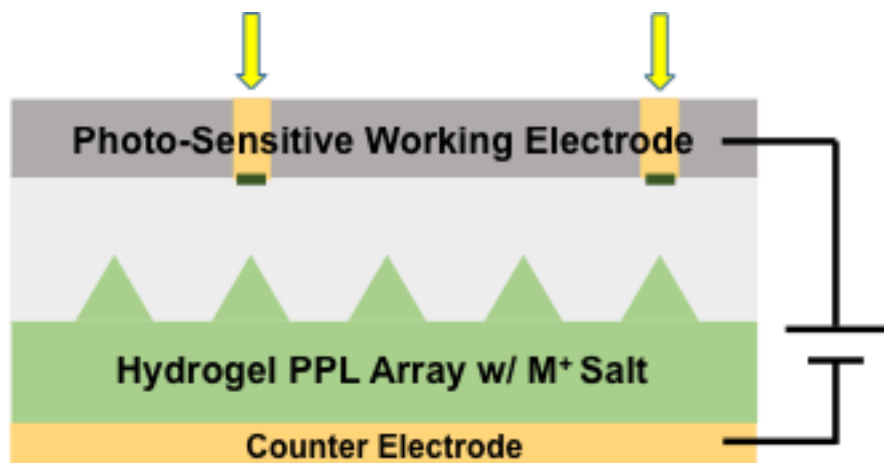


**Figure 5.13.** Basic understanding of proposed active PPL mechanism. The working electrode will be replaced with the OEH device which can use the changing conductivity to apply potential selectively in regions where patterning is to occur. In this way, ePPL patterning could become a fully functional tool for arbitrary desktop nanolithography and 3D printing of metal nanostructures.

Successful completion of a new electronically active PPL technique will introduce entirely new worlds of patterning and material designs. One interesting application would be to discover possible new plasmonic metamaterial structures using simulation and modeling and then rapidly print many different structures to experimentally discover the next most promising structure.

Another future prospect is to use electronically-active PPL to pattern multiple inks atop one another by coating each tip with a different ink by massively multiplexed inkjet printing. Then, different inks can react with one another and nanoscale chemical reactors can be observed

in a huge combinatorial library. Otherwise, inks can form on top of one another as well for use in multi-layered structures in plasmonics and electronics. Lastly, these tools would make ideal candidates for the design and fabrication of large area nanoscale electronic connections. This is enabled by the tool's unique ability to pattern with independent pens at various locations over a single substrate.

**CHAPTER SIX:**  
**CONCLUSIONS AND FUTURE OUTLOOK**

## 6.1 Summary and Conclusions

Lithography is one of the cornerstones of technological development in society. In order to synthesize, prototype, discover, and apply materials in the real world, lithography tools are crucial. As computers become smaller and nanomaterials show new promise, our collective understanding of the properties, synthesis, and applications of nanomaterials has become ever more important. For that reason, lithography must become smaller as well with technology, and tools must be developed for the widespread use of nanolithography in both research and commercial settings. In fact, lithography tools are even important for the average home user when we consider the widespread use of tools like ballpoint pens, laserjet printers, and home-use 3D printers. The development of nanolithography tools has been prolific in recent decades, but we have yet to see high-throughput nanolithography methods become widespread, versatile, inexpensive, and user-friendly. The work done in this thesis represents a small step towards that goal.

Our existing nanolithography tools work well, but they don't cover all their bases yet. Notably, CF-SPL techniques offer uniquely high-throughput arbitrary patterning, but they, too, are insufficient for truly widespread use without further fine-tuning and development. In this thesis, the architectures developed previously have been improved upon and thoroughly investigated such that they can become more widespread in terms of materials, environments, and capabilities. Beginning with negative PPL, we have expanded the capabilities of PPL to include patterning in aqueous environments and through material removal rather than deposition. t-PPL has expanded our capabilities to high-throughput thermal patterning, such that localized thermochemistries may occur at each tip over a massively parallel (>10,000 tips) scale, and

opened more avenues to high-throughput 3D nanoprinting, analogous to fused deposition modeling. The invention of ePPL has expanded our capabilities to more materials, including any metal, metal alloy, or other charged material that may be electrodeposited, and opens more avenues for 3D printing of metallic structures. Finally, the work done here towards active PPL demonstrates the potential for arbitrary patterning on a single substrate that does not repeat the same pattern at each tip location, which would enormously transform the field of CF-SPL and its usage. By the combination of both these architectures (ePPL and active PPL), we can achieve not only arbitrary electrochemical patterning but also arbitrary 3D printing of metals in the future. Likewise, this may be done with t-PPL and active PPL. These tools can be utilized to explore new plasmonic 3D metamaterials, multi-metallic features, and multi-component nanoparticle patterning over centimeter-scale areas for a desktop nanofabrication tool compatible with either academic or industrial research and advancement.

## **6.2 Future Outlook**

While all four of the methods described in this thesis have been thoroughly investigated and developed over countless iterations of troubleshooting, all of them may be further improved with more experimentation and technology development, as any good technological development might. In all four cases, resolution, materials exploration, z-direction printing, and analysis of printed materials may be further explored in order to contribute to the wealth of technology related to nanolithography. Beyond these expected improvements and investigations, however, it is important to be imaginative and creative with the directions one might take with each of these nanolithography tools.

For example, using n-PPL of PAEs, control over ordering and microfluidic flow might make complex multicomponent patterning very interesting. In that case, we can develop patterned structures made up of ordered, amorphous, different sizes, and different core material PAE assemblies all at once. Hierarchical patterns of multiple functionalities can be easily synthesized. Proteins, for example, can be made into a PAE and printed similarly. Furthermore, other materials besides PAEs could be explored for n-PPL, such as direct cellular patterning or removal of enzymes or different DNA-based assemblies.

With the invention of t-PPL, the preliminary conceptual promise is shown, but this work has barely scratched the surface of possibility. By merely observing the myriad applications of t-SPL, we know that extending this to millions of probes working in parallel, those applications could be done as well. However more interestingly, one exciting prospect lies in lab-on-a-chip style tissue engineering, but doing so with such high control over  $x$ ,  $y$ , and  $z$  directions, and so rapidly in a desktop nanofab environment, expands capabilities immensely.

ePPL, on the other hand, is a more thoroughly investigated technology, and it provides very unique capabilities that have not been previously observed. With this new method to rapidly prototype metallic structures, 3D metallic nanoprinting with high-throughput may be attainable for the first time. In addition, patterning alloyed metal nanoparticles is facile, as is controlling the size and composition across a single substrate. In this way, megalibraries with compositional and size gradients of alloys may be patterned across a single substrate, then probed for catalytic or magnetic activity, such that new materials discovery may be performed rapidly. Finally, the success of ePPL with metals indicates that any charged molecule may be patterned, as long as it can be electro-deposited and captured within a hydrogel. In this manner, all types of biological

molecules like enzymes and DNA, as well as functionalized diazonium or conducting polymers may be synthesized with high throughput and dimensional control as well as spatial-arrangement over a large-area substrate.

Finally, upon the successful completion of active PPL, one of the most significant uses of the technology lies in studies of biological materials, especially in cellular assays. For the first time, different shapes and structures can be patterned all across a single substrate, paving the way for tissue engineering and more, but also encouraging a more controlled study of cell-environment interactions, as in cell migration studies. In addition, the technology could feasibly be used towards circuit building and repairs. Lastly, this project could be utilized in a different way, as well, where the optoelectronic heater is used as the substrate rather than a backing layer, such that a new method of thermal CF-SPL is born, and localized heating can occur at each polymer pen location.

## REFERENCES

1. Brown, K. A.; Hedrick, J. L.; Eichelsdoerfer, D. J.; Mirkin, C. A. "Nanocombinatorics with Cantilever-Free Scanning Probe Arrays." *ACS Nano*. 2019.
2. Levenson, M. D.; Viswanathan, N. S.; Simpson, R. A. "Improving Resolution in Photolithography with a Phase-Shifting Mask." *IEEE Trans. Electron Devices* **1982**, *29* (12), 1828–1836.
3. Vieu, C.; Carcenac, F.; Pepin, A.; Chen, Y.; Mejias, M.; Lebib, A.; Manin-Ferlazzo, L.; Couraud, L.; Launois, H. "Electron Beam Lithography - Resolution Limits and Applications." *Appl. Surf. Sci.* **2000**, *164*, 111–117.
4. Bernard, A.; Renault, J. P.; Michel, B.; Bosshard, H. R.; Delamarche, E. "Microcontact Printing of Proteins." *Adv. Mater.* **2000**, *12* (14), 1067–1070.
5. Xia, Y.; Whitesides, G. M. "SOFT LITHOGRAPHY." *Annu. Rev. Mater. Sci.* **1998**, *28* (1), 153–184.
6. Garcia, R.; Knoll, A. W.; Riedo, E. "Advanced Scanning Probe Lithography." *Nature Nanotechnology*. 2014, pp 577–587.
7. Piner, R. D. "'Dip-Pen' Nanolithography." *Science (80-. )*. **1999**, *283* (5402), 661–663.
8. Ginger, D. S.; Zhang, H.; Mirkin, C. A. "The Evolution of Dip-Pen Nanolithography." *Angewandte Chemie - International Edition*. 2004, pp 30–45.
9. Huo, F.; Zheng, Z.; Zheng, G.; Giam, L. R.; Zhang, H.; Mirkin, C. A. "Polymer Pen Lithography." *Science (80-. )*. **2008**, *321* (5896), 1658–1660.

10. Eichelsdoerfer, D. J.; Liao, X.; Cabezas, M. D.; Morris, W.; Radha, B.; Brown, K. A.; Giam, L. R.; Braunschweig, A. B.; Mirkin, C. A. "Large-Area Molecular Patterning with Polymer Pen Lithography." *Nat. Protoc.* **2013**, 8 (12), 2548–2560.
11. Braunschweig, A. B.; Huo, F.; Mirkin, C. A. "Molecular Printing." *Nat. Chem.* **2009**.
12. Kluender, E. J.; Hedrick, J. L.; Brown, K. A.; Rao, R.; Meckes, B.; Du, J. S.; Moreau, L. M.; Maruyama, B.; Mirkin, C. A. "Catalyst Discovery through Megalibraries of Nanomaterials." *Proc. Natl. Acad. Sci. U. S. A.* **2019**.
13. Cabezas, M. D.; Eichelsdoerfer, D. J.; Brown, K. A.; Mrksich, M.; Mirkin, C. A. "Combinatorial Screening of Mesenchymal Stem Cell Adhesion and Differentiation Using Polymer Pen Lithography." *Methods Cell Biol.* **2014**, 119, 261–276.
14. Giam, L. R.; Mirkin, C. A. "Cantilever-Free Scanning Probe Molecular Printing." *Angewandte Chemie - International Edition.* 2011.
15. Cabezas, M. D.; Meckes, B.; Mirkin, C. A.; Mrksich, M. "Subcellular Control over Focal Adhesion Anisotropy, Independent of Cell Morphology, Dictates Stem Cell Fate." *ACS Nano* **2019**.
16. Chai, J.; Huo, F.; Zheng, Z.; Giam, L. R.; Shim, W.; Mirkin, C. a. "Scanning Probe Block Copolymer Lithography." *Proc. Natl. Acad. Sci. U. S. A.* **2010**, 107 (47), 20202–20206.
17. Chen, P.-C.; Liu, G.; Zhou, Y.; Brown, K. a.; Chernyak, N.; Hedrick, J. L.; He, S.; Xie, Z.; Lin, Q.-Y.; Dravid, V. P.; et al. "Tip-Directed Synthesis of Multimetallic Nanoparticles." *J. Am. Chem. Soc.* **2015**, 150706082404002.

18. Chen, P. C.; Liu, X.; Hedrick, J. L.; Xie, Z.; Wang, S.; Lin, Q. Y.; Hersam, M. C.; Dravid, V. P.; Mirkin, C. A. "Polyelemental Nanoparticle Libraries." *Science* (80-. ). **2016**.
19. Chen, P. C.; Liu, M.; Du, J. S.; Meckes, B.; Wang, S.; Lin, H.; Dravid, V. P.; Wolverton, C.; Mirkin, C. A. "Interface and Heterostructure Design in Polyelemental Nanoparticles." *Science* (80-. ). **2019**.
20. Shim, W.; Braunschweig, A. B.; Liao, X.; Chai, J.; Lim, J. K.; Zheng, G.; Mirkin, C. A. "Hard-Tip, Soft-Spring Lithography." *Nature* **2011**.
21. Hedrick, J. L.; Brown, K. A.; Kluender, E. J.; Cabezas, M. D.; Chen, P. C.; Mirkin, C. A. "Hard Transparent Arrays for Polymer Pen Lithography." *ACS Nano* **2016**.
22. Shim, W.; Brown, K. A.; Zhou, X.; Rasin, B.; Liao, X.; Mirkin, C. A. "Multifunctional Cantilever-Free Scanning Probe Arrays Coated with Multilayer Graphene." *Proc. Natl. Acad. Sci. U. S. A.* **2012**.
23. Huo, F.; Zheng, G.; Liao, X.; Giam, L. R.; Chai, J.; Chen, X.; Shim, W.; Mirkin, C. A. "Beam Pen Lithography." *Nat. Nanotechnol.* **2010**, 5 (9), 637–640.
24. Liao, X.; Brown, K. A.; Schmucker, A. L.; Liu, G.; He, S.; Shim, W.; Mirkin, C. A. "Desktop Nanofabrication with Massively Multiplexed Beam Pen Lithography." *Nat. Commun.* **2013**, 4.
25. Xie, Z.; Gordiichuk, P.; Lin, Q. Y.; Meckes, B.; Chen, P. C.; Sun, L.; Du, J. S.; Zhu, J.; Liu, Y.; Dravid, V. P.; et al. "Solution-Phase Photochemical Nanopatterning Enabled by High-Refractive-Index Beam Pen Arrays." *ACS Nano* **2017**.

26. Carbonell, C.; Valles, D. J.; Wong, A. M.; Tsui, M. W.; Niang, M.; Braunschweig, A. B. “Massively Multiplexed Tip-Based Photochemical Lithography under Continuous Capillary Flow.” *Chem* **2018**, *4* (4), 857–867.
27. Carbonell, C.; Valles, D.; Wong, A. M.; Carlini, A. S.; Touve, M. A.; Korpanty, J.; Gianneschi, N. C.; Braunschweig, A. B. “Polymer Brush Hypersurface Photolithography.” *Nat. Commun.* **2020**.
28. Valles, D. J.; Naeem, Y.; Carbonell, C.; Wong, A. M.; Mootoo, D. R.; Braunschweig, A. B. “Maskless Photochemical Printing of Multiplexed Glycan Microarrays for High-Throughput Binding Studies.” *ACS Biomater. Sci. Eng.* **2019**.
29. Talapin, D. V.; Shevchenko, E. V. “Introduction: Nanoparticle Chemistry.” *Chemical Reviews*. 2016.
30. Khan, I.; Saeed, K.; Khan, I. “Nanoparticles: Properties, Applications and Toxicities.” *Arabian Journal of Chemistry*. 2019.
31. Kagan, C. R.; Lifshitz, E.; Sargent, E. H.; Talapin, D. V. “Building Devices from Colloidal Quantum Dots.” *Science* (80-. ). **2016**.
32. Boles, M. A.; Engel, M.; Talapin, D. V. “Self-Assembly of Colloidal Nanocrystals: From Intricate Structures to Functional Materials.” *Chemical Reviews*. 2016.
33. Isaacoff, B. P.; Brown, K. A. “Progress in Top-Down Control of Bottom-Up Assembly.” *Nano Letters*. 2017.
34. Laramy, C. R.; O’Brien, M. N.; Mirkin, C. A. “Crystal Engineering with DNA.” *Nature*

*Reviews Materials*. 2019.

35. Macfarlane, R. J.; Lee, B.; Jones, M. R.; Harris, N.; Schatz, G. C.; Mirkin, C. A. “Nanoparticle Superlattice Engineering with DNA.” *Science* (80-. ). **2011**.
36. Senesi, A. J.; Eichelsdoerfer, D. J.; Macfarlane, R. J.; Jones, M. R.; Auyeung, E.; Lee, B.; Mirkin, C. A. “Stepwise Evolution of DNA-Programmable Nanoparticle Superlattices.” *Angew. Chemie - Int. Ed.* **2013**.
37. Wang, M. X.; Seo, S. E.; Gabrys, P. A.; Fleischman, D.; Lee, B.; Kim, Y.; Atwater, H. A.; Macfarlane, R. J.; Mirkin, C. A. “Epitaxy: Programmable Atom Equivalents Versus Atoms.” *ACS Nano* **2017**.
38. Lin, Q. Y.; Mason, J. A.; Li, Z.; Zhou, W.; O’Brien, M. N.; Brown, K. A.; Jones, M. R.; Butun, S.; Lee, B.; Dravid, V. P.; et al. “Building Superlattices from Individual Nanoparticles via Template-Confined DNA-Mediated Assembly.” *Science* (80-. ). **2018**.
39. Howell, S. T.; Grushina, A.; Holzner, F.; Brugger, J. “Thermal Scanning Probe Lithography—a Review.” *Microsystems and Nanoengineering*. 2020.
40. Paul, P. C. “Thermal Scanning Probe Lithography.” In *Frontiers of Nanoscience*; 2016.
41. Cheong, L. L.; Paul, P.; Holzner, F.; Despont, M.; Coady, D. J.; Hedrick, J. L.; Allen, R.; Knoll, A. W.; Duerig, U. “Thermal Probe Maskless Lithography for 275 Nm Half-Pitch Si Technology.” *Nano Lett.* **2013**.
42. Mamin, H. J.; Rugar, D. “Thermomechanical Writing with an Atomic Force Microscope Tip.” *Appl. Phys. Lett.* **1992**.

43. Carroll, K. M.; Lu, X.; Kim, S.; Gao, Y.; Kim, H. J.; Somnath, S.; Polloni, L.; Sordan, R.; King, W. P.; Curtis, J. E.; et al. "Parallelization of Thermochemical Nanolithography." *Nanoscale* **2014**.
44. Vettiger, P.; Despont, M.; Drechsler, U.; Durig, U.; Haberle, W.; Lutwyche, M. I.; Rothuizen, H. E.; Stutz, R.; Widmer, R.; Binnig, G. K. "The 'Millipede'—More than Thousand Tips for Future AFM Storage." *IBM J. Res. Dev.* **2000**, *44* (3), 323–340.
45. Lee, W. K.; Dai, Z.; King, W. P.; Sheehan, P. E. "Maskless Nanoscale Writing of Nanoparticle-Polymer Composites and Nanoparticle Assemblies Using Thermal Nanoprobes." *Nano Lett.* **2010**.
46. Zhu, J.; Hu, L.; Zhao, P.; Lee, L. Y. S.; Wong, K. Y. "Recent Advances in Electrocatalytic Hydrogen Evolution Using Nanoparticles." *Chemical Reviews*. 2020.
47. Boken, J.; Khurana, P.; Thatai, S.; Kumar, D.; Prasad, S. "Plasmonic Nanoparticles and Their Analytical Applications: A Review." *Applied Spectroscopy Reviews*. 2017.
48. Neiva, E. G. C.; Oliveira, M. M.; Bergamini, M. F.; Marcolino, L. H.; Zarbin, A. J. G. "One Material, Multiple Functions: Graphene/Ni(OH)<sub>2</sub> Thin Films Applied in Batteries, Electrochromism and Sensors." *Sci. Rep.* **2016**.
49. Vazquez-Mena, O.; Sannomiya, T.; Villanueva, L. G.; Voros, J.; Brugger, J. "Metallic Nanodot Arrays by Stencil Lithography for Plasmonic Biosensing Applications." *ACS Nano* **2011**.
50. Huang, L.; Chen, P. C.; Liu, M.; Fu, X.; Gordiichuk, P.; Yu, Y.; Wolverton, C.; Kang, Y.;

- Mirkin, C. A. “Catalyst Design by Scanning Probe Block Copolymer Lithography.” *Proc. Natl. Acad. Sci. U. S. A.* **2018**.
51. Mahenderkar, N. K.; Chen, Q.; Liu, Y. C.; Duchild, A. R.; Hofheins, S.; Chason, E.; Switzer, J. A. “Epitaxial Lift-off of Electrodeposited Single-Crystal Gold Foils for Flexible Electronics.” *Science* (80-. ). **2017**.
52. Yan, Z.; Sun, H.; Chen, X.; Liu, H.; Zhao, Y.; Li, H.; Xie, W.; Cheng, F.; Chen, J. “Anion Insertion Enhanced Electrodeposition of Robust Metal Hydroxide/Oxide Electrodes for Oxygen Evolution.” *Nat. Commun.* **2018**.
53. Therese, G. H. A.; Kamath, P. V. “Electrochemical Synthesis of Metal Oxides and Hydroxides.” *Chemistry of Materials*. 2000.
54. Hirt, L.; Ihle, S.; Pan, Z.; Dorwling-Carter, L.; Reiser, A.; Wheeler, J. M.; Spolenak, R.; Vörös, J.; Zambelli, T. “Template-Free 3D Microprinting of Metals Using a Force-Controlled Nanopipette for Layer-by-Layer Electrodeposition.” *Adv. Mater.* **2016**, 28 (12), 2311–2315.
55. Xu, J.; Ren, W.; Lian, Z.; Yu, P.; Yu, H. “A Review: Development of the Maskless Localized Electrochemical Deposition Technology.” *Int. J. Adv. Manuf. Technol.* **2020**.
56. Li, Y.; Maynor, B. W.; Liu, J. “Electrochemical AFM ‘Dip-Pen’ Nanolithography [24].” *Journal of the American Chemical Society*. 2001.
57. Eliyahu, D.; Gileadi, E.; Galun, E.; Eliaz, N. “Atomic Force Microscope-Based Meniscus-Confined Three-Dimensional Electrodeposition.” *Adv. Mater. Technol.* **2020**.

58. Chen, M.; Lee, H.; Yang, J.; Xu, Z.; Huang, N.; Chan, B. P.; Kim, J. T. “Parallel, Multi-Material Electrohydrodynamic 3D Nanoprinting.” *Small* **2020**.
59. Hu, J.; Yu, M. F. “Meniscus-Confined Three-Dimensional Electrodeposition for Direct Writing of Wire Bonds.” *Science* (80-. ). **2010**.
60. Hirt, L.; Grüter, R. R.; Berthelot, T.; Cornut, R.; Vörös, J.; Zambelli, T. “Local Surface Modification via Confined Electrochemical Deposition with FluidFM.” *RSC Adv.* **2015**.
61. Seol, S. K.; Kim, D.; Lee, S.; Kim, J. H.; Chang, W. S.; Kim, J. T. “Electrodeposition-Based 3D Printing of Metallic Microarchitectures with Controlled Internal Structures.” *Small* **2015**, *11* (32), 3896–3902.
62. Seol, S. K.; Pyun, A. R.; Hwu, Y.; Margaritondo, G.; Je, J. H. “Localized Electrochemical Deposition of Copper Monitored Using Real-Time X-Ray Microradiography.” *Adv. Funct. Mater.* **2005**.
63. Kang, H.; Hwang, S.; Kwak, J. “A Hydrogel Pen for Electrochemical Reaction and Its Applications for 3D Printing.” *Nanoscale* **2015**, *7* (3), 994–1001.
64. Yun, C.; Kang, H.; Kwak, J.; Hwang, S. “Do-It-Yourself Pyramidal Mold for Nanotechnology.” *ACS Omega* **2019**.
65. Chen, X.; Liu, X.; Ouyang, M.; Chen, J.; Taiwo, O.; Xia, Y.; Childs, P. R. N.; Brandon, N. P.; Wu, B. “Multi-Metal 4D Printing with a Desktop Electrochemical 3D Printer.” *Sci. Rep.* **2019**.
66. Reiser, A.; Lindén, M.; Rohner, P.; Marchand, A.; Galinski, H.; Sologubenko, A. S.;

- Wheeler, J. M.; Zenobi, R.; Poulikakos, D.; Spolenak, R. “Multi-Metal Electrohydrodynamic Redox 3D Printing at the Submicron Scale.” *Nat. Commun.* **2019**.
67. Rozhok, S.; Piner, R.; Mirkin, C. A. “Dip-Pen Nanolithography: What Controls Ink Transport?” *J. Phys. Chem. B* **2003**.
68. Brown, K. A.; Eichelsdoerfer, D. J.; Liao, X.; He, S.; Mirkin, C. A. “Material Transport in Dip-Pen Nanolithography.” *Frontiers of Physics*. 2014.
69. Ovshinsky, S. R.; Fetcenko, M. A.; Ross, J. “A Nickel Metal Hydride Battery for Electric Vehicles.” *Science (80-. )*. **1993**.
70. Jana, M.; Sivakumar, P.; Kota, M.; Jung, M. G.; Park, H. S. “Phase- and Interlayer Spacing-Controlled Cobalt Hydroxides for High Performance Asymmetric Supercapacitor Applications.” *J. Power Sources* **2019**.
71. Diehl, K. A.; Foley, J. D.; Nealey, P. F.; Murphy, C. J. “Nanoscale Topography Modulates Corneal Epithelial Cell Migration.” *J. Biomed. Mater. Res. - Part A* **2005**, 75 (3), 603–611.
72. Mahmud, G.; Campbell, C. J.; Bishop, K. J. M.; Komarova, Y. A.; Chaga, O.; Soh, S.; Huda, S.; Kandere-Grzybowska, K.; Grzybowski, B. A. “Directing Cell Motions on Micropatterned Ratchets.” *Nat. Phys.* **2009**, 5 (8), 606–612.
73. Cabezas, M. D.; Mirkin, C. A.; Mrksich, M. “Nanopatterned Extracellular Matrices Enable Cell-Based Assays with a Mass Spectrometric Readout.” *Nano Lett.* **2017**, 17 (3), 1373–1377.

74. Watanabe, T.; Akiyama, M.; Totani, K.; Kuebler, S. M.; Stellacci, F.; Wenseleers, W.; Braun, K.; Marder, S. R.; Perry, J. W. "Photoresponsive Hydrogel Microstructure Fabricated by Two-Photon Initiated Polymerization." *Adv. Funct. Mater.* **2002**, *12* (9), 611–614.
75. White, T. J.; Broer, D. J. "Programmable and Adaptive Mechanics with Liquid Crystal Polymer Networks and Elastomers." *Nat. Mater.* **2015**, *14* (11), 1087–1098.
76. Salaita, K.; Mirkin, C. A. "Massively Parallel Dip-Pen Nanolithography with 55000-Pen Two-Dimensional Arrays." *Angew. Chemie-International Ed.* **2006**, *45* (43), 7220–7223.
77. Wang, X. F.; Bullen, D. A.; Zou, J.; Liu, C.; Mirkin, C. A. "Thermally Actuated Probe Array for Parallel Dip-Pen Nanolithography." *J. Vac. Sci. Technol. B* **2004**, *22* (6), 2563–2567.
78. Bullen, D.; Liu, C. "Electrostatically Actuated Dip Pen Nanolithography Probe Arrays." *Sensors Actuators, A Phys.* **2006**, *125* (2), 504–511.
79. Bullen, D.; Chung, S. W.; Wang, X.; Zou, J.; Mirkin, C. A.; Liu, C. "Parallel Dip-Pen Nanolithography with Arrays of Individually Addressable Cantilevers." *Appl. Phys. Lett.* **2004**, *84* (5), 789–791.
80. Han, Y.; Liu, C. "Pneumatically Actuated Active Polymer Pen Lithography." *Sensors Actuators, A Phys.* **2011**, *167* (2), 433–437.
81. Brown, K. A.; Eichelsdoerfer, D. J.; Shim, W.; Rasin, B.; Radha, B.; Liao, X.; Schmucker, A. L.; Liu, G.; Mirkin, C. A. "A Cantilever-Free Approach to Dot-Matrix Nanoprinting."

- Proc. Natl. Acad. Sci.* **2013**, *110* (32), 12921–12924.
82. Huang, Z.; Li, L.; Zhang, X. A.; Alsharif, N.; Wu, X.; Peng, Z.; Cheng, X.; Wang, P.; Brown, K. A.; Wang, Y. H. “Photoactuated Pens for Molecular Printing.” *Adv. Mater.* **2018**, *30* (8).
  83. Street, R. A. “Hydrogenated Amorphous Silicon.” *Cambridge Univ. Press* **1991**, No. 2, 62–91.
  84. Chiou, P. Y.; Chang, Z.; Wu, M. C. “Droplet Manipulation with Light on Optoelectrowetting Device.” *J. Microelectromechanical Syst.* **2008**, *17* (1), 133–138.
  85. Chiou, P. Y.; Park, S. Y.; Wu, M. C. “Continuous Optoelectrowetting for Picoliter Droplet Manipulation.” *Appl. Phys. Lett.* **2008**, *93* (22).
  86. Park, S.-Y.; Teitell, M. A.; Chiou, E. P. Y. “Single-Sided Continuous Optoelectrowetting (SCOEW) for Droplet Manipulation with Light Patterns.” *Lab Chip* **2010**, *10* (13), 1655.
  87. Chiou, P.; Ohta, A.; Wu, M. “Massively Parallel Manipulation of Single Cells and Microparticles Using Optical Images.” *Nature* **2005**, *436* (July), 370–372.
  88. Haulot, G.; Ho, C. M. “Optoelectronic Heating for Fabricating Microfluidic Circuitry.” *Adv. Optoelectron.* **2011**, *2011*.
  89. Takeuchi, M.; Hagiwara, M.; Haulot, G.; Ho, C. M. “Reconfigurable Microfluidic Pump Enabled by Opto-Electrical-Thermal Transduction.” *Appl. Phys. Lett.* **2013**, *103* (17).
  90. Attaf, N.; Aida, M. S.; Hadjeris, L. “Thermal Conductivity of Hydrogenated Amorphous Silicon.” *Solid State Commun.* **2001**, *120* (12), 525–530.

91. Heller, D. E.; Dawson, R. M.; Malone, C. T.; Nag, S.; Wronski, C. R. "Electron-Transport Mechanisms in Metal Schottky Barrier Contacts to Hydrogenated Amorphous Silicon." *J. Appl. Phys.* **1992**, 72 (6), 2377–2384.

# CURRICULUM VITAE

**RUSTIN GOLNABI**

Evanston, IL 60201 USA

(201) 983-7452; rustin313@gmail.com

## EDUCATION

- **Northwestern University**, Evanston, IL; Sep 2015 – Dec 2020
  - Ph.D. in Materials Science and Engineering
- **The Johns Hopkins University**, Baltimore, MD; Sep 2012 – May 2015
  - Bachelor of Science in Materials Science and Engineering (*Concentration in Nanomaterials*)

## RESEARCH EXPERIENCE

- **Northwestern University**, Evanston, IL; Sep 2015 – Dec 2020
  - Advisor: Dr. Chad A. Mirkin
  - Collaborated with a chemist to develop a nanoscale analog to a 3D printer for use in prototyping and developing new electronic, biological, and metamaterial devices
  - Engineered an optoelectronic heater for polymer pen lithography in order to selectively print nanoparticles over a large area substrate
  - Co-wrote and edited proposals and presentations for multimillion-dollar funding from DoD for nanoscale 4D printer development while leading communications monthly with 5 lab groups across 4 different campuses
  - Mentored and advised younger students, and presented regularly at sub-group and group meetings
- **Johns Hopkins University**, Baltimore, MD; Nov 2012 – Aug 2015
  - Advisor: Dr. Robert C. Cammarata
  - Investigated A/C dielectrophoretic separation of carbon nanotubes and nanoparticles for applications in electronics

- Presented both oral and poster sessions at two international materials science conferences, and published two peer-reviewed articles
- Mobilized results and research towards founding of start-up company, NanoDirect, LLC in Baltimore, MD
- **IMEC (Inter-University Microelectronics Center)**, Leuven, Belgium; Jun 2014 – Aug 2014
  - Advisor: Dr. Pol Van Dorpe
  - Designed and evaluated Finite-Difference Time-Domain (FDTD) simulations of light propagation in Bragg mirrors and MMI devices, and performed corresponding transmission measurements in SiN waveguides for next generation photonics

### **TEACHING EXPERIENCE**

- **Northwestern Materials Science Department**, Evanston, IL; Apr 2018 – Dec 2019
  - Courses:
    - MSE 201: Introduction to Materials Science and Engineering
    - MSE 314: Thermodynamics of Materials
- **Northwestern Center for Talent Development**, Evanston, IL; Oct 2016 – Dec 2019
  - Developed and wrote three new and distinct courses in nanotechnology, engineering, and smart sensors, and taught weekend courses to gifted students grades 3-9 in the Chicagoland area

### **LEADERSHIP EXPERIENCE**

- **Northwestern Materials Science Umbrella Society (MSUS)**, Evanston, IL; Aug 2018 – Mar 2020
  - **Vice President**
  - Organized professional development events with 7-member executive board for Northwestern graduate students, and applied for and helped manage annual funding

- **Northwestern Materials Science Student Association (MSSA)**, Evanston, IL; Jul 2016 – Jul 2017
  - **President**
  - Managed a 12-member executive board to organize recruitment and orientation events, social and professional events, and fundraising for a department of over 300 students
- **Johns Hopkins Iranian Cultural Society**, Baltimore, MD; Dec 2012 – May 2015
  - **President**
  - Organized events to bring together students interested in Persian culture, in particular three events surrounding major Iranian holidays for the community in the Baltimore area, including an annual Norooz banquet event for over 300 people

## PUBLICATIONS

- EunBi Oh\*, **Rustin Golnabi\***, David A. Walker, Chad A. Mirkin. “Electrochemical Polymer Pen Lithography.” *In Preparation*.
- **Rustin Golnabi\***, Jinghan Zhu\*, Ziyi Miao, Chad A. Mirkin. “Polymer Pen Negative Lithography.” *In Preparation*.
- Liliang Huang, Haixin Lin, Cindy Y. Zheng, Edward J. Kluender, **Rustin Golnabi**, Bo Shen, Chad A. Mirkin. “Multimetallic High-Index Facet Heterostructured Nanoparticles.” *Journal of the American Chemical Society* 142 (2020).
- **Rustin Golnabi**, Su (Ike) Chih Chi, Stephen L. Farias and Robert C. Cammarata. “A Continuous Flow Device for the Purification of Semiconducting Nanoparticles by AC Dielectrophoresis.” *MRS Proceedings* 1700 (2014).
- **Rustin Golnabi**, Won Ik Lee, Deok-Yang Kim, and Glen R Kowach. “Effects of Crystallographic Planes on Focused Ion Beam Milled Patterns of Single Crystal Diamonds.” *MRS Proceedings* 1395 (2012).

- W Lee, **R Golnabi**, A Calabro, C Queenan, D Becker and D Kim. “Effect of Ion Currents on the Morphology of Focused Ion Beam Milled Patterns on a Single Crystalline Diamond.” *Microscopy and Microanalysis* 17 (Suppl. 2), pp 698-699 (2011).
- **Rustin Golnabi**, Won I. Lee, Deok-Yang Kim and Glen R. Kowach. “Focused Ion Beam Milling of Crystalline Diamonds.” *MRS Proceedings* 1282 (2011).

### **SKILLS & INTERESTS**

- **Software:** MATLAB, AutoCAD, Adobe Illustrator, LabView, Microsoft Office (Excel, PowerPoint, Access, Word)
- **Language:** Fluent in written and spoken Farsi and Spanish
- **Interests:** Cooking, Biking, Backgammon